Low-Flow Push-Pull Perfusion for Measuring Neurotransmitters with High Spatial and Temporal Resolution within the Living Brain

by

Thomas R. Slaney

A dissertation submitted in partial fulfillment
of the requirements for the degree of
Doctor of Philosophy
(Chemistry)
in the University of Michigan
2013

Doctoral Committee:

Professor Robert T. Kennedy, Chair
Professor Raoul Kopelman
Assistant Professor Stephen Maldonado
Professor Euisik Yoon

© Thomas R. Slaney 2013

DEDICATION

To my mother Jeanne Thomas, my father Frederick Slaney, and my sister Heidi Slaney whose love and support has made me who I am today.

ACKNOWLEDGEMENTS

I would like to thank my advisor, Dr. Kennedy, for all his guidance, encouragement, and support throughout the years. By never accepting less than my best, he has taught me to be a better scientist. I would also like to thank my committee, Dr. Kopelman, Dr. Maldonado and Dr. Yoon, for their invaluable guidance and feedback throughout my dissertation research.

I would like to thank Dr. Mark Burns and Dr. Gregory Roman for valuable guidance in research with vacuum-generated segmented flow. I would like to thank Neil Hershey, as well as Dr. Kristin Schultz and Dr. Maura Perry for training me in neurosurgery. Neil also was a valuable resource in capillary electrophoresis. I would also like to thank Jing Nie for her assistance in optimization of segmented flow reagent addition. I am also grateful to Dr. Peng Song and Dr. Omar Mabrouk for their training and feedback in developing and using LC-MS. I would like to thank both Dr. Meng Wang and Erik Guetschow for their assistance with microchip CE of plug samples. Lastly, I am grateful for all the assistance that Kirsten Porter-Stransky from Dr. Brandon Aragona's lab has provided related to tissue histology.

PREFACE

This work describes improvements to a technique called low-flow push-pull perfusion for measuring neurotransmitters within the brains of anesthetized or awake, freely-moving animals. This method is advantageous given its multianalyte measurement capabilities and high (~200 μm) spatial resolution. This work introduces methods to collect samples as nanoliter droplet fractions, providing from 7 s to 200 ms temporal resolution. It further discusses methods for analyzing neurotransmitters using reagent addition to droplets to perform enzyme assays or mass spectrometry. Push-pull probes were then used to demonstrate how concentrations of neurotransmitters and their metabolites can vary significantly between small nuclei (200 μm apart) using liquid chromatography – mass spectrometry, demonstrating differences in neuronal abundance, function and local metabolism.

TABLE OF CONTENTS

LIST OF TABLES

TABLE

LIST OF FIGURES

LIST OF APPENDICES

ABSTRACT

Low-flow push-pull perfusion is a technique for measuring neurotransmitters within the brain with ~200 μm resolution. Activity of neurotransmitters can vary on this size scale; therefore, low-flow push-pull may offer new insights into physiology. Flow rates used by this technique (50 nL/min) may present challenges for sample handling and assay sensitivity due to nL sample fractions. In this work, the temporal resolution of low-flow push-pull was advanced to 7 s *in vivo*, several different neurochemical assays were implemented, and gradients of neurotransmitters were mapped across sub-mm distances.

To address collection and manipulation of 7 s fractions collected in vivo, push-pull samples were stored as 6 nL plugs in an oil carrier phase. A tee was developed to address each fraction discretely for reagent addition. L-glutamate was measured within the striatum of anesthetized rats by using a fluorogenic enzyme assay. Microinjection of a potassium solution at the probe tip evoked L-glutamate concentration transients that had maxima of 4.5 ± 1.1 μM and rise times of 22 ± 2 s.

Nanospray ionization mass spectrometry was used to simultaneously measure three neurochemicals in plug samples. After microinjection of neostigmine at the push-pull probe tip, rapid extracellular concentration increases of neostigmine (14 ± 3 s), acetylcholine (35 ± 4 s) and a gradual decrease in choline (60 ± 13 s) were observed. This experiment highlights the ability of low-flow push-pull perfusion to observe drug-

neurotransmitter dynamics *in vivo*. A GABA enzyme assay and capillary electrophoresis were demonstrated for analysis of push-pull perfusion plugs.

A miniaturized push-pull probe was adapted for awake, freely moving animals and used to measure 13 neurotransmitters and metabolites. Concentration gradients were observed between proximate brain regions. For example, dopamine in the ventral tegmental area was 4.8 ± 1.5 nM, but in the red nucleus (200 μm apart) was 0.5 ± 0.2 nM.

This collection of work illustrates that low-flow push-pull perfusion is a versatile tool for monitoring many different neurotransmitters within the brain with 200 μm spatial and 7 s or faster temporal resolution. Future research directions may include ms temporal resolution *in vivo* measurements and microfabricated probes.

Chapter I

Introduction

Realizing the Next Generation of in Vivo Neurochemical Monitoring

Much of our understanding of how the brain works has been gleaned from chemical measurements made within the intact organ. Though cell and tissue preparations provide valuable information about the anatomy and physiology of the neurons that comprise the brain[1-10], they require great care in making inferences about higher-order physiology of the brain[11]. *In vivo* chemical measurements permit direct observation of normal brain function and can be associated with behavioral cues, external stimuli, and animal models of disease[12-14]. The technology to make these measurements was originally introduced during the 1950s. Since that time, it has undergone years of innovation, from the cortical cup, to microdialysis, then to the miniaturized probes and electrodes of the present. Whereas early experiments focused on simple identification of the presence and release of neurotransmitters[15], state-of-the-art techniques allow behavior to be correlated with the rapid chemical concentration fluctuations of specific neurotransmitters within spatially distinct, even sub-mm regions of the brain[14]. Although *in vivo* electrochemical sensors have revealed the presence of ms chemical transients, further development is required to create universal and selective techniques which provide the same resolution.

The objectives of this chapter are to review the chemical basis of neuronal communication within the brain and to place the topic of chemical sampling technology in a historical context. This section will highlight currently used instrumentation outlining the benefits and limitations of each detection method. An examination of the information provided by *in vivo* microelectrodes will indicate the importance of spatial and temporal resolution in neurochemical measurements. Finally, this chapter will discuss current microfluidic technologies that can be utilized to allow measurements of neurotransmitters on the μm size scale and s to ms time scale within the brain.

Neurons and Neurotransmitters

Neurons are discrete, highly interconnected cells that communicate with each other and control the functions of the body. Neurons transmit signals by conducting electrochemical impulses, or action potentials, through their excitable cell membranes. Axons are projections which conduct signals away from the cell body (soma) while dentrites conduct signals towards the cell body. Their membranes are maintained in a polarized state (-70 mV, cytosol versus extracellular fluid) by the action of sodium-potassium pumps and contain voltage-gated ion channels that can open when the membrane is sufficiently depolarized (approximately -55 mV)[16]. Upon reaching this threshold potential, the rapid influx of sodium ions across the membrane triggers further depolarization, and this action potential propagates along the cell membrane until reaching a junction with another neuron, called a synapse.

While a small fraction of synapses are gap junctions which directly link the cytosol of the two cells through channels, the majority are chemical synapses in which the neuronal membranes are in close proximity (~20 nm)[17] but not connected (shown in

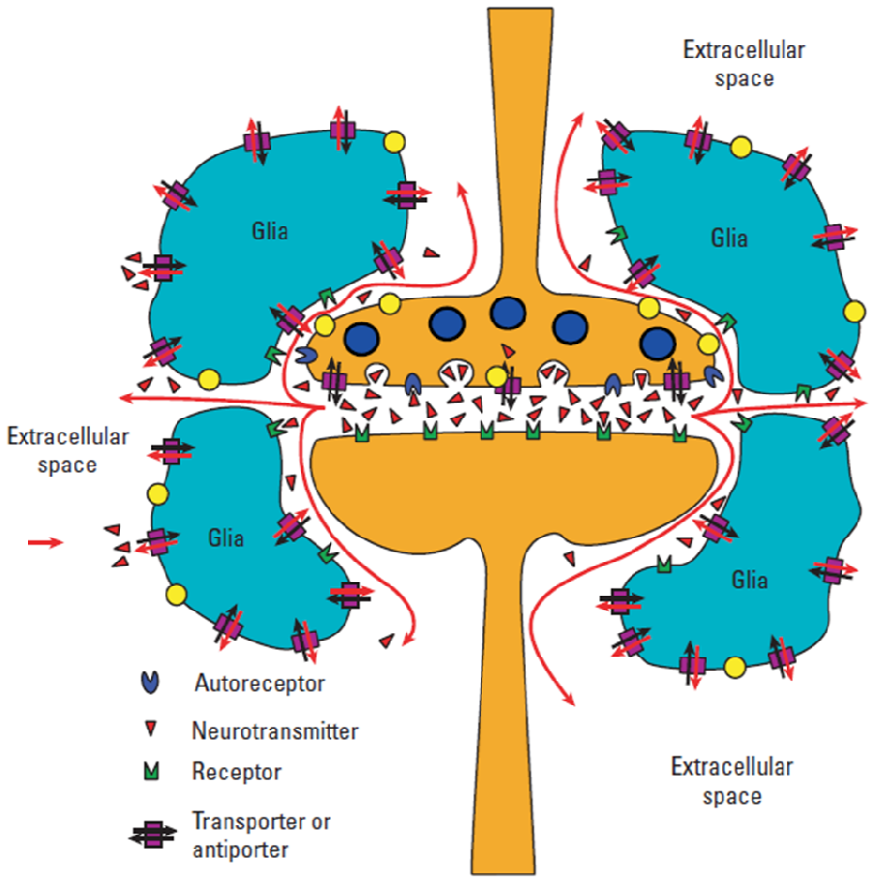

Figure 1.1. A chemical synapse. An action potential reaching the synapse from the afferent neuron (top) triggers release of neurotransmitters into the synaptic cleft. These bind specific receptors on the post-synaptic neuron (bottom) or autoreceptors on the afferent neuron. Reuptake then rapidly removes the neurotransmitter while a fraction diffuses into the extracellular milieu. Some neurotransmitters such as glutamate are maintained at tonic levels by the actions of glia cells. Reprinted with permission from[18], copyright 2006 American Chemical Society.

Figure 1.1)[16]. At chemical synapses, the action potential triggers the rapid exocytosis of synaptic vesicles which release chemical messengers into the synaptic cleft. These chemical messengers, or neurotransmitters, rapidly diffuse to the post-synaptic membrane where they then bind to specific receptors[16].

After release, most neurotransmitter molecules are actively transported or metabolized from the brain extracellular compartment to prevent continued action, but a certain fraction escapes into the extracellular space. This fraction can vary between the

specific neurotransmitter and the region of release as rates of reuptake or degradation vary[19]. Extracellular neurotransmitters can agonize receptors on nearby or distant neurons, in a process known as "volume transmission"[1, 19, 20]. While some neurotransmitters are found within the extracellular compartment primarily as a consequence of neuronal release, others, such as glutamate, are maintained at tonic concentrations by the actions of glia, the support cells within the brain which surround neurons and regulate their functions (Figure 1.1)[21-23].

There are hundreds of neurotransmitters and although some have highly specialized roles, others can be diverse in their actions[24]. The function of a neurotransmitter is dependent upon what receptor it binds, and can have an excitatory (depolarizing), inhibitory (hyperpolarizing) or modulatory effect. The roles of glutamate as the universal excitatory neurotransmitter[25] and γ-aminobutyric acid (GABA) as the universal inhibitory neurotransmitter are well established. However, the neurotransmitter glycine can function in either capacity as it is a major inhibitory neurotransmitter within the spinal cord but a required cofactor for glutamate receptors in the brain[26]. The cellular roles of the "excitatory" and "inhibitory" neurotransmitters cannot be generalized to their effect on the entire organism, as glutamate disregulation is implicated in the etiology of addiction[27] and decreased GABA is implicated in mood disorders[28].

Modulatory neurotransmitters such as the monoamines have more abstract roles, affecting higher order mental processes. For example, dopamine is associated with reward, movement, and congnition[19], whereas serotonin is associated with mood, cognition, memory and other processes[29, 30]. Rather than directly affecting membrane

potential, these bind G-protein-coupled receptors, affecting sub-cellular processes[31]. Much about the roles and behavior of different neurotransmitters remains obscure.

Measurement of neurotransmitters released can provide not only an assay of neuronal activity, but of what chemical messages are being sent. Synaptic clefts are very difficult to measure within due to their small (~20 nm) width[17], but the spillover from these clefts has been well established to correlate with local neuronal activity[14, 32, 33]. A salient feature of neurotransmission that presents an analytical challenge is the fast rates of release and reuptake of neurotransmitters into the extracellular space. Extracellular concentrations can vary on the s to ms timescale, correlating with behaviors, stimuli, and other events[32, 34, 35]. Another feature is that neuronal populations are highly organized into discrete nuclei within the brain and vary in size from mm to hundreds of μm. This organization reflects the different roles of neurons throughout the brain, such as the "hedonic hotspot" within the rat brain, a 1 mm^3 region which modulates how an animal responds to a pleasurable or noxious stimuli[36]. Additionally, the chemical concentrations in the extracellular compartment can range from pM to μM concentrations, necessitating techniques with adequate sensitivity to make such measurements.

Evolution of in Vivo Neurotransmitter Sampling

Cortical Cup

One of the first established techniques for monitoring neurochemical release from the intact brain was developed in 1953 by MacIntosh and Oborin[37]. Known as the "cortical cup", a cylinder ~5-10 mm in diameter[37, 38] (Figure 1.2A) was placed on the cortex through a burr hole in the skull. This allowed physiological saline to be passed over the surface of the brain and analyzed for content[38]. In doing so, the release of

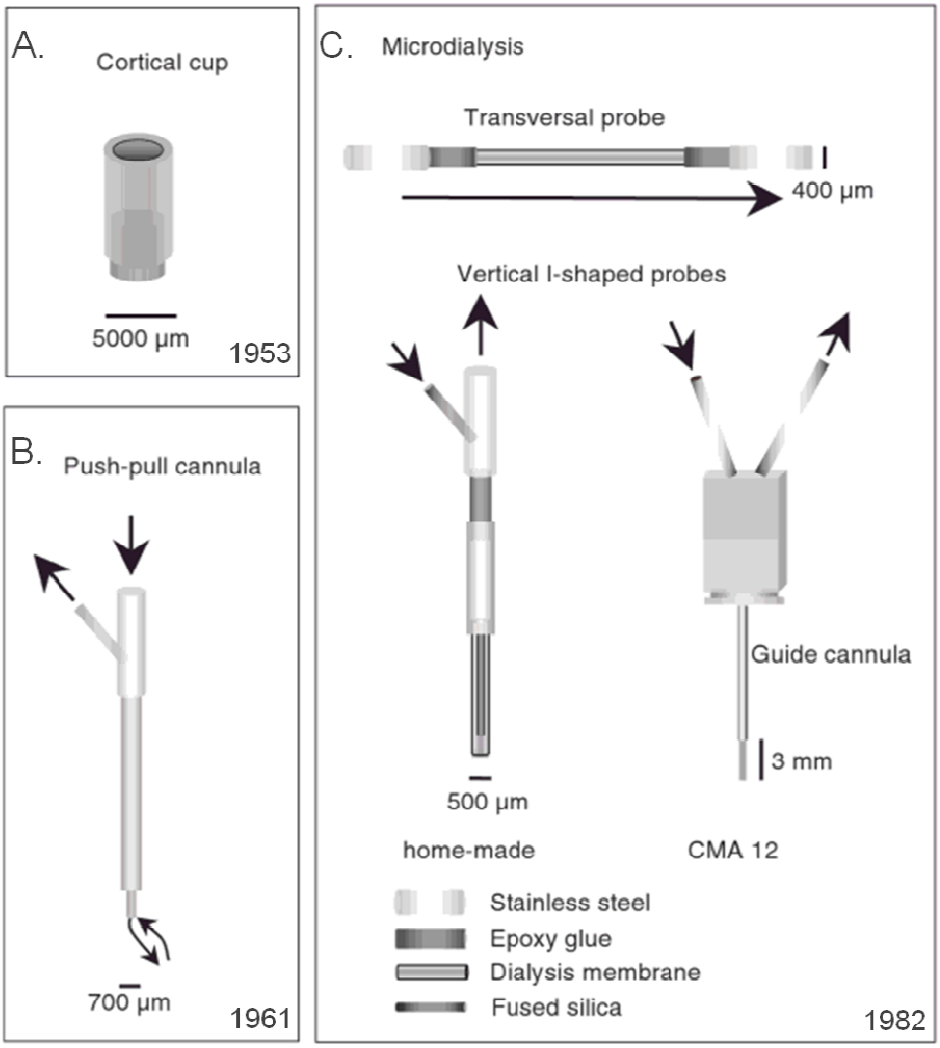

Figure 1.2. Devices for *in vivo* neurochemical sampling, including year of introduction. (A) The cortical cup involved passing saline over the exposed cortex of an animal and collecting it to observe transmitter release. (B) A push-pull cannula allowed deep brain samples to be conducted by perfusing fluid through concentric tubings implanted within the brain. (C) Microdialysis provided deep brain measurements by passing saline through an implanted dialysis fiber, either linearly (top) or through concentric tubing (bottom). Guide cannulae (implanted prior to surgery) allow microdialysis or push-pull experiments to be performed after an animal has recovered. Adapted with permission from[39], copyright Elsevier 2007.

acetylcholine and amino acids could be observed at rest and during stimulation[37, 38] and gave insight to the interactions of different neurotransmitters[38]. Despite new observations, the drawbacks of the cortical cup were apparent: a large device requiring the surface of

the brain be exposed. This made small animal experiments, deep brain measurements, and awake, freely moving experiments impractical[39].

"Conventional" Push-Pull Perfusion

By 1961, an alternative to the cortical cup had been developed known as push-pull perfusion[40]. Like the cortical cup, push-pull perfusion probes bathed neurons directly with physiological saline and collected the effluent. By doing so at the ends of concentric cannulae (Figure 1.2B), the extracellular neurotransmitters could be measured throughout the intact brain[41]. Push-pull perfusion allowed an animal to be sampled after recovery from the implantation surgery. To accomplish this, the outer cannula of the push-pull probe was inserted with an obturator instead of the inner cannula, and the animal was allowed to recover for several days. The obturator was then removed and inner cannula was inserted to enable sampling[42].

As the surface of the brain was not exposed, more freedom of motion could be achieved. However, with the benefits of this design came some challenges. Flow rates in the range of 10-100 μL/min were necessary to avoid probe occlusion which bore the potential for tissue lesioning, and continuous monitoring was also necessary to maintain operation[42]. Push-pull perfusion is still used for neurochemical measurements[43, 44], particularly large molecules[45], but has declined in use in lieu of newer techniques.

Microdialysis

Delgado and others first experimented with implanting and perfusing dialysis membranes within the brain in the 1970's (the "dialytrode")[46]. However, it was the work of Urban Ungerstedt in 1982 that introduced the technique of microdialysis[47]. Microdialysis probes consist of a hollow dialysis fiber which is implanted into the brain

region of interest, and perfused at ~1 to 2 μL/min flow rates with physiological saline (Figure 1.2C). Molecules such as neurotransmitters can then diffuse into the probe and be collected for analysis. Additionally, drugs and other molecules can be delivered simultaneously by diffusion from the probe. Concentrations within the sample collected at the probe outlet are proportional to the concentration within the tissue[48]. This technique is advantageous as it eliminates the risk of tissue lensioning poised by push-pull[42], and requires less monitoring as vacuum is not required. Microdialysis is to this day the *in vivo* method of choice for most neuroscientists making chemical measurements within the brain. Challenges for microdialysis include spatial resolution, as membrane lengths shorter than 1 mm are typically not used due to low concentrations recovered by the probe. Regions of interest may potentially be hundreds of microns in diameter[49].

Low-Flow Push-Pull Perfusion

Within the past decade, efforts to improve on the spatial resolution of *in vivo* sampling have resulted in new, ultra-low flow rate sampling methods. One such example is "direct sampling," or inserting a ~90 μm diameter capillary into the brain region of interest and withdrawing extracellular fluid at 1-50 nL/min[50]. This technique was improved upon with the development of low-flow push-pull perfusion[51]. Low-flow push-pull perfusion is similar to Gaddum's "conventional" push-pull perfusion (Figure 1.2B), except that tissue trauma is minimized by using 50 nL/min flow rates[51]. Concentric low-flow push-pull probes as small as 170 μm diameter have been utilized[52]. Another variation of the low-flow push-pull probe is the side-by-side capillary probe[53-55]. This design uses a 26 gauge hypodermic needle sheath to prevent occlusion during

implantation, but provides the advantages of low internal volume fluidics for both push and pull, facilitating probe use at nL/min flow rates[53-55].

Of *in vivo* sampling techniques, low-flow push-pull perfusion affords the finest spatial resolution. This is because sampling is confined to the area occupied by the probe tips. Though most studies have been conducted in the relatively large striatum[51, 53, 54] or lateral hypothalamus[56], there is the potential to selectively sample regions of the brain hundreds of μm in diameter. However, the low flow rate presents an analytical challenge for high temporal resolution, both in sample handling and sensitivity.

Instrumentation for Neurotransmitter Measurements

As sampling methodology to collect neurotransmitters from the brain has evolved, demands on analytical instrumentation have increased. Modern analytical techniques allow multiple neurotransmitters to be measured at basal levels within the brain[57]. However, sensitivity and selectivity presents a challenge when adapting to higher time resolution or lower flow rate techniques due to the smaller sample volumes produced. This is because the extracellular matrix of the brain is highly complex, and concentrations of neurotransmitters vary from μM to pM levels[57]. The advent of liquid chromatography (LC) and capillary electrophoresis (CE) mitigate these problems by separating neurotransmitters from the matrix and each other, reducing demands on the detector[39, 57]. Detection can then be conducted utilizing electrochemical detectors, fluorescence, or mass spectrometry[57]. Methods not requiring separations are immunoassays, enzyme assays and mass spectrometry and may increase analysis throughput by eliminating separation time.

Liquid Chromatography-Based Analyses

Liquid chromatography (LC)-based analyses are amongst the most frequently utilized methods of quantifying neurotransmitters collected by microdialysis[57]. In most cases, LC is performed in an offline fashion, collecting fractions for later analysis[57, 58]. Common techniques involve coupling LC to electrochemical detectors for electroactive molecules such as the catecholamines and serotonin[57, 59]. For quantifying non-electroactive species, pre-column derivatization makes LC amenable to fluorescence or electrochemical detectors[57, 59]. Another method of analysis is to place an enzyme bed at the end of the chromatography column for generation of an electroactive species from the analyte of interest. Enzyme reactors are commonly used for measurement of choline and acetylcholine[60, 61].

A disadvantage of LC as an analytical tool is that temporal resolution may be sacrificed if a larger sample volume is necessary for adequate sensitivity[57]. This can preclude use with ultra-low flow rate techniques such as low-flow push-pull perfusion[51]. Despite these concerns, LC with electrochemical or fluorescence detection remain mainstays of *in vivo* neuroscience research[57, 62].

More recently, advancements in mass spectrometry (MS) coupled to LC have offered high sensitivity measurements of neurotransmitters with and without derivatization[57]. MS has been used for label-free online detection and quantification of neuropeptides[63]. For separating small molecule neurotransmitters prior to MS detection, hydrophilic interaction chromatography (HILIC) and ion pairing have been utilized for simultaneous measurement of 4 to 6 neurotransmitters[64, 65]. Strong cation exchange can also be used for separation of neurotransmitters such as acetylcholine, improving

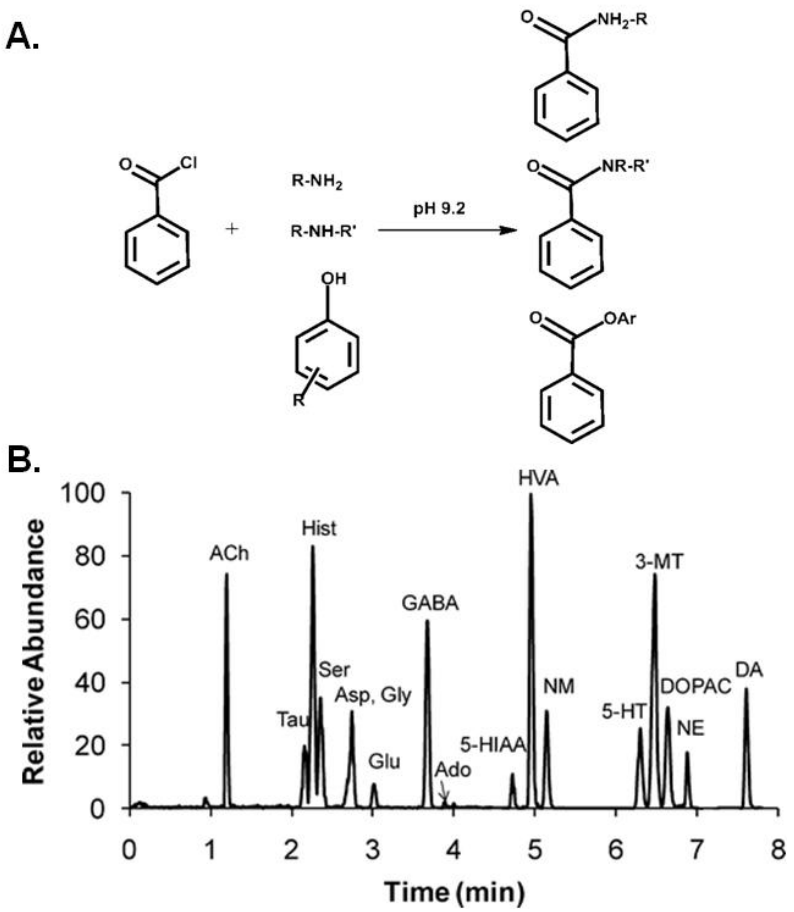

Figure 1.3. Benzoyl chloride derivatization of neurotransmitters for LC-MS analysis. (A) Benzoyl chloride reacts with primary amine, secondary amine and phenol moieties on neurotransmitters and metabolites. (B) High sensitivity and resolution of 17 neurotransmitters and their metabolites can be achieved from as little as a few µL of sample. Adapted with permission from [66], copyright 2012 American Chemical Society.

detection limits over electrochemical techniques[67]. Recently, derivatization prior to LC-MS detection has greatly increased the number of analytes which can be simultaneously measured. Diethylation labeling was shown to allow measurement of 4 monoamine neurotransmitters and metabolites[68]. To improve upon this technique, another group used benzoyl chloride to simultaneously measure 17 neurotransmitters and metabolites, as shown in Figure 1.3[66].

LC-MS with derivatization is particularly amenable to higher temporal resolution microdialysis or lower flow rate sampling methods due to its very high sensitivity,

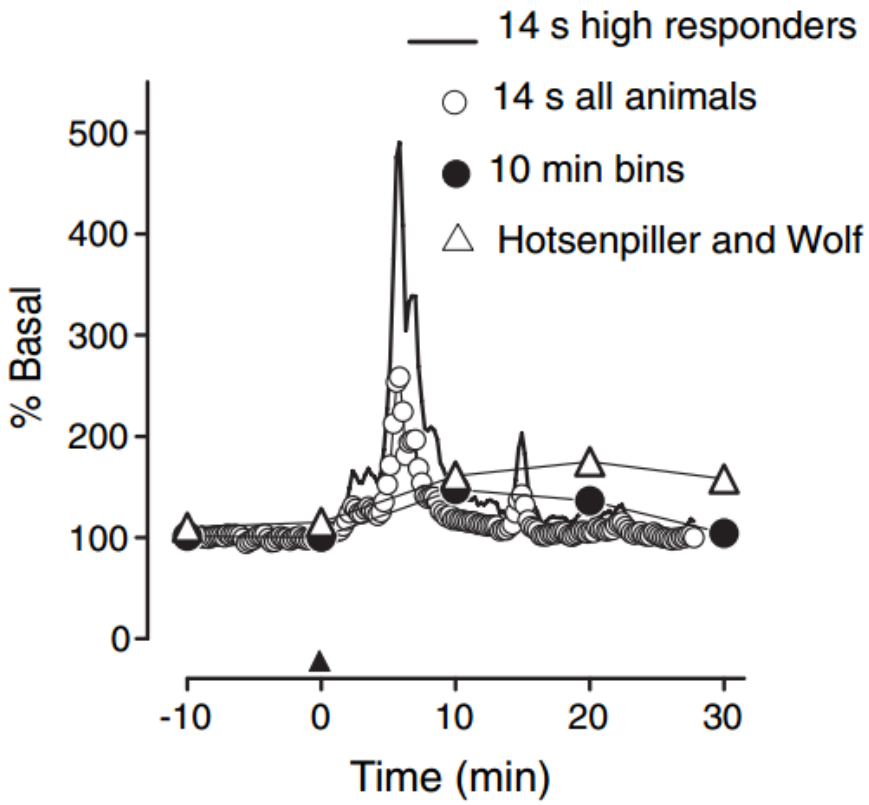

Figure 1.4. Online CE analysis of microdialysate in awake animals. In rats exposed to a fox scent, a rapid increase in L-glutamate is detected within their nucleus accumbens, as shown with 14 s resolution (CE-LIF). These dynamics are not visible with 10 min resolution sampling (LC-fluorescence). The 14 s data binned to 10 min is comparable to previous results. Reprinted with permission from [35], copyright 2006 International Society for Neuroscience.

achieving nM to pM detection limits with only a few μL of sample[66, 68, 69]. This high sensitivity of derivatized analytes is attributable to high fragmentation within the MS collision cell, better ionization efficiency due to increased hydrophobicity, and reduced matrix interference[66, 68]. As derivatized neurotransmitters are more stable, storage prior to offline analysis is simplified[66].

Capillary Electrophoresis

Capillary electrophoresis (CE) with laser-induced fluorescence (LIF) detection has emerged as a way of making fast time resolution chemical measurements with microdialysis and low-flow push-pull perfusion. Sensitivity and throughput of CE-LIF is

sufficient that effluent can be transmitted directly from the dialysis probe to instrument, a reagent (such as *o*-phthalaldehyde or naphthalene-2,3-dicarboxaldehyde[57, 70, 71]) added online to fluorescently label neurotransmitters, and a pL volume plug injected onto the separation capillary[18, 35, 71, 72]. Higher electric fields (~4 kV/cm) for CE allow for faster separation of amino acid neurotransmitters[73]. With high temporal resolution comes the ability to observe rapid concentration dynamics, such as responses to environmental stimuli. Figure 1.4 shows measurements of glutamate collected by microdialysis from the nucleus accumbens of rats in response to a fox scent with fast CE (14 s resolution) or LC analysis (10 min)[35]. While LC reveals a glutamate increase, the fast dynamics involved are not uncovered without higher time resolution. Binning the CE data to the same time scale reveals comparable results.

The sensitivity of CE-LIF has also made it the most common method of detection for low-flow push-pull perfusion[51-54, 56]. By collecting sample fractions into capillaries for offline analysis, temporal resolutions of 5 min (~0.25 μL per fraction) have been achieved[56]. In an online low-flow push-pull analysis, CE coupled to an ultraviolet detector has been utilized to measure ascorbate within the eye at 16 s resolution[74]. Other studies have utilized microfluidic devices to control push and pull flow while incorporating derivatization, CE separation and LIF detection with ~45 s resolution (described below)[53, 54].

Direct Methods of Neurotransmitter Analysis

While the majority of neurotransmitter analyses incorporate a separation, there are some techniques with sufficient selectivity and sensitivity to measure neurotransmitters within the sample matrix[57]. Electrochemical detectors are attractive for compact systems

as they do not require complex components such as optics. In particular, enzyme-based electrochemical detection has been developed for quantification of glucose and lactate[75] and has been applied for the study of spreading depolarizations within the human brain[76, 77]. As for neurotransmitters, glutamate has been detected with glutamate oxidase/horseradish peroxidase-based electrochemical detection[78, 79]. Challenges of incorporating enzyme-based electrochemical detectors are strategies to avoid background interference from sources such as ascorbic acid.

Another technique for direct detection of neurotransmitters is enzyme-based fluorogenic assays. A number of such assays have been developed previously for neurochemicals such as glutamate[80-82], GABA[82], acetylcholine[83], and choline[83]. For monitoring brain metabolism, a glucose oxidase assay has been used with microdialysis[84]. Laser-induced fluorescence can be utilized to achieve high sensitivity detection with small sample volumes[84, 85]. The minimal manipulation required for an enzyme assay makes them attractive for continuous flow detection schemes.

Though LC-MS has recently been utilized for detection of neuropeptides from microdialysis samples, radioimmunoassays are more well established[57]. While useful, these techniques often require large sample volumes (~25 μL) which may be impractical for observing chemical changes on the min time scale, and hourly fractions are not uncommon[86].

Recently, MS with electrospray ionization has been utilized for direct quantification (without LC) of neurotransmitters within microdialysate[87]. A makeup flow containing organic solvent to increase sensitivity, a chelating agent to remove adduct interferences, and an isotopically labeled internal standard enabled nM detection limits of

acetylcholine and choline[87]. The flow rates required during analysis made this method impractical for low-flow push-pull perfusion. However, nanospray ionization provides better mass sensitivity than eletrospray with nL/min flow rates and therefore may be amenable to this assay for push-pull samples[88].

Despite very rapid analysis times and high sensitivity, the temporal resolution of microdialysis and low-flow push-pull perfusion are limited by Taylor dispersion[89]. Taylor dispersion is the accelerated diffusion of a solute due to laminar flow within a capillary. This reduces the temporal resolution of sampling methods depending on the capillary lengths and flow rates[73]. With nL/min flow rates as with low-flow push-pull, this dispersion becomes severe and the 16 s resolution demonstrated previously is near the theoretical limit of the short (50 cm, 50 μm ID) inlet used[74]. A detailed description of temporal resolution and dispersion is presented in Chapter II.

Microelectrodes for in Vivo Measurements

Implantable microelectrodes have developed in parallel to sampling techniques for *in vivo* neurotransmitter measurements. These methods have been reviewed in detail elsewhere[14, 90-92]. Using cyclic voltammetry or amperometry, microelectrodes can provide chemical measurements on the s to ms timescale with hundreds of μm spatial resolution[14]. Two electrode types which have been especially popular in recent years are carbon fiber microelectrodes and microfabricated electrodes[14, 32-34, 93-103]. Carbon fiber electrodes are beneficial as they can be less than 30 μm in diameter, providing excellent spatial resolution while minimizing tissue trauma[104]. Microfabricated electrodes, constructed from silicon or ceramic, provide the benefits of small size (~100-200 μm

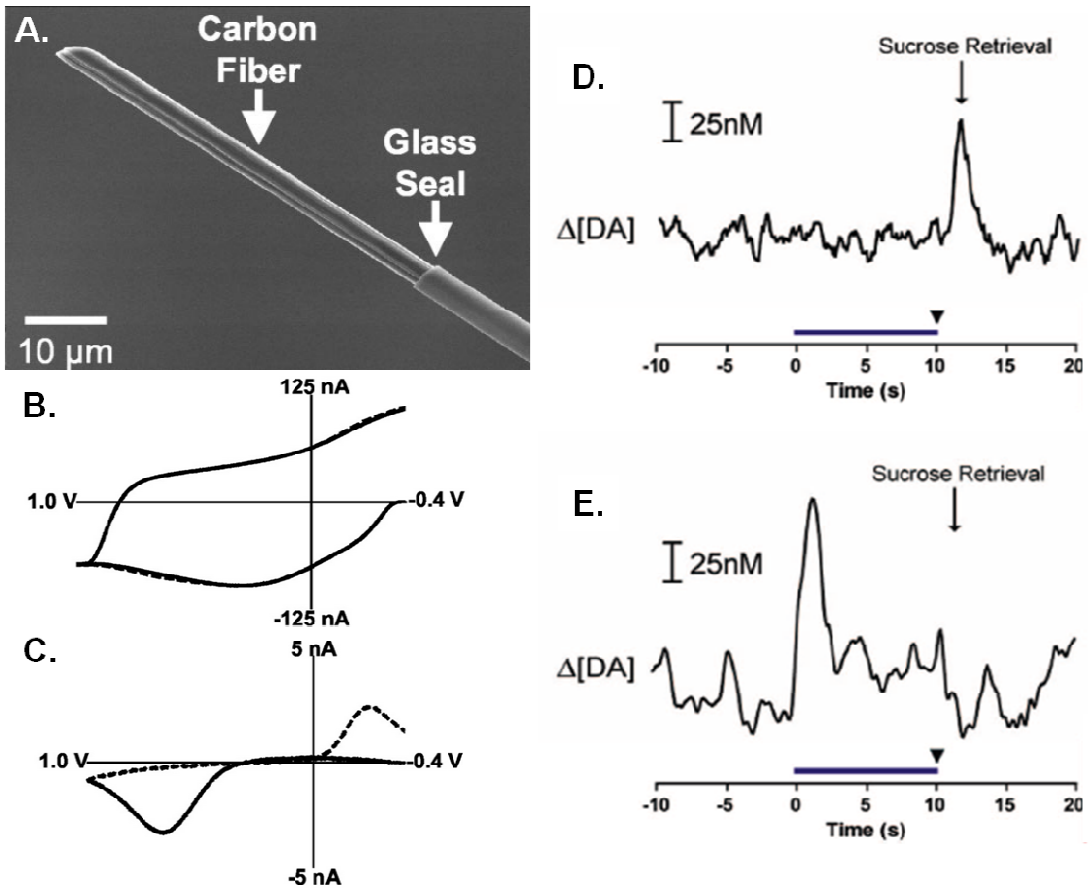

Figure 1.5. Fast-scan cyclic voltammetry using carbon fiber microelectrodes. (A). The small size of carbon fiber microelectrodes provides the highest spatial resolution of *in vivo* analytical devices. (B) Signals are collected and dopamine maxima (dashed line) located above background by subtracting the lowest signal during a collection window (solid line), revealing a dopamine voltammogram (C). Animals were presented a cue at t = 0 s and a sucrose pellet at t = 10 s. Whereas naïve animals (D) show no response to the cue in anticipation of the pellet, conditioned animals elicit dopamine increase in the nucleus accumbens at time of cue rather than time of pellet. A-C reproduced with permission from [32], copyright 2003 American Association for Clinical Chemistry; D,E reproduced with permission from[14] copyright 2008 American Chemical Society, and [105] copyright 2007 Macmillan Publishers: Nature Neuroscience.

diameter)[95, 101, 102], multiple sensing elements for background subtraction[101, 102], and multiple recording sites[94, 101].

The fastest *in vivo* electrochemical measurements have been accomplished for analytes that can be directly detected on a bare electrode within the extracellular compartment[14]. Molecules such as the catecholamines (particularly dopamine) can be

detected with hundreds of ms temporal resolution on carbon fiber microelectrodes (Figure 1.5A)[14, 32, 93]. Fast-scan cyclic voltammetry (FSCV) provides some selectivity for specific neurotransmitters while making measurements every ~100 ms (Figure 1.5B-C)[14, 90]. This has revealed much information about the nature of chemical communication, as the frequency of exocytotic events can be monitored and correlated with behavior (Figure 1.5D-E)[34, 93, 105].

Amperometric electrodes can be used for measuring neurotransmitters and substances not easily oxidized by an electrode[14, 102]. This is accomplished by coating an electrode with an enzyme selective for the neurotransmitter of interest which generates an electroactive product. Common analysis targets include glutamate[99, 101, 102, 106-109], acetylcholine and choline[100, 110], lactate[92, 111, 112], and glucose[113, 114]. Though lactate and glucose are not neurotransmitters, they provide information about local metabolic activity within the brain[112, 113].

There are some technical limitations to implantable microelectrodes. Fewer than 20 neurotransmitters have been measured *in vivo*[14], indicating a significant number of neurotransmitters are not yet compatible with these techniques[24]. Another challenge is making selective, quantitative measurements. While FSCV can resolve neurotransmitters with different redox potentials[14], some neurotransmitters such as norepinephrine and dopamine have identical voltammograms and cannot be directly distinguished[32]. Additionally, FSCV generates a relatively high background current which must be subtracted, as shown in Figure 1.5B-C. To avoid interference from background shifts, no greater than 90 s measurement windows should be utilized[93]. Amperometric microelectrodes utilize specialized coatings and background electrodes to remove signals

from interferents such as ascorbic acid[97, 101, 102]. However, selectivity of measurements remains a challenge[97].

The spatial and temporal resolution of microelectrodes has highlighted the significance of rapid chemical changes in small regions within the brain. In particular, they have revealed that "hot spots" of neural activity can be detected even within seemingly homogenous nuclei[49]. Moreover, it highlights the need for use of high spatial resolution sampling techniques such as low-flow push-pull perfusion, but with higher temporal resolution than the ~5 min of previous offline analyses[56].

Microfluidics for Improving Temporal Resolution

Given the spatial heterogeneity and rapid concentration fluctuations revealed by microelectrodes, there is a need to develop new techniques which allow accurate multi-analyte measurement with the same spatial and temporal resolutions. While bench-top CE systems can provide a great deal of information and improved temporal resolution, they have not been as successful in increasing the time resolution of ultra-low flow rate techniques. Microfluidic chips can further push the temporal limits of *in vivo* sampling while integrating analytical functions within the device. Several substrates for microfabrication have been developed including glass and polydimethyl siloxane (PDMS) [115, 116]. By miniaturizing, integrating and automating the processes of collecting, derivatizing and analyzing flow from a sampling probe, there is a potential to reduce reagent consumption, reduce instrument size, and facilitate sample handling.

Capillary electrophoresis on a chip provides integrated analysis. Glass microfluidic chips have been used to analyze microdialysate collected from the brain[70, 84, 117-119]. By integrating the derivatization and analysis on one device, precise control of

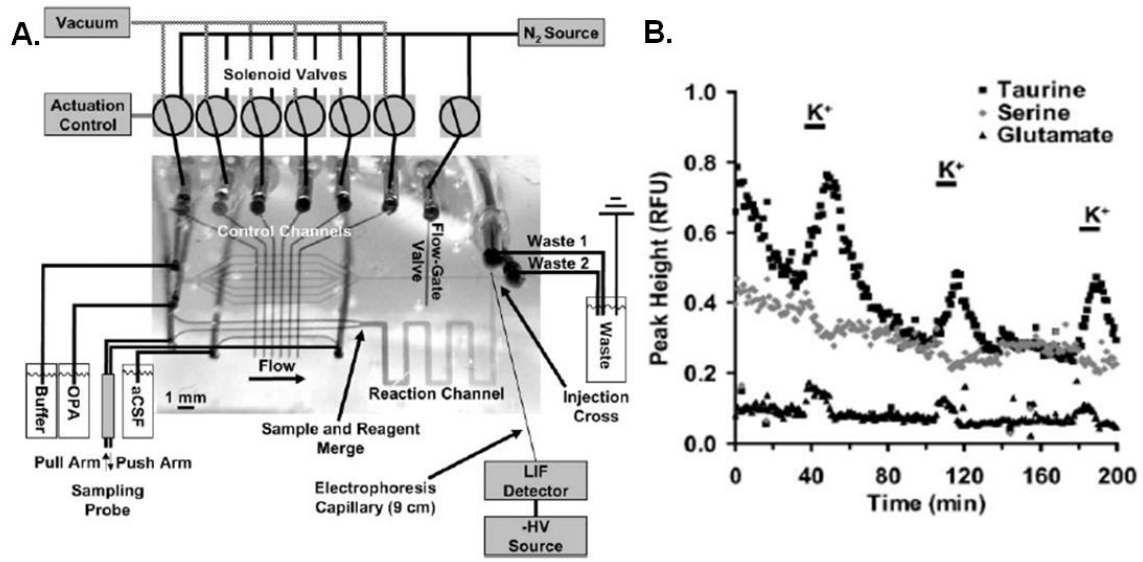

Figure 1.6. (A) Microfluidic chip incorporating a pneumatic peristaltic pump, fluorescence derivatization, and CE separation channel for analysis of neurotransmitters. (B) Transient increases in amino acid neurotransmitters glutamate and taurine were observed following neuronal stimulation with high potassium (K^+) aCSF. Reproduced from [53] with permission of the Royal Society of Chemistry.

derivatization parameters and separation channels can be obtained, however temporal resolution for this work was no greater than those demonstrated in non-microfabricated online analyses due to dispersion during flow[73].

Microfluidic pumps have been used to automate and simplify control of low-flow push-pull perfusion sampling. One advantage of PDMS as a microfluidic substrate is its flexibility and multilayer capabilities make it amenable to valving and pumping[120]. The basis of these devices is a layer of "control channels" over a thin PDMS membrane which incorporates the fluidic channels. By applying pneumatic pressure to the control channels, the membrane flexes to pinch the fluidic channels, sealing them off. As the volume of the channel is displaced by this motion, a series of these valves become an effective pump[53, 54, 120]. Figure 1.6A shows a PDMS microfluidic chip which integrates all the operations of low-flow push-pull perfusion and sample analysis. Figure 1.6B

shows the results obtained from within the anesthetized brain following potassium depolarizations of neurotransmitters. A multi-channel pump provides both push and pull flow to the implanted probe, and propels a separation buffer to an integrated microfluidic flow gate[53, 54]. A valve to stop the flow of separation buffer is actuated by a computer program to make an injection into the electrophoresis channel. To improve CE separation efficiency, a fused silica capillary can be inserted into the PDMS chip at the flow gate exit and utilized for the separation channel, improving heat transfer versus PDMS[53]. By integrating all functions and minimizing dispersion lengths, these devices have demonstrated the highest temporal resolution (~45 s) of any neurotransmitter analysis using low-flow push-pull (excluding this work)[53, 54].

Segmented flow microfluidics offer much potential for sampling methods to reduce dispersion during transport, manipulation, derivatization, and analysis of microdialysate or low-flow push-pull perfusate[121]. Segmented flow is the use of plugs or droplets of aqueous phase in an immiscible oil carrier on-chip[121]. If the channel is hydrophobic, then the oil phase wets the walls with a thin film, isolating each aqueous segment as a discrete sample[122-124]. Much progress has been achieved in the handling of nanoliter droplets. Methods for reagent addition[125, 126], splitting[127, 128], storage[118], phase separation[129], and rapid mixing[124] have been demonstrated without cross-talk between droplets. Analytical methodologies have been utilized with droplets including enzyme assays[84], immunoassays[130], capillary electrophoresis[70, 118, 119, 129], and mass spectrometry[87, 131, 132].

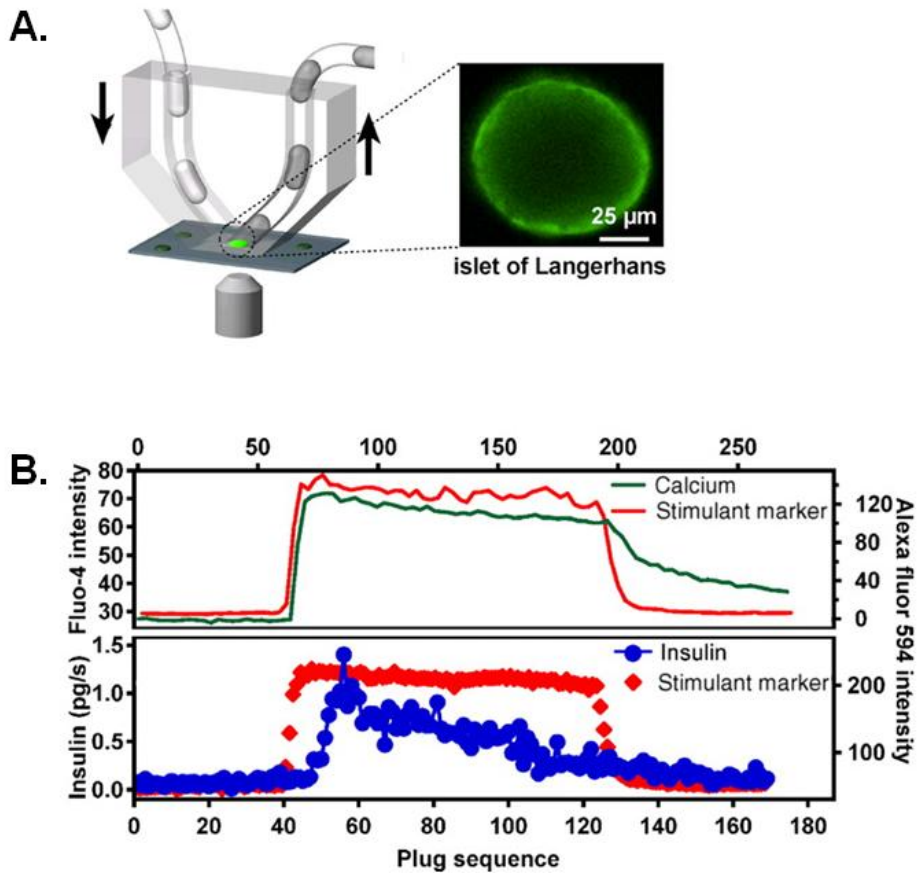

Figure 1.7. Chemistrode sampling using droplets for high temporal resolution. (A) An islet was monitored during exposure to high glucose concentration for intracellular calcium concentration and insulin secretion. (B) Analyzing plugs collected for insulin (competitive immunoassay) revealed a delayed insulin increase following glucose stimulation, and a decreasing insulin release over time as opposed to a more constant calcium concentration. Reproduced with permission from [130] copyright 2008 the National Academy of Sciences of the USA.

Nanoliter droplets were successfully incorporated with microdialysis sampling for up to 2 s temporal resolution[70, 118, 119]. By utilizing an offline analysis format, plugs could be generated at a high frequency and individually analyzed at a slower pace with electrophoresis[119]. This enables high resolution separations without compromising on temporal resolution. Despite this benefit, faster than 2 s temporal resolution was not achieved, a temporal limit attributed to the probe dialysis membrane[119].

Sampling methods not requiring a membrane may offer higher temporal resolution than microdialysis by not having a membrane to limit diffusion[119]. One novel

device so named the "chemistrode" has demonstrated this possibility, achieving up to 50 ms temporal resolution sampling *in vitro*[130]. This device functioned by bouncing nL plugs off the surface of an islet being analyzed (Figure 1.7). While this device clearly illustrates the potential of plugs for improving temporal resolution, the "chemistrode" is not amenable to deep brain sampling as measurements occurred at an orifice of a PDMS microchip.

In previous studies, the temporal resolution of low-flow push-pull perfusion was significantly affected by Taylor dispersion, reducing resolution to 16 s without derivatization or ~45 s with derivatization[54, 74]. This is due to practical limits imposed by how close the analytical instrumentation can be placed near an animal, increasing the length of the capillary inlet and dispersion time. However, segmented flow can be generated much closer to the inlet of the probe, preserving the temporal resolution for online or offline analysis[70, 84, 119]. As no membrane is present to limit diffusion, temporal resolutions in the ms range should be possible. The spatial resolution of these devices is greater than microdialysis, thus offering the potential to observe changes within small (~ 200 μm) nuclei of the brain. Since plugs are amenable to different assays, this should allow many different neurotransmitters to be analyzed.

Conclusions

Technologies for *in vivo* neurochemical sampling have evolved significantly as sampling probes have become less invasive, more practical, and finer spatial resolution. Improvements in analytical methodology allow multianalyte measurements and higher temporal resolution. Microelectrodes have highlighted the significance of high spatial and temporal resolution for observing concentration dynamics and spatial heterogeneity

of the brain. Droplet-based microfluidics have improved microdialysis to comparable temporal resolution of microelectrodes but with multianalyte resolution. By coupling droplet microfluidics to low-flow push-pull perfusion, sampling with both spatial and temporal resolution comparable to microelectrodes within the brain should be achievable, providing the potential for many different and multianalyte analyses.

Dissertation Overview

The goal of this dissertation is to improve upon low-flow push-pull perfusion to create a high spatial and temporal resolution *in vivo* method without the limitations of microelectrodes. First, a reliable and simple method for integrating droplet microfluidics with push-pull is described, which provides 7 s temporal resolution. To process the samples collected, a novel Teflon reagent addition tee was fabricated. This high temporal resolution methodology was demonstrated *in vivo* with several different assays, including an enzyme assay, capillary electrophoresis, and mass spectrometry. The spatial resolution and multianalyte potential of low-flow push-pull perfusion were demonstrated *in vivo* by using novel miniaturized probes implanted in awake, freely moving animals to map 13 neurotransmitters and metabolites with 200 μm resolution. Future projects are proposed to improve upon the spatial and temporal resolution of these devices, including designs to improve temporal resolution, microfabrication of probes for smaller geometries, improved temporal resolution of comprehensive neurotransmitter analyses, and elucidating regional differences in dopamine uptake and metabolism.

Chapter II

Push-pull perfusion was coupled to segmented flow to generate 6 nL plug samples at 7 s intervals. This was achieved by using a vacuum source coupled to a tee at the

probe outlet for plug generation. By balancing the flow resistance of an oil inlet, stable plug generation was achieved and up to 45 min of samples stored for offline analysis. A novel Teflon-based reagent addition tee was fabricated to allow addition of a glutamate enzyme assay reagent to each plug, which was then quantified by laser-induced fluorescence. This allowed 7 s resolution measurement of glutamate transients within the striatum of anesthetized rats. Microinjections of 70 mM potassium created rapid glutamate transients with an average maxima of 4.5 ± 1.1 μM. It was also demonstrated that reducing inlet size and geometry can provide up to 200 ms temporal resolution.

Chapter III

Multianalyte *in vivo* measurements were demonstrated by low-flow push-pull perfusion sampling coupled to nanospray ionization mass spectrometry. Acetylcholine, its metabolite choline, and the drug neostigmine were analyzed simultaneously. A reagent was added to each plug to improve ionization, remove background interferences and increase accuracy by an iosotopic internal standard using the tee demonstrated in Chapter II. Basal concentrations of ACh and Ch were 5.0 ± 1.9 nM and 490 ± 90 nM in the striatum of anesthetized rats. Following microinjection of neostigmine, extracellular concentration increases of as fast as 7 s could be observed for neostigmine (14 ± 3 s average) while acetylcholine increased over 35 ± 4 s. Choline was observed to decrease over 60 ± 13 s following microinjection, relating to a decrease in metabolism of acetylcholine.

Chapter IV

Low-flow push-pull perfusion was used to test if extracellular chemical gradients exist between several small brain nuclei. A miniaturized polyimide-encased push-pull

probe was developed and used to measure basal neurotransmitter spatial gradients within brain of live animals with 0.004 mm^3 resolution. Dopamine, norepinephrine, serotonin, glutamate, γ-aminobutyric acid, aspartate, glycine, acetylcholine and several neurotransmitter metabolites were measured simultaneously by LC-MS. Significant differences in basal concentrations between midbrain regions as little as 200 μm apart were observed. For example, dopamine in the ventral tegmental area was 4.8 ± 1.5 nM but in the red nucleus was 0.5 ± 0.2 nM. Regions of high glutamate concentration and variability were found within the VTA of some individuals suggesting hot spots of glutamatergic activity. Measurements were also made within the nucleus accumbens core and shell. Differences were not observed in dopamine and 5-HT in the core and shell; but their metabolites homovanillic acid (460 ± 60 nM and 130 ± 60 nM respectively) and 5-hydroxyindoleacetic acid (720 ± 200 nM and 220 ± 50 nM respectively) did differ significantly suggesting differences in dopamine and 5-HT activity in these brain regions. Maintenance of these gradients depends upon a variety of mechanisms. Such gradients likely underlie highly localized effects of drugs and control of behavior that have been found using other techniques.

Chapter V

To further increase the applications of segmented flow-coupled low-flow push pull perfusion, two analytical methods were adapted. First, a novel droplet-based enzyme assay for the neurotransmitter GABA was developed. By incorporating laser-induced fluorescence, a detection limit of 0.7 μM for GABA within samples was achieved using similar methodology to that described within Chapter II. Second, the reagent addition tee was used to fluorescently tag amine neurotransmitters and a microfabricated

electrophoresis chip was used to measure neurotransmitters within each sample plug. Rise times could be observed within 1 plug, indicating that 7 s temporal resolution is conserved in this microchip. Potassium-evoked changes of glutamate and aspartate were measured *in vivo* by electrophoresis.

Chapter VI

This body of work is summarized, and several future areas for research are proposed to build on this work. The first project is to improve the temporal resolution to 1 s or better for low-flow push-pull perfusion when applied to *in vivo* measurements. This can be accomplished by modifying probe geometry and flow rates and using segmented flow. Additionally, adding a makeup volume to probe effluent can allow higher frequency plugs without the technical challenges of reducing to pL plug volumes. The second project is to integrate segmented flow microfluidics with a silicon microfabricated push-pull probe. Prototypes of this probe have been constructed and tested successfully *in vivo* with 20 minute fraction collection but as of yet, segmented flow has not been utilized. Design modifications can additionally provide benefits such as sampling from other sites and incorporation of microinjectors. A third project would improve on the temporal resolution of benzoyl chloride analysis of push-pull fractions. As the 1 μL fractions collected in Chapter IV yielded amply detectable signals for basal neurotransmitter concentrations, 0.1 μL (2 minute) fractions should be readily detected and highly informative. Lastly, low-flow push-pull perfusion can be utilized to study the fate and metabolism of dopamine within regions such as the accumbens shell, which may provide insight to the mechanisms of certain drugs which are not well understood.

Appendices

Three appendices are provided to supplement experimental procedures for probe use and fabrication, performing histology, and microfabricating push-pull probes. Appendix A contains a description of practical aspects for low-flow push-pull perfusion probe fabrication and operation. Though the data chapters give an overview of instrumentation and parameters needed for low-flow push-pull sampling, the goal of this section is to provide a comprehensive description of fabrication protocols and probe operation. It offers an overview of parameters observed to be relevant to maintaining stable flow rates over several hours and how to prevent probe occlusion. Appendix B describes in detail the procedures for performing histology for probe tracking. This allows not only probe placement to be verified, but can be helpful in troubleshooting sampling issues. Appendix C provides a detailed description of the fabrication procedures for a new design of silicon microfabricated push-pull probe. It also provides results and observations from preliminary experiments utilizing this probe and a discussion of the significance of these preliminary results.

References

(1) Fuxe, K.; Dahlstroem, A. B.; Jonsson, G.; Marcellino, D.; Guescini, M.; Dam, M.; Manger, P.; Agnati, L. *Prog. Neurobiol. (Amsterdam, Neth.)* **2010**, *90*, 82-100.
(2) D'Este, L.; Casini, A.; Puglisi-Allegra, S.; Cabib, S.; Renda, T. G. *J. Chem. Neuroanat.* **2007**, *33*, 67-74.
(3) Furuta, A.; Rothstein, J. D.; Martin, L. J. *J. Neurosci.* **1997**, *17*, 8363-8375.
(4) Oakman, S. A.; Faris, P. L.; Kerr, P. E.; Cozzari, C.; Hartman, B. K. *J. Neurosci.* **1995**, *15*, 5859-5869.
(5) Jongen-Rêlo, A. L.; Voorn, P.; Groenewegen, H. J. *Eur. J. Neurosci.* **1994**, *6*, 1255-1264.
(6) Woolf, N. J.; Butcher, L. L. *Brain Res. Bull.* **1986**, *16*, 603-637.
(7) Brown, P.; Molliver, M. E. *J. Neurosci.* **2000**, *20*, 1952-1963.

(8) Yung, K. K. L.; Bolam, J. P.; Smith, A. D.; Hersch, S. M.; Ciliax, B. J.; Levey, A. I. *Neuroscience* **1995**, *65*, 709-730.
(9) Freed, C.; Revay, R.; Vaughan, R. A.; Kriek, E.; Grant, S.; Uhl, G. R.; Kuhar, M. J. *J. Comp. Neurol.* **1995**, *359*, 340-349.
(10) Lehre, K. P.; Levy, L. M.; Ottersen, O. P.; Storm-Mathisen, J.; Danbolt, N. C. *J. Neurosci.* **1995**, *15*, 1835-1853.
(11) Reid, K. H.; Edmonds Jr, H. L.; Schurr, A.; Tseng, M. T.; West, C. A. *Prog. Neurobiol.* **1988**, *31*, 1-18.
(12) Willuhn, I.; Wanat, M. J.; Clark, J. J.; Phillips, P. E. M.; Self, D. W.; Staley Gottschalk, J. K. In *Behavioral Neuroscience of Drug Addiction*; Self, D. W., Staley, J. K., Eds.; Springer Berlin Heidelberg: Heidelberg, 2009; Vol. 3, pp 29-71.
(13) Bruno, J. P.; Sarter, M.; Arnold, H. M.; Himmelheber, A. M. *Reviews in the Neurosciences* **1999**, *10*, 25-48.
(14) Robinson, D. L.; Hermans, A.; Seipel, A. T.; Wightman, R. M. *Chem. Rev.* **2008**, *108*, 2554-2584.
(15) Pepeu, G. *Prog. Neurobiol.* **1973**, *2*, 259-288.
(16) Klein, S. B.; Thorne, B. M. *Biological Psychology*; Worth: New York, 2007.
(17) Palay, S. L. *J. Biophys. Biochem. Cytol.* **1956**, *2*, 193-202.
(18) Watson, C. J.; Venton, B. J.; Kennedy, R. T. *Anal. Chem.* **2006**, *78*, 1391-1399.
(19) Rice, M. E.; Patel, J. C.; Cragg, S. J. *Neuroscience* **2011**, *198*, 112-137.
(20) Agnati, L. F.; Leo, G.; Zanardi, A.; Genedani, S.; Rivera, A.; Fuxe, K.; Guidolin, D. *Acta Physiologica* **2006**, *187*, 329-344.
(21) Timmerman, W.; Westerink, B. H. C. *Synapse* **1997**, *27*, 242-261.
(22) Melendez, R. I.; Vuthiganon, J.; Kalivas, P. W. *J. Pharmacol. Exp. Ther.* **2005**, *314*, 139-147.
(23) Knackstedt, L. A.; LaRowe, S.; Mardikian, P.; Malcolm, R.; Upadhyaya, H.; Hedden, S.; Markou, A.; Kalivas, P. W. *Biol. Psychiatry* **2009**, *65*, 841-845.
(24) Greengard, P. *Science* **2001**, *294*, 1024-1030.
(25) Meldrum, B. S. *The Journal of Nutrition: International Symposium on Glutamate* **2000**, *130*, 1007S-1015S.
(26) Hernandes, M.; Troncone, L. *J. Neural Transm.* **2009**, *116*, 1551-1560.
(27) Kalivas, P. W. *Nat. Rev. Neurosci.* **2009**, *10*, 561-572.
(28) Petty, F. *Journal of Affective Disorders* **1995**, *34*, 275-281.
(29) Zangen, A.; Overstreet, D. H.; Yadid, G. *J. Neurochem.* **1997**, *69*, 2477-2483.
(30) Roth, B. L.; Hanizavareh, S. M.; Blum, A. E. *Psychopharmacology* **2004**, *174*, 17-24.
(31) Gilman, A. G. *Annu. Rev. Biochem.* **1987**, *56*, 615-649.
(32) Robinson, D. L.; Venton, B. J.; Heien, M. L. A. V.; Wightman, R. M. *Clin. Chem.* **2003**, *49*, 1763-1773.
(33) Westerink, B. H. C.; Timmerman, W. *Anal. Chim. Acta* **1999**, *379*, 263-274.
(34) Garris, P. A.; Kilpatrick, M.; Bunin, M. A.; Michael, D.; Walker, Q. D.; Wightman, R. M. *Nature* **1999**, *398*, 67-69.
(35) Venton, B. J.; Robinson, T. E.; Kennedy, R. T. *J. Neurochem.* **2006**, *96*, 236-246.
(36) Peciña, S.; Berridge, K. C. *J. Neurosci.* **2005**, *25*, 11777-11786.
(37) Mitchell, J. F. *The Journal of Physiology* **1963**, *165*, 98-116.

(38) Jasper, H. H.; Koyama, I. *Can. J. Physiol. Pharmacol.* **1969**, *47*, 889-905.
(39) Pepeu, G.; Giovannini, M. G. In *Handbook of Microdialysis*; Westerink, B. H. C., Cremers, T. I. F. H., Eds.; Elsevier: Amsterdam, 2007, pp 377-398.
(40) Gaddum, J. H. *J. Physiol. (Lond.)* **1961**, *155*, 1P-2P.
(41) Szerb, J. C. *Can. J. Physiol. Pharmacol.* **1967**, *45*, 613-620.
(42) Myers, R. D.; Adell, A.; Lankford, M. F. *Neurosci. Biobehav. Rev.* **1998**, *22*, 371-387.
(43) Sirivelu, M. P.; Shin, A. C.; Perez, G. I.; MohanKumar, P. S.; MohanKumar, S. M. J. *Human Reproduction* **2009**, *24*, 718-725.
(44) Misztal, T.; Gorski, K.; Tomaszewska-Zaremba, D.; Molik, E.; Romanowicz, K. *J. Endocrinol.* **2008**, *198*, 83-89.
(45) Fiedler, J.; Jara, P.; Luza, S.; Dorfman, M.; Grouselle, D.; Rage, F.; Lara, H. E.; Arancibia, S. *J. Neuroendocrinol.* **2006**, *18*, 367-376.
(46) Delgado, J. M. R.; Lerma, J.; del Río, R. M.; Solís, J. M. *J. Neurochem.* **1984**, *42*, 1218-1228.
(47) Zetterstrom, T.; Vernet, L.; Ungerstedt, U.; Tossman, U.; Jonzon, B.; Fredholm, B. B. *Neurosci. Lett.* **1982**, *29*, 111-115.
(48) Olson, R. J.; Justice, J. B. *Anal. Chem.* **1993**, *65*, 1017-1022.
(49) Robinson, D. L.; Howard, E. C.; McConnell, S.; Gonzales, R. A.; Wightman, R. M. *Alcohol.: Clin. Exp. Res.* **2009**, *33*, 1187-1196.
(50) Kennedy, R. T.; Thompson, J. E.; Vickroy, T. W. *J. Neurosci. Methods* **2002**, *114*, 39-49.
(51) Kottegoda, S.; Shaik, I.; Shippy, S. A. *J. Neurosci. Methods* **2002**, *121*, 93-101.
(52) Kottegoda, S.; Pulido, J. S.; Thongkhao-on, K.; Shippy, S. A. *Molecular Vision* **2007**, *13*, 2073-2082.
(53) Cellar, N. A.; Kennedy, R. T. *Lab Chip* **2006**, *6*, 1205-1212.
(54) Cellar, N. A.; Burns, S. T.; Meiners, J. C.; Chen, H.; Kennedy, R. T. *Anal. Chem.* **2005**, *77*, 7067-7073.
(55) Slaney, T. R.; Nie, J.; Hershey, N. D.; Thwar, P. K.; Linderman, J.; Burns, M. A.; Kennedy, R. T. *Anal. Chem.* **2011**, *83*, 5207-5213.
(56) Thongkhao-on, K.; Wirtshafter, D.; Shippy, S. A. *Pharmacol. Biochem. Behav.* **2008**, *89*, 591-597.
(57) Perry, M.; Li, Q.; Kennedy, R. T. *Anal. Chim. Acta* **2009**, *653*, 1-22.
(58) Nandi, P.; Lunte, S. M. *Anal. Chim. Acta* **2009**, *651*, 1-14.
(59) Kissinger, P. T. In *Microdialysis in the Neurosciences*; Robinson, T. E., Justice, J. B., Eds.; Elsevier: Amsterdam, 1991, pp 103-116.
(60) Tsai, T.-R.; Cham, T.-M.; Chen, K.-C.; Chen, C.-F.; Tsai, T.-H. *Journal of Chromatography B: Biomedical Sciences and Applications* **1996**, *678*, 151-155.
(61) Huang, T.; Yang, L.; Gitzen, J.; Kissinger, P. T.; Vreeke, M.; Heller, A. *Journal of Chromatography B: Biomedical Sciences and Applications* **1995**, *670*, 323-327.
(62) McKittrick, C. R.; Abercrombie, E. D. *J. Neurochem.* **2007**, *100*, 1247-1256.
(63) Li, Q.; Zubieta, J.-K.; Kennedy, R. T. *Anal. Chem.* **2009**, *81*, 2242-2250.
(64) Zhang, X.; Rauch, A.; Lee, H.; Xiao, H.; Rainer, G.; Logothetis, N. K. *Rapid Commun. Mass Spectrom.* **2007**, *21*, 3621-3628.
(65) Eckstein, J. A.; Ammerman, G. M.; Reveles, J. M.; Ackermann, B. L. *J. Neurosci. Methods* **2008**, *171*, 190-196.

(66) Song, P.; Mabrouk, O. S.; Hershey, N. D.; Kennedy, R. T. *Anal. Chem.* **2012**, *84*, 412-419.
(67) Shackman, H. M.; Shou, M.; Cellar, N. A.; Watson, C. J.; Kennedy, R. T. *J. Neurosci. Methods* **2007**, *159*, 86-92.
(68) Ji, C.; Li, W.; Ren, X.-d.; El-Kattan, A. F.; Kozak, R.; Fountain, S.; Lepsy, C. *Anal. Chem.* **2008**, *80*, 9195-9203.
(69) Mabrouk, O. S.; Li, Q.; Song, P.; Kennedy, R. T. *J. Neurochem.* **2011**, *118*, 24-33.
(70) Wang, M.; Roman, G. T.; Perry, M. L.; Kennedy, R. T. *Anal. Chem.* **2009**, *81*, 9072-9078.
(71) Bowser, M. T.; Kennedy, R. T. *Electrophoresis* **2001**, *22*, 3668-3676.
(72) Venton, B. J.; Robinson, T. E.; Kennedy, R. T.; Maren, S. *Eur. J. Neurosci.* **2006**, *23*, 3391-3398.
(73) Lada, M. W.; Vickroy, T. W.; Kennedy, R. T. *Anal. Chem.* **1997**, *69*, 4560-4565.
(74) Patterson, E. E., II; Pritchett, J. S.; Shippy, S. A. *Analyst* **2009**, *134*, 401-406.
(75) Dempsey, E.; Diamond, D.; Smyth, M. R.; Urban, G.; Jobst, G.; Moser, I.; Verpoorte, E. M. J.; Manz, A.; Michael Widmer, H.; Rabenstein, K.; Freaney, R. *Anal. Chim. Acta* **1997**, *346*, 341-349.
(76) Feuerstein, D.; Manning, A.; Hashemi, P.; Bhatia, R.; Fabricius, M.; Tolias, C.; Pahl, C.; Ervine, M.; Strong, A. J.; Boutelle, M. G. *J Cereb Blood Flow Metab* **2010**, *30*, 1343-1355.
(77) Parkin, M.; Hopwood, S.; Jones, D. A.; Hashemi, P.; Landolt, H.; Fabricius, M.; Lauritzen, M.; Boutelle, M. G.; Strong, A. J. *J Cereb Blood Flow Metab* **2005**, *25*, 402-413.
(78) Obrenovitch, T. P.; Zilkha, E. *Methods* **2001**, *23*, 63-71.
(79) Miele, M.; Boutelle, M. G.; Fillenz, M. *Journal of Physiology-London* **1996**, *497*, 745-751.
(80) McElroy, K. E.; Bouchard, P. J.; Harpel, M. R.; Horiuchi, K. Y.; Rogers, K. C.; Murphy, D. J.; Chung, T. D. Y.; Copeland, R. A. *Anal. Biochem.* **2000**, *284*, 382-387.
(81) Chapman, J.; Zhou, M. *Anal. Chim. Acta* **1999**, *402*, 47-52.
(82) Graham, L. T.; Aprison, M. H. *Anal. Biochem.* **1966**, *15*, 487-497.
(83) Browning, E. T. *Anal. Biochem.* **1972**, *46*, 624-638.
(84) Wang, M.; Roman, G. T.; Schultz, K.; Jennings, C.; Kennedy, R. T. *Anal. Chem.* **2008**, *80*, 5607-5615.
(85) Bradley, A. B.; Zare, R. N. *J. Am. Chem. Soc.* **1976**, *98*, 620-621.
(86) Gruber, S. H. M.; Nomikos, G. G.; Mathe, A. A. *European Neuropsychopharmacology* **2006**, *16*, 592-600.
(87) Song, P.; Hershey, N. D.; Mabrouk, O. S.; Slaney, T. R.; Kennedy, R. T. *Anal. Chem.* **2012**, *84*, 4659-4664.
(88) Juraschek, R.; Dülcks, T.; Karas, M. *J. Am. Soc. Mass Spectrom.* **1999**, *10*, 300-308.
(89) Aris, R. *Proc. R. Soc. London, Ser. A* **1956**, *235*, 67-77.
(90) Kawagoe, K. T.; Zimmerman, J. B.; Wightman, R. M. *J. Neurosci. Methods* **1993**, *48*, 225-240.
(91) O'Neill, R. D.; Lowry, J. P.; Mas, M. **1998**, *12*, 69-127.

(92) Wilson, G. S.; Gifford, R. *Biosensors Bioelectron.* **2005**, *20*, 2388-2403.
(93) Heien, M. L. A. V.; Khan, A. S.; Ariansen, J. L.; Cheer, J. F.; Phillips, P. E. M.; Wassum, K. M.; Wightman, R. M. *Proceedings of the National Academy of Sciences of the United States of America* **2005**, *102*, 10023-10028.
(94) Johnson, M. D.; Franklin, R. K.; Gibson, M. D.; Brown, R. B.; Kipke, D. R. *J. Neurosci. Methods* **2008**, *174*, 62-70.
(95) Kipke, D. R. *Engineering in Medicine and Biology Society, 2003. Proceedings of the 25th Annual International Conference of the IEEE* **2003**, *4*, 3337-3339.
(96) Oldenziel, W. H.; Dijkstra, G.; Cremers, T. I. F. H.; Westerink, B. H. C. *Brain Res.* **2006**, *1118*, 34-42.
(97) Oldenziel, W. H.; Dijkstra, G.; Cremers, T. I. F. H.; Westerink, B. H. C. *Anal. Chem.* **2006**, *78*, 3366-3378.
(98) Bruno, J. P.; Gash, C.; Martin, B.; Zmarowski, A.; Pomerleau, F.; Burmeister, J.; Huettl, P.; Gerhardt, G. A. *Eur. J. Neurosci.* **2006**, *24*, 2749-2757.
(99) Day, B. K.; Pomerleau, F.; Burmeister, J. J.; Huettl, P.; Gerhardt, G. A. *J. Neurochem.* **2006**, *96*, 1626-1635.
(100) Parikh, V.; Pomerleau, F.; Huettl, P.; Gerhardt, G. A.; Sarter, M.; Bruno, J. P. *Eur. J. Neurosci.* **2004**, *20*, 1545-1554.
(101) Burmeister, J. J.; Pomerleau, F.; Palmer, M.; Day, B. K.; Huettl, P.; Gerhardt, G. A. *J. Neurosci. Methods* **2002**, *119*, 163-171.
(102) Burmeister, J. J.; Gerhardt, G. A. *Anal. Chem.* **2001**, *73*, 1037-1042.
(103) Gerhardt, G. A.; Ksir, C.; Pivik, C.; Dickinson, S. D.; Sabeti, J.; Zahniser, N. R. *J. Neurosci. Methods* **1999**, *87*, 67-76.
(104) Wightman, R. M.; Heien, M. L. A. V.; Wassum, K. M.; Sombers, L. A.; Aragona, B. J.; Khan, A. S.; Ariansen, J. L.; Cheer, J. F.; Phillips, P. E. M.; Carelli, R. M. *Eur. J. Neurosci.* **2007**, *26*, 2046-2054.
(105) Day, J. J.; Roitman, M. F.; Wightman, R. M.; Carelli, R. M. *Nat Neurosci* **2007**, *10*, 1020-1028.
(106) Hu, Y.; Mitchell, K. M.; Albahadily, F. N.; Michaelis, E. K.; Wilson, G. S. *Brain Res.* **1994**, *659*, 117-125.
(107) Hascup, K. N.; Hascup, E. R.; Stephens, M. L.; Glaser, P. E. A.; Yoshitake, T.; Mathe, A. A.; Gerhardt, G. A.; Kehr, J. *Neuropsychopharmacology* **2011**, *36*, 1769-1777.
(108) Hascup, E. R.; Hascup, K. N.; Stephens, M.; Pomerleau, F.; Huettl, P.; Gratton, A.; Gerhardt, G. A. *J. Neurochem.* **2010**, *115*, 1608-1620.
(109) Quintero, J. E.; Day, B. K.; Zhang, Z.; Grondin, R.; Stephens, M. L.; Huettl, P.; Pomerleau, F.; Gash, D. M.; Gerhardt, G. A. *Exp. Neurol.* **2007**, *208*, 238-246.
(110) Uutela, P.; Reinilä, R.; Piepponen, P.; Ketola, R. A.; Kostiainen, R. *Rapid Commun. Mass Spectrom.* **2005**, *19*, 2950-2956.
(111) Shram, N. F.; Netchiporouk, L. I.; Martelet, C.; Jaffrezic-Renault, N.; Bonnet, C.; Cespuglio, R. *Anal. Chem.* **1998**, *70*, 2618-2622.
(112) Hu, Y.; Wilson, G. S. *J. Neurochem.* **1997**, *69*, 1484-1490.
(113) Hu, Y.; Wilson, G. S. *J. Neurochem.* **1997**, *68*, 1745-1752.
(114) Netchiporouk, L. I.; Shram, N. F.; Jaffrezic-Renault, N.; Martelet, C.; Cespuglio, R. *Anal. Chem.* **1996**, *68*, 4358-4364.

(115) Duffy, D. C.; McDonald, J. C.; Schueller, O. J. A.; Whitesides, G. M. *Anal. Chem.* **1998**, *70*, 4974-4984.
(116) Reyes, D. R.; Iossifidis, D.; Auroux, P.-A.; Manz, A. *Anal. Chem.* **2002**, *74*, 2623-2636.
(117) Sandlin, Z. D.; Shou, M.; Shackman, J. G.; Kennedy, R. T. *Anal. Chem.* **2005**, *77*, 7702-7708.
(118) Wang, M.; Hershey, N.; Mabrouk, O.; Kennedy, R. *Anal. Bioanal. Chem.* **2011**, *400*, 2013-2023.
(119) Wang, M.; Slaney, T.; Mabrouk, O.; Kennedy, R. T. *J. Neurosci. Methods* **2010**, *190*, 39-48.
(120) Unger, M. A.; Chou, H.-P.; Thorsen, T.; Scherer, A.; Quake, S. R. *Science* **2000**, *288*, 113-116.
(121) Huebner, A.; Sharma, S.; Srisa-Art, M.; Hollfelder, F.; Edel, J. B.; deMello, A. J. *Lab Chip* **2008**, *8*, 1244-1254.
(122) Zheng, B.; Tice, J. D.; Ismagilov, R. F. *Anal. Chem.* **2004**, *76*, 4977-4982.
(123) Tice, J. D.; Song, H.; Lyon, A. D.; Ismagilov, R. F. *Langmuir* **2003**, *19*, 9127-9133.
(124) Song, H.; Tice, J. D.; Ismagilov, R. F. *Angew. Chem. Int. Ed.* **2003**, *42*, 768-772.
(125) Song, H.; Li, H.-W.; Munson, M. S.; Van Ha, T. G.; Ismagilov, R. F. *Anal. Chem.* **2006**, *78*, 4839-4849.
(126) Li, L.; Boedicker, J. Q.; Ismagilov, R. F. *Anal. Chem.* **2007**, *79*, 2756-2761.
(127) Nie, J.; Kennedy, R. T. *Anal. Chem.* **2010**, *82*, 7852-7856.
(128) Adamson, D. N.; Mustafi, D.; Zhang, J. X. J.; Zheng, B.; Ismagilov, R. F. *Lab Chip* **2006**, *6*, 1178-1186.
(129) Roman, G. T.; Wang, M.; Shultz, K. N.; Jennings, C.; Kennedy, R. T. *Anal. Chem.* **2008**, *80*, 8231-8238.
(130) Chen, D.; Du, W.; Liu, Y.; Liu, W.; Kuznetsov, A.; Mendez, F. E.; Philipson, L. H.; Ismagilov, R. F. *Proc. Natl. Acad. Sci. USA* **2008**, *105*, 16843-16848.
(131) Hatakeyama, T.; Chen, D. L.; Ismagilov, R. F. *J. Am. Chem. Soc.* **2006**, *128*, 2518-2519.
(132) Zhu, Y.; Fang, Q. *Anal. Chem.* **2010**, *82*, 8361-8366.

Chapter II

Push-Pull Perfusion Sampling with Segmented Flow for High Temporal and Spatial Resolution *in Vivo* Chemical Monitoring

*Reproduced with permission from Slaney, T.R. et al. Analytical Chemistry **2011**, 83, 5207-5213. Copyright 2011 American Chemical Society.*

Introduction

Monitoring neurotransmitters in the brain extracellular compartment is a necessary tool for studying neuronal function and psychological disorders[1-3]. In such measurements, temporal resolution is important because concentration changes of neurotransmitters in the extracellular space around synapses are known to occur in milliseconds to seconds [1, 4]. Spatial resolution is important because the brain contains many small structures with distinct functions, neuronal populations, and neurotransmitter dynamics. Microdialysis sampling coupled to analytical methods is a widely used approach for *in vivo* monitoring. If the sensitivity of the analytical method is sufficient, short sampling intervals can be used and temporal resolution of a few seconds can be achieved[5-8]; however, the relatively large size of the probes, which are typically over 2 mm long and 200 μm diameter, preclude their use for studying smaller brain regions. In this work, we combine the miniaturized sampling method low-flow push-pull perfusion with segmented flow to achieve 200 ms temporal resolution and spatial resolution of 0.016 mm^2.

Push-pull sampling has been used in the brain since 1961[9, 10]. In this method, artificial cerebrospinal fluid (aCSF) is continuously infused into tissue through one tube and withdrawn from a second tube that is placed beside or concentric with the infusion tube. Push-pull sampling fell out of favor because of tissue damage associated with direct tissue contact of fluids flowing at microliter per minute rates. Spatial resolution can be improved and tissue damage greatly reduced by using narrow bore capillaries as the sampler tubing and flow rates less than 50 nL/min[11]. Spatial resolution of low-flow push-pull perfusion is inherently better than microdialysis as the active sampling area is only limited by the spacing of the probe capillary inlets.

Achieving high temporal resolution with low-flow push-pull sampling places great demands on sample manipulation capability, assay throughput, and assay sensitivity. Consider that if sampling at 50 nL/min, then a 60 min experiment at 10 s temporal resolution would require collection and analysis of 360 samples of 8 nL volume each. Furthermore, Taylor dispersion during sampling can reduce temporal resolution. Initial experiments with low flow push-pull perfusion achieved 5 min temporal resolution by off-line fraction collection and analysis by CE[11]. Coupling low-flow push pull perfusion on-line with CE has allowed 16 s[12] and 45 s[13, 14] temporal resolution sampling from the eye and brain respectively; however, in these cases Taylor dispersion was minimized by using short tubing that would be impractical for freely moving subjects. This approach also precludes off-line analysis which is often advantageous.

In this work, we have coupled low-flow push-pull perfusion to segmented flow to both improve temporal resolution and facilitate manipulation of the nanoliter fractions that are collected. In segmented flow, fractions are collected into a tube or channel as

discrete plugs separated by an immiscible carrier phase that wets the tubing surface. As previously shown for microdialysis and "chemistrode" sampling, this approach prevents loss of temporal resolution due to Taylor dispersion during transport to an analytical system[15-17]. This method also provides a convenient way to manipulate nanoliter samples in view of the operations that have been developed for plugs[18-24]. Furthermore, several methods have been developed to analyze plug samples including enzyme assay[23], immunoassay[25], electrophoresis[15, 26], and mass spectrometry[27, 28].

A significant challenge for coupling segmented flow with push-pull perfusion is developing flow control for plug formation from the "pull" or sampling capillary. We found that this problem could be solved by using vacuum at the outlet of collection tubing to pull oil and brain perfusate into a tee where flow segmentation occurred. As an initial application of this approach, we demonstrate *in vivo* monitoring of L-glutamate, a primary excitatory neurotransmitter in the brain known to have rapid concentration dynamics[29]. L-glutamate was determined by fluorescent enzyme assay of the plugs in an off-line system. The assay allowed hundreds of samples with ~6 nL volume to be measured at 15 samples/min. The system is shown to provide an efficient means of collecting, manipulating, and analyzing the large number of low volume samples required for high temporal and spatial resolution sampling.

Materials and Methods

Chemicals and Materials

Unless otherwise specified, all reagents were purchased from Fisher Scientific (Fairlawn, NJ) and were certified ACS grade or better. L-glutamic acid and 1*H*,1*H*,2*H*,2*H*-perfluoro-1-octanol (PFO) were purchased from Sigma-Aldrich (St. Louis,

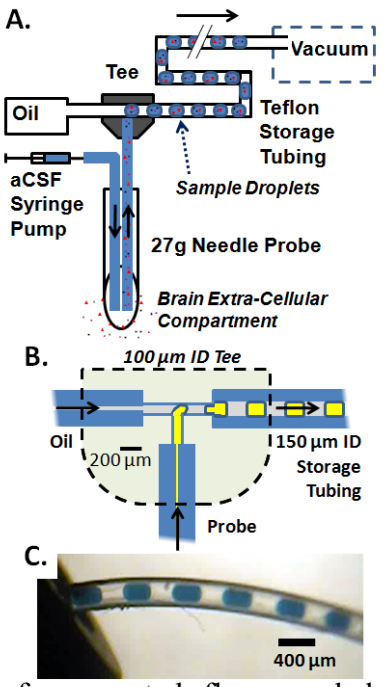

Figure 2.1. (A) Diagram of segmented flow-coupled low-flow push-pull probe. Artificial cerebrospinal fluid (aCSF) is infused directly into the tissue, while simultaneously extracellular fluid is withdrawn at an equal flow rate. Suction for sampling flow is generated by vacuum applied to the outlet of Teflon storage tubing, which also pulls the oil to generate the segmented sample stream. (B) Diagram of the internal tee geometry (tee outline not to scale). (C) Photograph of 6 nL sample segments (blue food dye) entering the storage tubing at the tee outlet.

MO). Perfluorodecalin and FC-72 were purchased from Acros (Morris Plains, NJ). L-glutamate oxidase, glutamate pyruvate transaminase, horseradish peroxidase, L-alanine, dimethylsulfoxide, and Amplex Red were purchased as a kit from Invitrogen (Carlsbad, CA). Fused silica capillaries were purchased from Polymicro (Phoenix, AZ). Teflon PFA tubing was purchased from Upchurch (Oak Harbor, WA). 1/32" polyvinylidine difluoride (PVDF) sheets were purchased from Small Parts (Lexington, KY).

Probe Fabrication

"Side-by-side" push-pull probes were constructed as described previously[13]. Briefly, two 10 cm lengths of 20 µm inner diameter (ID), 90 µm outer diameter (OD) capillary were inserted through a 27-gauge stainless steel hypodermic needle as

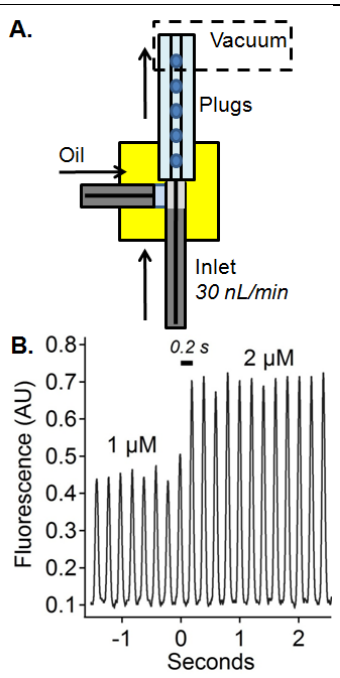

Figure 2.2. System for high temporal resolution sampling. (A) A tee from PVDF was molded so to place the probe inlet adjacent to the segmentation tubing. Oil enters the tee by flowing over the end of the inlet capillary within the tee. (B) Fluorescence of plugs in non-fluorescent oil was measured while switching between 1 and 2 µM resorufin standards, demonstrating 0.2 s temporal resolution (1 plug to observe a 10-90% concentration change, 30 nL/min sampling rate).

illustrated in Figure 2.1A (BD, Franklin Lakes, NJ). The capillaries were cemented in place by applying cyanoacrylate adhesive to the opposite end of the needle (Duro Super Glue, Henkel, Rocky Hill, CT). To adapt these capillaries to 360 µm fittings, 2 cm lengths of 150 µm ID, 360 µm OD capillary were glued concentrically over the ends of these using thixotropic optical epoxy (353ND-T, Epoxy Technology, Billerica, MA). Additional fabrication details are provided in Appendix A.

A tee was fabricated from PVDF and capillaries for use in temporal resolution experiments. Figure 2.2A illustrates the assembled tee design. To mold the PVDF, a 150 µm OD capillary was placed inside a 150 µm ID, 360 µm OD Teflon tubing and a 360 µm OD capillary was placed perpendicular to the 150 µm OD capillary to form a tee. These capillaries were fixed to a piece of glass using labeling tape and an approximately

1 cm square piece of PVDF was placed over these capillaries. Another piece of glass was placed over the PVDF, and the assembly was heated in an oven at 170°C until the PVDF melted. After cooling at room temperature, a second piece of approximately 1 cm square PVDF was slid underneath the PVDF assembly to form a bottom layer and this assembly was again melted in the oven. The capillaries were removed and the PVDF was trimmed to reduce channel lengths to ~4 mm using a high-speed rotary cutoff tool (Dremel, Robert Bosch, Farmington Hills, MI). The perpendicular channel was extended to intersect the 150 μm ID channel using a 360 μm drill bit (Kyocera, Costa Mesa, CA). A flat tipped 360 μm drill bit was used to bore out the 360 μm axial tubing channel. A 25 cm length of 50 μm ID, 360 μm OD capillary was inserted into the axial channel. The polyimide was removed from approximately 2 mm at the end of a 1 cm length of 10 μm ID, 150 μm OD capillary and this end was inserted into the 150 μm ID channel until adjacent to the Teflon tubing. A 10 cm long, 25 μm ID x 360 μm OD oil inlet capillary was inserted in the perpendicular channel. The tee was sealed with StickyWax (KerrLab, Orange, CA) to prevent leaks and primed with oil (10:1 FC-72:PFO, v:v) to remove trapped air bubbles before use.

Surgical Procedures

All surgical procedures were performed according to a protocol approved by the University Committee on Use and Care of Animals. Male Sprague-Dawley rats between 250 and 350 g were anesthetized by intraperitoneal administration of 75 mg/kg ketamine and 0.25 mg/kg dexmedetomidine. Boosters of 25 mg/kg ketamine and 0.08 mg/kg dexmedetomidine were given as needed. Anesthetized rats were mounted in a stereotaxic frame and the push-pull sampling probe was inserted into the striatum at 1.0 mm anterior

and ± 2.6 mm lateral to bregma, and 5.0 mm ventral to the dura. During insertion, both capillaries were flushed with aCSF to prevent clogging as described elsewhere[11]. The aCSF contained 145 mM NaCl, 2.68 mM KCl, 1.01 mM $MgSO_4$, 1.22 mM $CaCl_2$, 1.55 mM Na_2HPO_4, and 0.45 mM NaH_2PO_4, pH 7.4[14]. For K^+ stimulation experiments, a capillary microinjector[30] mounted on a second stereotaxic arm, angled 10° to vertical in the coronal plane, was inserted 0.1 mm right of the sampling probe inlet. The sampling probe was positioned so that the beveled side faced the injector. After probes were inserted, 45 min equilibration time was allowed as preliminary experiments showed that for 30 min after insertion L-glutamate concentrations were not stable. Stimulated L-glutamate release was achieved by infusing 100 nL of high-K^+ aCSF over 6 s. High-K^+ aCSF was prepared the same as aCSF, except with 70.0 mM KCl and 77.7 mM NaCl.

Probe Operation

An overview of the fluidic system for *in vivo* sampling and analysis is shown in Figure 2.1. To provide the "push" flow, one capillary of the probe was connected to a 25 μL syringe (Gastight, Hamilton Co., Reno, NV) using 360 μm capillary fittings and approximately 30 cm of 40 μm ID capillary, and this syringe was placed in a syringe pump (Fusion 400, Chemyx, Stafford, TX). After probe insertion, the "pull" capillary was connected to a 100 μm ID tee (C360QTPKG4, Valco Instruments, Houston, TX). One inlet of this tee was attached to a 20 cm length of 40 μm ID capillary which was placed in a vial of a 50:1 (v:v) solution of perfluorodecalin:PFO, the immiscible oil phase. A 50 cm length of 150 μm ID, 360 μm OD Teflon PFA tubing was attached to the third inlet of the tee. 610 mm Hg of vacuum was applied to the outlet of the Teflon tube to provide 50 nL/min of "pull" through the probe inlet and approximately 70 nL/min of

oil flow simultaneously. To provide a constant flow rate, this Teflon storage tubing was primed with plugs of aCSF before sampling. To monitor the aqueous flow, plug frequency and quality were visually observed. Detailed procedures for probe use and troubleshooting are provided in Appendix A.

After sampling from the brain, the probe was removed and sequentially placed into a series of standards of L-glutamate in aCSF for calibration. To prevent clogging during removal, vacuum was stopped and the "push" flow was increased to 500 nL/min. Standards were sampled without "push" flow to calibrate for absolute recovered concentrations.

Fabrication of a Teflon-Based Reagent Addition Tee

A hydrophilic capillary placed orthogonal to a hydrophobic channel has been shown to provide carry-over free reagent addition to segmented flow[22, 24]. A reusable Teflon-based reagent addition tee with a hydrophilic reagent inlet was therefore constructed by melt casting polyvinylidine difluoride (PVDF) sheet over capillary tubing as shown in Figure 2.3. A 20 cm length of 150 μm ID Teflon tubing was first protected by inserting a ~30 cm length of 150 μm OD capillary through it. This was placed on a piece of glass, and a 200 μm OD capillary was placed perpendicular to this. To ensure vertical alignment, the 200 μm capillary was placed inside a ~2 cm length of 250 μm ID, 360 μm OD capillary and approximately 3 mm of 200 μm OD capillary was left exposed (not pictured). These capillaries were fastened to the glass with labeling tape. An approximately 1 cm square piece of PVDF sheet was aligned over the tubing as shown in Figure 2.3A. Another piece of glass was placed above this assembly which was then heated at 170°C until the PVDF melted. After cooling to room temperature, another

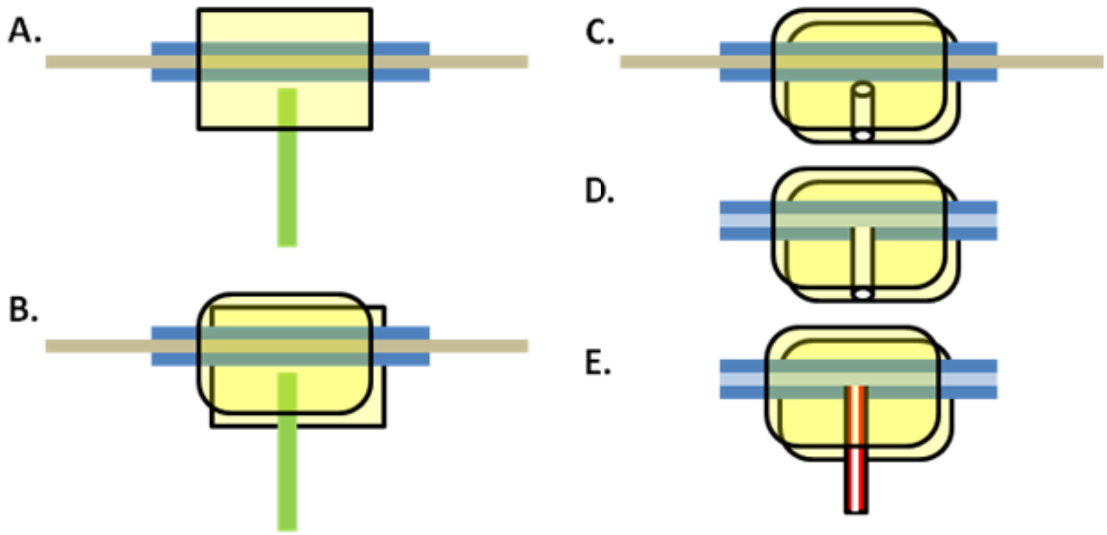

Figure 2.3. Fabrication procedure of a Teflon tubing-based reagent addition tee. A 10 cm length of 150 µm ID, 360 µm OD Teflon tubing (blue) was protected by filling with a 150 µm OD capillary (gray). A 200 µm OD capillary (green) was placed perpendicular to this Teflon tubing, and a ~2x2 cm long rectangular piece of PVDF (yellow) was placed over these tubings (A). This was sandwiched between two glass plates and melted at 170°C. Another piece of PVDF was slid under the tubing (B) and this was again melted at 170°C. The 200 µm capillary was then removed (C), the hole was extended to the lumen of the Teflon tubing with a 92-gauge drill bit, and the 150 µm OD capillary was removed (D). A 10 cm, 50 µm ID, 190 µm OD capillary was then inserted until flush with the lumen (E) and sealed with wax.

PVDF piece was slid underneath the tubing as in Figure 2.3B and the tee was then placed in the oven at 170°C until melted. The chip was then cooled to room temperature, and the perpendicular capillary was pulled out (Figure 2.3C). The PVDF was trimmed to reduce the length of the capillary molded channel to less than 4 mm using a high-speed rotary cutting tool. The 200 µm hole was extended through the wall of the Teflon tubing (Figure 2.3D) using a 92-gauge bit mounted in a high-speed drill controlled by a micropositioner. The 150 µm OD capillary was removed, and a 10 cm 50 µm ID 190 µm OD capillary inserted through the 200 µm inlet until flush with the edge of the lumen of the Teflon tubing. To prevent leaks, the Teflon tubing and capillary were sealed to the PVDF tee using Sticky Wax.

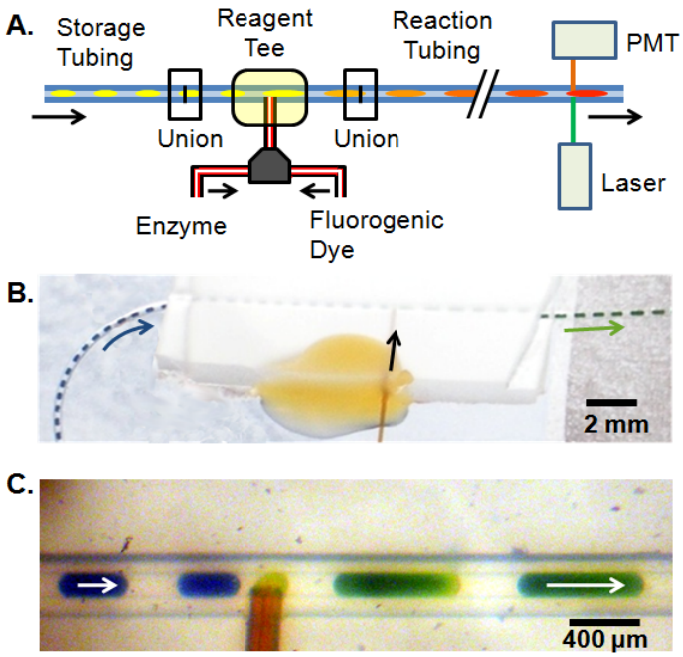

Figure 2.4. Operation of a Teflon-based reagent addition tee. (A) Scheme for enzyme assay analysis setup with reagent-addition tee. A 150 µm ID, 360 µm OD Teflon storage tube containing the push-pull sample plugs is connected to the inlet of the reagent-addition tee with a PDMS union. Stored plugs are pushed by a syringe pump through the tee, where the assay reagents (enzyme and fluorogenic dye) are added at an approximately 1:2 reagent:sample volume ratio. These plugs travel through Teflon for approximately 35 minutes while the enzyme reaction incubates. Fluorescence is continuously measured with a green HeNe laser and photomultiplier tube. (B) Photograph illustrating passive tee operation. For visualization, yellow food coloring (from bottom) was added to blue food coloring plugs (left) to yield green plugs (right). (C) Micrograph of reagent addition in the tee as described in B. Arrows indicate flow direction.

Enzyme Assay and Plug Analysis

Plugs were collected into and stored in 150 µm ID by 360 µm OD Teflon tubing. For analysis, the sample plugs were pumped into a Teflon reagent addition tee at 200 nL/min (see Figure 2.4A) using a syringe pump (Fusion 400, Chemyx, Stafford, TX).

Enzyme assay reagents were pumped through the orthogonal inlet of the tee at 50 nL/min using another syringe pump yielding a total flow rate of 250 nL/min. The reagent inlet was a 50 µm ID fused silica tube. The hydrophilic material was important to

prevent carry-over of sample[22]. PDMS unions consisting of a ~5 mm long x 360 μm ID channel were used to connect Teflon tubings.

Glutamate assay reagents were prepared to achieve the reaction concentrations recommended by the manufacturer when added at a 1:2 reagent:sample volume ratio. These reagents were prepared as two solutions in 100 mM Tris-HCl pH 7.5, the first containing 0.3 mM Amplex Red, and the second 7.5 U/mL of horseradish peroxidase, 0.24 U/mL L-glutamate oxidase, 15 U/mL glutamate-pyruvate transaminase, and 6 mM l-alanine. These reagents were mixed at a tee fitting while being injected into plugs. The resulting plugs passed out of the third arm of the tee and into a 150 μm ID by 60 cm long Teflon tube. Fluorescence of plugs was measured in this tube 50 cm downstream of the tee as they passed through the detector. The laser-induced fluorescence detector utilized a 543 nm 1.5 mW He-Ne laser (Melles Griot, Carlsbad, CA) for excitation, a 580 nm emission filter (XF3022, Omega Optical, Brattleboro, VT), and a photomultiplier tube for detection.

Safety Considerations

Perfluorinated surfactants have been shown to cause chronic health effects. Proper care and personal protective equipment should be utilized to avoid contact with these liquids.

Results and Discussion

Backpressure and Temporal Resolution Considerations of a Sampling Probe Inlet

In selecting the vacuum and capillary dimensions, it is necessary to balance the desire to use short and narrow bore tubing to minimize dispersion with the practical

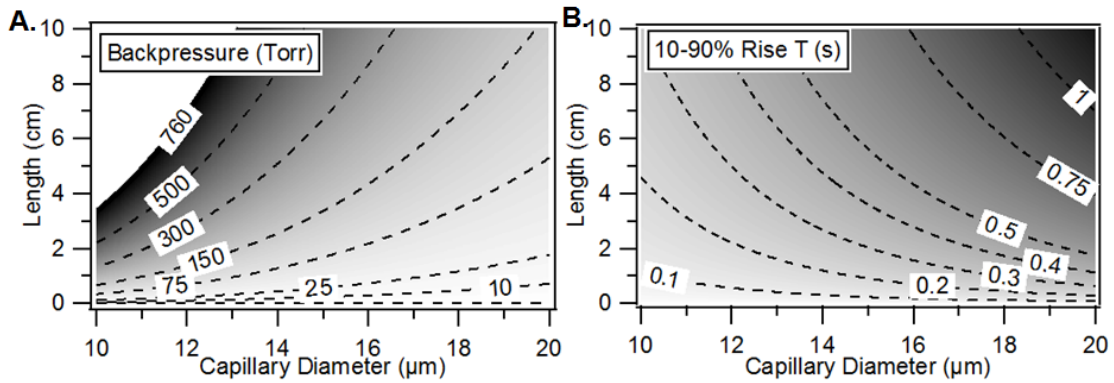

Figure 2.5. Contour plots of effects of varying probe inlet capillary lengths and inner diameter on (A) backpressures (0.89 cPa viscosity) and (B) temporal resolution (rise time) for l-glutamate (D = 7.6x10-10 m2/s) at 50 nL/min.

considerations of useful backpressures. The backpressure must be greater than the capillary pressure at the oil/aqueous interface within the tee of the probe to ensure constant flow; however, leaking and bubble formation become increasingly problematic at stronger vacuum. Using the Hagen-Poiseuille equation with 0.89 mPa·s and 5.1 mPa·s as the dynamic viscosities for the aqueous phase and perfluorodecalin, respectively, allows the desired backpressure and the aqueous/oil ratio to be selected. A 2D plot of inlet backpressures at 50 nL/min when diameter and length are varied is shown for the aqueous inlet in Figure 2.5.

While lower backpressures may provide more reliable flow, temporal resolution achieved will be worse with larger inlet dimensions due to Taylor dispersion and diffusion. The rise time required for 10% to 90% of a concentration step change was used as a metric of temporal resolution. The equation for the effective diffusion coefficient for Taylor dispersion[31, 32] can be substituted into the equation for diffusion from a finite concentration step to describe a flowing concentration step. This combined equation can be solved to find the distances from the center of the boundary for 10% and 90% of the step change after dispersing for the flush time of the capillary, and this

distance converted to rise time using the flow linear velocity. Iteratively solving this equation revealed a simpler expression:

$$Rise\ Time = \frac{3.62}{V}\sqrt{\left(1 + \frac{r^2V^2}{48D^2}\right)Dt} \quad (1)$$

where r is capillary radius, V is average flow velocity, D is diffusion coefficient, and t is flush time of the capillary. This equation for 10 to 90% rise time can be plotted for a fixed flow rate as shown in Figure 2.5B. Juxtaposing this with a plot of backpressure (Figure 2.5A) can visually allow considerations of the consequences of inlet dimensions at a fixed flow rate.

In this work, we used a 1 cm, 10 μm ID probe inlet to achieve sub-second resolution because it yielded 145 Torr backpressure and 0.15 s temporal resolution (for resorufin, D=4.6x10^{-10} m^2/s) at 32 nL/min. For *in vivo* sampling, a 10 cm length of 20 μm ID capillary was chosen as it provides not only a long probe length to work with, but a 142 Torr backpressure and 1.2 s resolution (for glutamate) at 50 nL/min, much faster than the 7 s plugs generated. Approximately 150 Torr was found to be small enough backpressure that air leaks in both probes were minimal.

Probe Design

The fluidics for *in vivo* sampling by push-pull perfusion and collecting fractions as plugs are illustrated in Figure 2.1A. In this system, a syringe pump provides push flow and vacuum pulls both sample from the probe and oil from a reservoir through a tee and into a collection tube. Based upon considerations of flow resistance and temporal resolution, capillaries with 20 μm ID by 10 cm length and 40 μm ID by 20 cm length were selected for the aqueous phase (sampling) capillary and oil inlet capillary, respectively. The collection tubing was 150 μm ID Teflon for *in vivo* studies. This ID

tubing is compatible with previously published methods of reagent addition which is necessary for assays[22, 24]. Using this system, regularly shaped plugs were generated as illustrated in Figures 1B and 1C. By measuring the width and frequency of plugs generated, we determined the flow rate through the sampling capillary to be 48 ± 8 nL/min (n = 5 different probe and tee systems), which is within the desirable flow rates for low-flow push-pull perfusion[11], with 610 mm Hg absolute pressure applied. This vacuum was small enough that failure due to air leaks was eliminated. The flow rate in the collection tubing was 46 ± 5 % aqueous (n = 5) so that the oil spacers and sample plugs were similar widths. Sample plugs were measured to be 5.9 ± 1.2 nL using different probes (n = 5) corresponding to 7 s plugs of 330 μm length.

Spatial resolution is inherently better than microdialysis as the active sampling area is based on the spacing of the two capillary lumen between which the flow occurs. If the active sampling area is assumed equal to the tip surface area of these two capillaries, the sampling region is then approximately 90 μm by 180 μm, an area of about 0.016 mm^2. This area is approximately 80-fold less than the surface (i.e., sampling) area of a relatively small 2 mm long by 200 μm diameter microdialysis probe.

Temporal Resolution Characterization

Temporal resolution in a plug-based system can be defined as $t_{res} \approx \frac{\phi}{f}$ where is the number of plugs required to observe a change (from 10 to 90% of a concentration step), and f is the plug frequency (Hz)[16]. As shown in Figure 2.6A, a glutamate step change could be observed with just 1 plug within 150 μm ID Teflon collection tubing for 7 s resolution. Reducing the collection tubing ID to match that of the tee (100 μm) allows smaller, more frequent plugs, occurring at 1.7 ± 0.3 s (n = 3). Step changes of

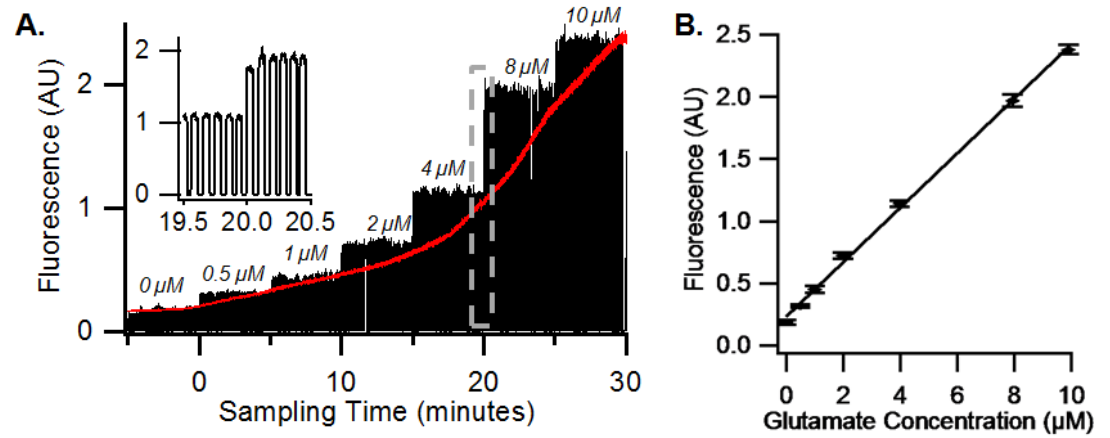

Figure 2.6. Calibration curve of recovered L-glutamate concentrations. A stirred vial was sampled without push flow, and was spiked at 5 minute intervals from 0 to 10 μM L-glutamate. Resulting plugs were analyzed using the system shown in Figure 2.4. (A) Recording of fluorescence of plugs for sampled step changes in L-glutamate concentration (black line). A comparable experiment without segmented flow revealed the loss of temporal associated with continuous flow (red line). (B) Calibration curve resulting from sampling experiments. Each point is the average of ~56 samples with 1 standard deviation as the error bar.

resorufin measured directly by laser induced fluorescence could be resolved within two plugs for 3.4 s resolution. Finite element analysis (not shown) suggested that this resolution was limited by the dead volume of the tee.

To test the limits of temporal resolution by push-pull perfusion with segmented flow, a PVDF tee with lowered internal volume was fabricated. As shown in figure 2.2A, this tee allowed the probe capillary outlet to be placed immediately adjacent to the plug storage tubing. A 10 μm ID, 1 cm long sampling capillary was used. A 50 μm bore Teflon storage tubing allowed faster plugs to be stably generated (0.2 s intervals, 0.1 nL volume, n = 3) for a 30 nL/min flow rate. Step changes of resorufin were observed within one plug for a 0.2 s rise time (as shown in Figure 2.2B). These results show that sub-second temporal resolution is possible by this method of sampling. For practical analysis, reagent addition tees for the lower volume plugs would need to be developed.

High Throughput Determination of L-Glutamate in Nanoliter Sample Plugs

This *in vivo* sampling probe generates 500 plugs of 5.9 nL volume in 1 h. Therefore, the analytical procedure used must have sufficient throughput and sensitivity to analyze the fractions. For this work, we chose a fluorescence enzyme assay for L-glutamate. The reaction scheme of the assay used is:

$$\text{L-glutamate} + O_2 \xrightarrow{\text{L-Glutamate Oxidase}} \alpha\text{-ketoglutarate} + H_2O_2$$

$$H_2O_2 + \text{Amplex Red} \xrightarrow{\text{Horseradish Peroxidase}} O_2 + \text{resorufin}$$

$$\alpha\text{-ketoglutarate} + \text{L-alanine} \xrightarrow{\text{Glutamate-Pyruvate Transaminase}} \text{L-glutamate} + \text{pyruvate}$$

where resorufin is the detected fluorescent product. This assay is attractive as it incorporates an enzyme (glutamate-pyruvate transaminase) to regenerate L-glutamate and amplify signal. Reaction time (35 minutes) was chosen based on manufacturer-recommended times and was verified experimentally to provide adequate sensitivity to observe sub-micromolar concentration changes (see Figure 2.6B).

To perform the assay on plugs, the fluidic system illustrated in Figure 2.4 was used. Reagents were reproducibly added to plugs with little cross-contamination by pumping them through a hydrophilic capillary that intersects the plug flow path in a hydrophobic tee similar to that described before[22, 24]. Previous work for reagent addition to pre-formed plugs has used tees fabricated in PDMS; however, because perfluorinated oils have low energy of interaction with PDMS, the surface had to be modified to prevent aqueous plugs from coalescing and splitting[33]. We found that although such modifications were suitable for *in vitro* studies, they were not sufficiently stable when exposed to samples collected *in vivo*. Therefore, we developed a reagent-addition tee

using 150 μm ID Teflon tubing as shown in Figure 2.4. Surface stability of this Teflon tee was sufficient to allow it to be reused for many experiments.

Using this tee, approximately 3 nL of reagent was added to each of the plug samples as they passed the tee junction. The resulting fluorescence was detected ~50 cm downstream, corresponding to a 35 min reaction time. At the flow rates used, samples were assayed at ~4 s intervals (15 samples/min) after the initial 35 min of incubation. Up to 500 sample and standard plugs were analyzed in one 75 min session demonstrating the stability of this high throughput system. A fluorescence trace during calibration of the system is shown in Figure 2.6A. For calibration, L-glutamate was spiked into a test solution in steps from 0 to 10 μM. The fluorescence changes are linear with concentration as shown in Figure 2.6B. The step changes were detected across 1-2 plugs, indicating that temporal resolution was preserved despite the long incubation time.

The system provided a convenient and automated way to manipulate and analyze the 5.9 nL plugs collected from the probe while maintaining temporal resolution and providing good throughput. Alternatives to the segmented flow approach would be to collect individual fractions into a multi-well plate or similar device; however collecting 5.9 nL fractions in a multi-well plate at high temporal resolution, storing them, and adding appropriate reagent amounts would be challenging. Another alternative would be to operate a continuous flow assay; however, this would greatly compromise temporal resolution. A direct comparison of continuous flow and segmented flow during calibration is shown in Figure 2.6A. Due to dispersion caused by flow and diffusion during transfer within the storage tubing (100 μm ID), 5 minute concentration steps produced a continuous increase in detected signal instead of the sharp steps observed

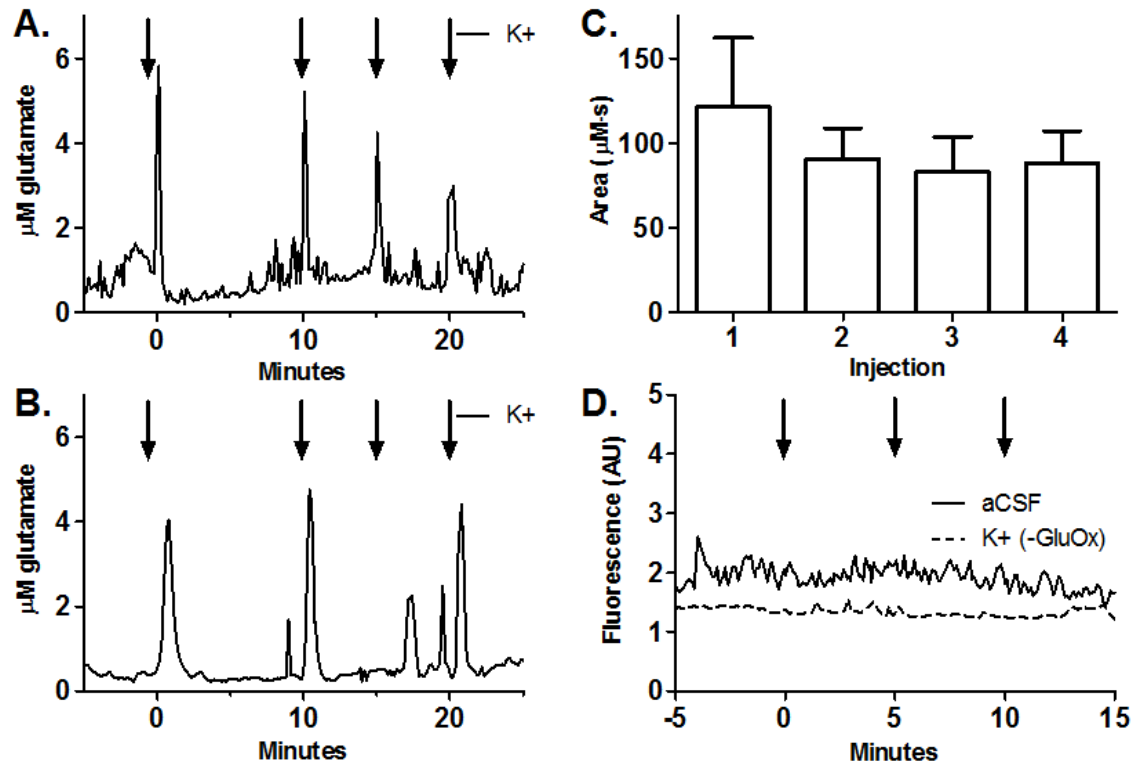

Figure 2.7. Segmented flow-coupled low-flow push-pull sampling of neurotransmitters in the rat striatum. (A) Measured striatal L-glutamate, with 100 nL 70 mM K^+ aCSF injected at times indicated by the arrows. (B) Same as A, but where brief probe occlusion occurred near third injection. (C) Mean evoked peak area of repeat injections in 5 rats, (4 rats for injection 4) with SEM. (D) Control injections of aCSF (solid), and 70 mM K^+ aCSF (dashes) analyzed without glutamate oxidase (arrows indicate approximate times).

with segmented flow.

In Vivo Monitoring of L-glutamate

We used this method to measure L-glutamate in the striatum of anesthetized rats as a demonstration of the potential for in vivo monitoring. Average basal L-glutamate concentration was 0.9 ± 0.2 μM (n = 8). For comparison, we measured 1 uL perfusate fractions using a capillary electrophoresis (CE) system described previously[34] and found basal glutamate to be 1.4 ± 0.1 μM (n = 3). We attribute this difference to ascorbic acid, which decreased the enzyme assay sensitivity at in vivo concentrations (not shown). The in vitro recovery of our probe was measured to be 57 ± 15 % (n = 3) by sampling

resorufin with and without "push" flow (2 μM in aCSF at 37°C). Correcting the CE-measured basal concentration for this recovery gives 2.5 ± 0.2 μM L-glutamate, which agrees with previously reported values of 2.0 ± 0.7, 1.9 ± 0.6, and 2.3 ± 1.2 μM for low-flow push-pull perfusion measurements of L-glutamate[11, 13, 14].

To demonstrate monitoring of rapid concentration changes, we microinjected 100 nL of 70 mM K^+ to evoke brief pulses of L-glutamate efflux. As shown by the example traces in Figures 2.7A and 2.7B, such injections resulted in transient increases in L-glutamate concentration recorded by measuring the fluorescence of plugs with reagent added. Average concentration maxima for the first microinjection was 5.6 ± 2.0 μM (n = 6) and 4.0 ± 0.9 μM for subsequent injections in the same animal (n = 6 rats, 2-3 injections each) spaced 5 or 10 min apart, an overall average of 4.5 ± 1.1 μM (n = 6). For a measure of evoked L-glutamate collected by the probe, area under the curve was calculated for each microinjection. Average peak area for the first stimulation was 121 ± 41 μM·s (n = 6), and 92 ± 16 μM·s for subsequent peaks as shown in Figure 2.7C (n = 6 rats, 2-3 injections each), an overall average of 102 ± 23 μM·s (n = 6). The average release of L-glutamate from the first microinjection was not significantly higher than for subsequent by either metric (T-test, $p > 0.05$).

To illustrate that the responses were not an artifact of the microinjection, we repeated the microinjections with normal aCSF and observed no response as shown in Figure 2.7D (solid line). If glutamate oxidase was omitted from the enzyme mixture, no response to potassium microinjections was observed, indicating transients are changes of glutamate and not hydrogen peroxide (Figure 2.7D, dashed line). These results are comparable to the 5.7 μM maxima observed in previous work with L-glutamate

microelectrodes where 100 nL of 70 mM high-K^+ aCSF was microinjected into the striatum[29].

As shown in Figure 2.7A, the rise to maximal response for high-K+ aCSF stimulation could be observed within 1 to 2 plugs. Achieving a 1 plug rise for all stimulations would require timing microinjections to be in phase with plug formation. In these preliminary experiments, the average number of plugs required was 2.8 ± 0.3 corresponding to a rise time of 22 ± 2 s (n = 21 injections in 6 rats). Some *in vivo* experiments experienced temporal resolution loss due to plugs coalescing during analysis as shown in Figure 2.7B (2-3 plugs required for rise time). A syringe driver was used for microinjections, at the disadvantage of requiring at least 6 s to infuse the full volume. A gas pressure microinjection system has allowed 1.6 s rise times to be observed in a comparable microelectrode study[29].

This temporal resolution is comparable to the "state-of-the-art" in microdialysis temporal resolution, while sampling from at least an 80-fold smaller area of the brain. The *in vitro* experiments shows temporal resolution that approaches what is possible with "chemistrode" sampling[16]. In the chemistrode, plugs are preformed and then passed through the sampling region. The present work shows that with relatively low dispersion in the sampling channel, 200 ms resolution is possible which is comparable to 50 ms achieved for the "chemistrode". The push-pull system achieves this resolution at much lower flow rates relative to the "chemistrode", which may be advantageous in sampling delicate tissues that might be disrupted by shear forces, and without concern of contaminating the sample with oil.

Segmented-flow coupled to push-pull sampling may also be compared to biosensors for in vivo monitoring. The segmented-flow method provides temporal and spatial resolution that approaches that of the best sensors. Glutamate enzyme sensors with 50 μm by 150 μm dimensions[35], compared to 90 x 180 μm capillary tips used here for sampling, and 0.8 s temporal resolution compared to 7 s here have been reported[29]. Aside from these issues, sensors presently provide advantages of ease of use (e.g. commercial products) and real time monitoring. In contrast, the sampling method should provide better opportunities for monitoring different compounds and multiple compounds simultaneously. In short, this approach to sampling closes the gap in spatial and temporal resolution performance between sampling and sensor methods, but each approach to *in vivo* monitoring retains distinct advantages.

Future Directions and Potential

A number of improvements and other applications seem feasible based on these initial results. This work used an enzyme assay to monitor L-glutamate in 7 s plugs. Development of a smaller reagent addition tee will allow assays to be performed on 200 ms plugs collected from push-pull sampling for detecting more rapid concentration changes. Other analytes could be targeted by using different enzyme systems. The resulting samples are also compatible with a variety of other plug manipulation and analysis techniques such as the "SlipChip" for handling arrays of nanoliter samples[36], immunoassays[25], capillary electrophoresis[15, 26, 37], electrochemical detection[38, 39], and mass spectrometry[27, 28]. While *in vivo* neurotransmitter sampling was the goal of the work described here, segmented flow-coupled low-flow push-pull or direct sampling is

adaptable to other applications such as spatially resolved sampling of secretions from tissues *in vitro* (e.g. brain slices, islets of Langerhans, or cultured cells).

In the course of these experiments, we observed several difficulties that will need to be addressed for future development. During the sampling procedure, 23% of probes were found to clog, a concession for the benefit of improved recovery granted by having the probe inlet directly in contact with the tissue. Figure 2.7B shows an experiment where clogging occurred briefly during the third microinjection resulting in a delayed appearance of the transient. Future work will investigate whether different probe designs are less susceptible to clogging. Another practical issue to address is materials and connections. Teflon tubing as the basis of assay fluidics proved to be robust as reagent addition tees could be used for many experiments. However, care in making connections between Teflon tubings was necessary to avoid trapping dust and debris, which could cause plug coalescence and compromise temporal resolution. Additionally, PDMS unions used exhibited a poor tolerance for high backpressure. Future work will focus on development of more reliable unions for analysis. Despite these obstacles, 74% of the sample tubes collected were successfully analyzed (n = 34 experiments). While this enzyme assay provided facile plug analysis and allowed visualization of glutamate transients, its non-specificity may be problematic if quantitative measurements are desired due to matrix interferences including ascorbic acid and hydrogen peroxide.

Conclusions

A method for high temporal resolution sampling using segmented flow coupled to a push-pull sampling probe was demonstrated with an 80-fold spatial resolution improvement over microdialysis. The method provides spatiotemporal resolution for

neurotransmitter measurement that approaches what has been achieved with electrochemical sensors, but as a sampling method it is adaptable to other segmented flow-based analyses to provide good versatility in chemical monitoring. The simplicity of the probes, the small dimensions of inlets, and high temporal resolution while maintaining picoliter to nanoliter volumes provides new opportunities for chemical monitoring by sampling.

References

(1) Robinson, D. L.; Hermans, A.; Seipel, A. T.; Wightman, R. M. *Chem. Rev.* **2008**, *108*, 2554-2584.
(2) Watson, C. J.; Venton, B. J.; Kennedy, R. T. *Anal. Chem.* **2006**, *78*, 1391-1399.
(3) Weiss, D. J.; Lunte, C. E.; Lunte, S. M. *TrAC, Trends Anal. Chem.* **2000**, *19*, 606-616.
(4) Venton, B. J.; Robinson, T. E.; Kennedy, R. T. *J. Neurochem.* **2006**, *96*, 236-246.
(5) Huynh, B. H.; Fogarty, B. A.; Martin, R. S.; Lunte, S. M. *Anal. Chem.* **2004**, *76*, 6440-6447.
(6) Lada, M. W.; Vickroy, T. W.; Kennedy, R. T. *Anal. Chem.* **1997**, *69*, 4560-4565.
(7) Parrot, S.; Sauvinet, V.; Riban, V.; Depaulis, A.; Renaud, B.; Denoroy, L. *J. Neurosci. Methods* **2004**, *140*, 29-38.
(8) Tucci, S.; Rada, P.; Sepúlveda, M. J.; Hernandez, L. *J. Chromatogr. B* **1997**, *694*, 343-349.
(9) Gaddum, J. H. *J. Physiol. (Lond.)* **1961**, *155*, 1P-2P.
(10) Myers, R. D.; Adell, A.; Lankford, M. F. *Neurosci. Biobehav. Rev.* **1998**, *22*, 371-387.
(11) Kottegoda, S.; Shaik, I.; Shippy, S. A. *J. Neurosci. Methods* **2002**, *121*, 93-101.
(12) Patterson, E. E., II; Pritchett, J. S.; Shippy, S. A. *Analyst* **2009**, *134*, 401-406.
(13) Cellar, N. A.; Kennedy, R. T. *Lab Chip* **2006**, *6*, 1205-1212.
(14) Cellar, N. A.; Burns, S. T.; Meiners, J. C.; Chen, H.; Kennedy, R. T. *Anal. Chem.* **2005**, *77*, 7067-7073.
(15) Wang, M.; Slaney, T.; Mabrouk, O.; Kennedy, R. T. *J. Neurosci. Methods* **2010**, *190*, 39-48.
(16) Chen, D.; Du, W.; Liu, Y.; Liu, W.; Kuznetsov, A.; Mendez, F. E.; Philipson, L. H.; Ismagilov, R. F. *Proc. Natl. Acad. Sci. USA* **2008**, *105*, 16843-16848.
(17) Wang, M.; Roman, G. T.; Schultz, K.; Jennings, C.; Kennedy, R. T. *Anal. Chem.* **2008**, *80*, 5607-5615.
(18) Song, H.; Tice, J. D.; Ismagilov, R. F. *Angew. Chem. Int. Ed.* **2003**, *42*, 768-772.
(19) Adamson, D. N.; Mustafi, D.; Zhang, J. X. J.; Zheng, B.; Ismagilov, R. F. *Lab Chip* **2006**, *6*, 1178-1186.

(20) Nie, J.; Kennedy, R. T. *Anal. Chem.* **2010**, *82*, 7852-7856.
(21) Zheng, B.; Tice, J. D.; Roach, L. S.; Ismagilov, R. F. *Angew. Chem. Int. Ed.* **2004**, *43*, 2508-2511.
(22) Song, H.; Li, H.-W.; Munson, M. S.; Van Ha, T. G.; Ismagilov, R. F. *Anal. Chem.* **2006**, *78*, 4839-4849.
(23) Song, H.; Chen, D. L.; Ismagilov, R. F. *Angew. Chem. Int. Ed.* **2006**, *45*, 7336-7356.
(24) Li, L.; Boedicker, J. Q.; Ismagilov, R. F. *Anal. Chem.* **2007**, *79*, 2756-2761.
(25) Liu, W.; Chen, D.; Du, W.; Nichols, K. P.; Ismagilov, R. F. *Anal. Chem.* **2010**, *82*, 3276-3282.
(26) Roman, G. T.; Wang, M.; Shultz, K. N.; Jennings, C.; Kennedy, R. T. *Anal. Chem.* **2008**, *80*, 8231-8238.
(27) Pei, J.; Li, Q.; Lee, M. S.; Valaskovic, G. A.; Kennedy, R. T. *Anal. Chem.* **2009**, *81*, 6558-6561.
(28) Hatakeyama, T.; Chen, D. L.; Ismagilov, R. F. *J. Am. Chem. Soc.* **2006**, *128*, 2518-2519.
(29) Day, B. K.; Pomerleau, F.; Burmeister, J. J.; Huettl, P.; Gerhardt, G. A. *J. Neurochem.* **2006**, *96*, 1626-1635.
(30) Kulagina, N. V.; Shankar, L.; Michael, A. C. *Anal. Chem.* **1999**, *71*, 5093-5100.
(31) Aris, R. *Proc. R. Soc. London, Ser. A* **1956**, *235*, 67-77.
(32) Bruus, H. *Theoretical Microfluidics*, First ed.; Oxford University Press: New York, NY, 2008.
(33) Roach, L. S.; Song, H.; Ismagilov, R. F. *Anal. Chem.* **2005**, *77*, 785-796.
(34) Bowser, M. T.; Kennedy, R. T. *Electrophoresis* **2001**, *22*, 3668-3676.
(35) Burmeister, J. J.; Pomerleau, F.; Palmer, M.; Day, B. K.; Huettl, P.; Gerhardt, G. A. *J. Neurosci. Methods* **2002**, *119*, 163-171.
(36) Du, W.; Li, L.; Nichols, K. P.; Ismagilov, R. F. *Lab Chip* **2009**, *9*, 2286-2292.
(37) Chiu, D. *Anal. Bioanal. Chem.* **2010**, *397*, 3179-3183.
(38) Han, Z.; Li, W.; Huang, Y.; Zheng, B. *Anal. Chem.* **2009**, *81*, 5840-5845.
(39) Liu, S.; Gu, Y.; Le Roux, R. B.; Matthews, S. M.; Bratton, D.; Yunus, K.; Fisher, A. C.; Huck, W. T. S. *Lab Chip* **2008**, *8*, 1937-1942.

Chapter III

Nanospray Mass Spectrometry for 7s Resolution *in Vivo* Simultaneous Monitoring of Drugs, Neurotransmitters and Metabolites

Introduction

Measuring neurotransmitters, metabolites and drugs simultaneously within the brain extracellular compartment is a powerful way to gain insight to the interactions of drugs with specific tissues. However, the brain is extremely delicate, requiring minimally invasive methods[1]. In rodents such as rats or mice, nuclei of interest may be less than 1 mm in diameter, requiring high spatial resolution. While tonic levels of neurotransmitters may vary on the min to h timescale[2, 3], sudden stimuli (such as behavioral cues or drug administration) may trigger dynamics on the s to ms timescale[4-6].

Enzyme-modified sensors have garnered much interest within the past decade given their abilities to observe rapid (~2 s resolution) chemical changes *in vivo* with high spatial resolution[7-11]. Advancements such as self-referencing designs and coatings[8, 11] compensate for some of the background interferents such as ascorbic acid. However, caution should be used in interpretation of any basal or absolute concentration measurements as effects of oxygen, ascorbate, glutathione, and other variable extracellular contents may not be compensated for by external calibrations[11]. Sensors are

also typically limited to one analyte per electrode, and developing sensors for new analytes including drugs is difficult.

Sampling methods such as microdialysis and low-flow push-pull allow multianalyte analyses to be performed without the selectivity concerns of electrodes. Microdialysis probes allow as rapid as 2 s temporal resolution[12], however their membranes are typically 1-4 mm long, precluding high spatial resolution. Low-flow push-pull perfusion probes have spatial resolution defined by their capillary inlets (~200 μm),[13-15] however the flow rates used (50 nL/min) present a significant analytical challenge both in sample handling and analytical sensitivity. Taylor dispersion must be minimized to maintain temporal resolution, often precluding use of continuous flow systems[16].

Segmented flow is a viable way to achieve 7 s temporal resolution with offline analysis of *in vivo* samples collected using low-flow push-pull (see Chapter II). Fractions collected are amenable to a variety of assays, and we both *in vitro* and *in vivo* multianalyte analyses have been conducted using a glass microchip CE system (see Chapter V)[17]. This device utilized fluorescence derivatization of analytes and a hydrophilic extraction bridge in a hydrophobic channel of a microchip to separate the aqueous and oil phases prior to separation. While a rapid and highly-sensitive technique, it nevertheless requires some microfabrication and a custom laser-induced fluorescence detector.

Mass spectrometry (MS) is an attractive tool for push-pull sample analysis given its sensitivity, multianalyte capability, and commercial availability. Multiple reaction monitoring (MRM) allows selective and sensitive measurement of analytes, and

isotopically labeled internal standards can ensure quantitative results. Using MS, microdialysate has been collected as oil-segmented fractions and analyzed online or offline to provide rapid measurements of acetylcholine (ACh), choline (Ch), and neostigmine, a cholinesterase inhibitor[18]. This method analyzed 160 nL plugs at 4 s/plug with a detection limit of 800 amol/sample. While this sensitivity greatly exceeds that of other detectors, it would limit temporal resolution of low-flow push-pull to approximately 3 minutes.

Nanospray ionization has the potential to provide high temporal resolution monitoring with low-flow push-pull. By using nL/min flow rates, much greater ionization efficiency is achieved compared to "conventional" ESI[19]. Commercially available metalized nanospray tips allow direct measurement of plug samples without the requirement of desegmentation. This method is also salt-tolerant, allowing measurement in 100's of mM ionic strengths as found within the brain[19]. To our knowledge, nanospray has not previously been used for direct analysis of brain perfusate.

In this work, we use nanospray for direct, label-free analysis of neurotransmitters collected from *in vivo* by low-flow push-pull perfusion sampling. We simultaneously measure 3 analytes and an internal standard with a 5 nM detection limit for ACh. This allows visualization of up to 7 s concentration dynamics limited by plug frequency, and permits the potential of much faster temporal resolution.

Materials and Methods

Reagents and Materials

Unless otherwise specified, all reagents were purchased from Fisher Scientific (Pittsburgh, PA) and were Certified ACS grade or better. Perfluorodecalin was

purchased from Acros (Fair Lawn, NJ). 1H,1H,2H,2H-perfluoro-1-octanol (PFO), acetylcholine chloride (ACh), choline chloride (Ch), and neostigmine bromide were purchased from Sigma-Aldrich (St. Louis, MO). Acetylcholine-d_4 was purchased from CDN Isotopes (Pointe-Claire, Quebec, CA). Cyanoacrylate glue was purchased from K & R International (E-Z Bond, Laguna Niguel, CA). Acetonitrile and water used were HPLC-grade. Artificial cerebrospinal fluid (aCSF) consisted of 145 mM NaCl, 2.68 mM KCl, 1.01 mM $MgSO_4$, 1.22 mM $CaCl_2$, 1.55 mM Na_2HPO_4, and 0.45 mM NaH_2PO_4, pH 7.4 [20].

Reagent Addition Tee

A reagent addition tee was fabricated from Teflon tubing and capillary encased in polyvinylidine difluoride sheet (PVDF). PVDF was purchased from AmazonSupply (1/32" thickness, Seattle, WA). Teflon high-purity PFA tubing (150 μm bore, 360 μm outer diameter) was purchased from IDEX Health and Science (Oak Harbor, WA). Capillaries were purchased from Polymicro (Phoenix, AZ).

A detailed fabrication protocol of the reagent addition tee is described elsewhere[14]. Briefly, a 190 μm outer diameter capillary was held perpendicular to the Teflon tubing on a glass support and PVDF was melted around it at 190°C in a convection oven. The capillary was then removed and a 200 μm drill bit (Kyocera, Costa Mesa, CA) inserted to drill through the wall of the Teflon. A 50 μm bore, 190 μm outer diameter capillary was then inserted until its tip was flush with the inner wall of the Teflon tubing, and was sealed and held in place using Sticky Wax (Kerr, Orange, CA).

Segmented flow compatible unions were used to connect to this tee. These unions were fabricated from ~4 mm of 1/16" outer diameter (OD), 0.01" inner diameter (ID)

polytetrafluoroethylene (PTFE) tubing (Grace, Albany, OR). A 360 μm OD capillary tubing was used to carefully ream the Teflon tubing ~5 times before use. For plug transfer, the 360 μm OD Teflon PFA tubings were cut uniformly and inserted until ends contacted within the union.

Push-Pull Probe Fabrication

Polyimide-encased push-pull probes were fabricated, as described in detail in Appendix A. Briefly, two lengths of 20 μm ID, 90 μm OD fused silica capillary were inserted into 3 cm of 180 μm ID, 220 μm OD polyimide tubing (AmazonSupply). The space between the capillaries and polyimide was backfilled with thixotropic epoxy (353ND-T, Epotek, Billerica, MA) and the epoxy was cured at 50°C for 30 minutes and 80°C until fully cured (~30 minutes). The polyimide and capillaries were cut flush with a razor blade and two 2 cm capillary adapters (150 μm ID, 360 μm OD) were glued with cyanoacrylate to the capillary ends to yield a length of 10 cm for the 20 μm ID, 90 μm OD capillaries. The polyimide-encased tip of the probe was polished smooth with 1500 grain sandpaper placed on a 1 Hz rotating disk (BV-10, Sutter, Novato, CA). To prevent occlusion while polishing, probe capillaries were backflushed at 500 nL/min with water. A 2 cm length of 250 μm ID, 360 μm OD capillary was coned on one end using the rotating sandpaper disk. The polyimide encased probe was then inserted through this capillary with the tip of the probe protruding 1 mm past the coned capillary tip, and was fastened with cyanoacrylate.

A microinjector was fabricated by gluing a 2 cm long 150 μm ID, 360 μm OD capillary adapter over a 20 μm ID, 90 μm OD capillary with a final length of 4.8 cm as described previously[18]. The microinjector was glued with cyanoacrylate to the side of the

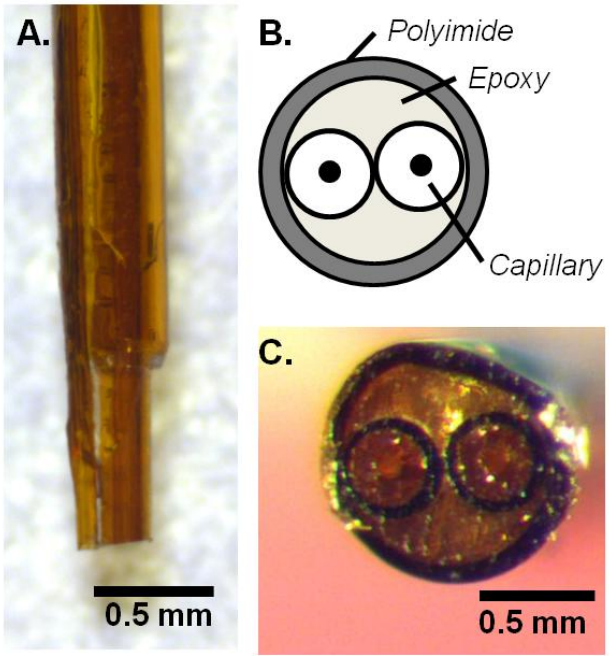

Figure 3.1. Miniaturized low-flow push-pull probes for neurochemical monitoring. (A) A probe (220 µm outer diameter) is placed within a 250 µm ID, 360 µm OD capillary sheath and a 90 µm OD microinjector attached with cyanoacrylate to the side. (B)The probe tip consists of 3 materials (polyimide, epoxy and fused silica capillary) polished to a flat surface. (C) Micrograph of a probe tip.

polyimide-encased probe to place the injector tip in contact and flush with the probe tip. Figure 3.1 shows a picture of an assembled probe with microinjector, as well as a polished probe tip.

Surgical Procedures

All animal use was performed according to a protocol approved by the University Committee for the Use and Care of Animals. Male Sprague-Dawley rats between 300 and 390 g were anesthetized by intraperitoneal administration of 65 mg/kg ketamine and 0.25 mg/kg dexmedetomidine. Boosters of 22 mg/kg ketamine and 0.08 mg/kg dexmedetomidine were administered as needed. Anesthetized animals were mounted in a stereotaxic frame (David Kopf, Tujunga, CA). A burr hole was drilled 1.0 mm anterior and ± 2.6 mm lateral to bregma.

Probes were fixed to a stereotaxic electrode holder (1770, David Kopf) and connected to a syringe pump. The probe microinjector was connected with a Teflon union to a 10 cm length of 200 μm ID, 360 μm OD capillary filled with either 5 μM neostigmine or aCSF. This reservoir capillary was connected to a Picospritzer (General Valve, Fairfield, NJ) set to 80 PSI.Probe capillaries were backflushed at 500 nL/min and implanted to a depth of 5.0 mm from dura. Probes were lowered slowly at ~1 mm per 20 s, and backflushing was immediately reduced to 50 nL/min at depth. Both capillaries were backflushed for 8 minutes.

Before starting pull, one of the probe inlets was connected to a 100 μm bore polyether ether ketone (PEEK) tee as described previously[14]. A second inlet of this tee contained a 20 cm capillary of 40 μm ID, 360 μm OD which connected to an oil reservoir containing a 50:1 (vol:vol) solution of PFD:PFO. The outlet of this tee contained a 20 cm length of 150 μm ID, 360 μm OD Teflon tubing. To start pull flow, the Teflon tubing was connected to 150 mm Hg of vacuum. This generated pull flow of 50 nL/min through the probe and ~1:1 aq:oil plugs. Flow rate was monitored by visual observation of plug size and frequency.

Push-pull flow was continued for 1 hour following implantation to allow basal concentrations of neurotransmitters to stabilize[14, 20]. After 1 h, a 4 s (200 nL) microinjection was performed. After 10 minutes, this injection was repeated and following another 10 minutes, the Teflon tubing "cartridge" was removed. A new tubing was then immediately started to collect additional samples.

Sample Preparation

After collection, the Teflon tubing cartridge containing plug fractions was connected to a syringe filled with oil via a 360 μm capillary union (Valco, Houston, TX). The other end of this tubing was connected to the Teflon reagent addition tee using a Teflon union. The outlet of the union was coupled to another Teflon storage tubing (150 μm ID, 360 μm OD).

A reagent containing 3 mM ethylenediamine tetraacetic acid disodium salt (EDTA) and 100 nM acetylcholine-d_4 in 1:1 (vol:vol) water:acetonitrile was added to plugs. The reagent was added at a 1:1 plug:reagent volume ratio using this tee[14, 18]. Stable addition was achieved by infusing the reagent at 600 nL/min. Plug aqueous:oil ratio was observed microscopically prior to reagent addition, and plug flow rate was set to ensure 1:1 reagent addition (typically 1200 nL/min). If sample plugs were non-uniform, they were discarded prior to reagent addition.

Mass Spectrometry Analysis

Following reagent addition, the Teflon cartridge containing the samples was again connected to an oil-filled syringe in a syringe pump. The other end of the tubing was connected with a Teflon union to a metalized nanospray tip. This tip consisted of a 75 μm ID, 360 μm OD fused silica capillary pulled to a tip inner diameter of 15 μm and coated with a conductive metal (NewObjective, Woburn, MA). Sample plugs were infused at 200 nL/min through this nanospray tip.

Samples were analyzed using a Micromass QuattroUltima triple-quadrupole (QQQ) mass spectrometer in MRM mode. MRM parameters are shown in Table 3.1. Nanospray tips were replaced as needed, at least daily. Plug intensities were measured

Mass Spectrometer - MRM Parameters				
	m/z Transition	*Dwell Time (ms)*	*Cone V*	*Collision energy (eV)*
Acetylcholine	146 → 87	40	35	15
Choline	104 → 60	40	35	15
Neostigmine	223 → 208	40	35	15
Acetylcholine-d_4	150 → 91	40	35	20

Table 3.1. Three analytes and an internal standard were simultaneously monitored in plug push-pull perfusate samples. The QQQ mass spectrometer additionally had a capillary voltage of 1.9 kV, cone gas of 150 L/h, and a source temperature of 140°C.

using Igor Pro 6.2.0.4 (WaveMetrics, Lake Oswego, OR). To analyze each MRM transition, the "Identify and measure peaks in steps" procedure of the "Unipolar Peak Areas" feature was utilized for the acetylcholine-*d4* internal standard trace. From this procedure, a list of peak center points was generated (average of peak start and end points). A 3-point boxcar average was performed on each MRM trace and the intensity of the midpoint (determined from d4-ACh) of each peak for each analyte was measured. The ratio of peak intensities to the internal standard intensity was then calculated and used for calibration.

After each animal experiment, plugs were collected for calibration. Initially plugs of aCSF were collected, then 3 solutions of aCSF containing ACh, Ch and Neostigmine standards. Three levels of calibration standards were collected for ACh, and one or three levels for Ch and Neostigmine. For example, one set of standards included 10, 50, and 100 nM ACh; 500, 250, and 50 nM Ch; and 2500, 1250 and 250 nM neostigmine, respectively. Calibration curves were generated based on ratio to internal standard intensity and were linear over the range tested.

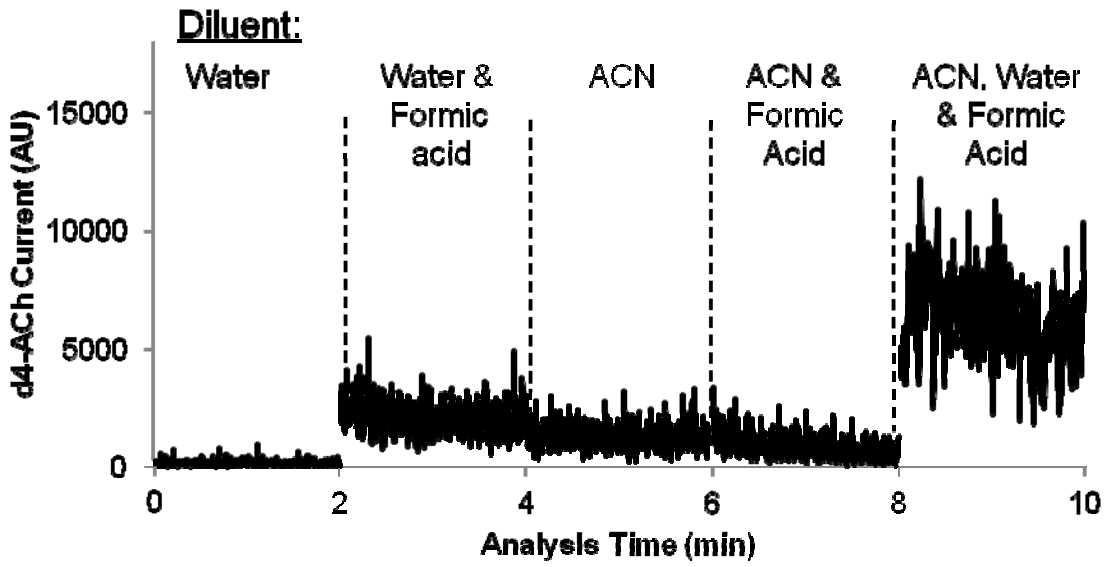

Figure 3.2. The effects of diluents (added 1:1 to 100 nM d4-ACh in aCSF) were tested on signal intensity. Diluents of water, 3% (vol) formic acid, and acetonitrile (ACN) were tested. Current of d4-ACh was greatest with 1:1 ACN:water containing 3% formic acid.

Results and Discussion

Probe and Microinjector Design

Polyimide-encased push-pull probes were utilized to minimize tissue trauma around the sampling area. The diameter of these probes was half that of needle-encased probes used previously (220 μm versus 400 μm)[14, 20, 21]. The success rate of these probes was much improved, with 91% (9 of 11) flowing without occlusion versus 78 % with needle-encased probes[14]. This success rate improvement is attributed to reduced implantation trauma by the smaller probe geometry, slower implantation rate and decreased time of backflushing at final depth.

Initial experiments tested microinjectors attached 100 μm apart from the probe tip, as previous work with *in vivo* microelectrodes has found this spacing advantageous[10].

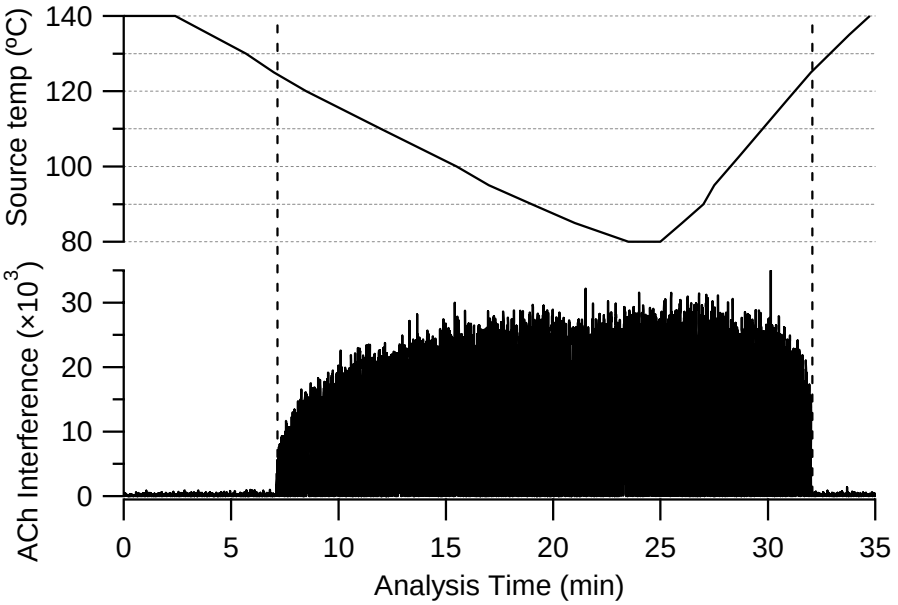

Figure 3.3. Effect of source temperature was examined on ACh interference. Plugs of aCSF containing no ACh were diluted 1:1 with a reagent of 3 mM EDTA in 50% (vol) of ACN were examined as source temperature was varied. Above 125°C, no interference was observed.

However, detection of pharmacological effects was not reliably achieved (1 in 5 probes), including failure to observe the drug. This was indicative of the drug not reaching the sampling area of the probe, and suggests that the spatial resolution of the probe was finer than the tip diameter of 220 μm. When the injector was instead attached with its tip in contact with the probe tip, neostigmine, ACh and Ch concentration transients were observed with every microinjection.

Optimization of Nanospray source parameters

Collision energy and ionization settings were previously characterized in a study using conventional electrospray ionization for ACh, Ch, Neo and d4-ACh[18]. However, a number of concerns are encountered with nanospray, including the need for stable spray throughout the experiment, risk of clogging, and potential cluster ion interferences not necessarily encountered with conventional electrospray. As tissue damage is minimal

during low-flow push-pull[15], the sample collected was debris free and clogging of the nanospray emitter tip never occurred during these experiments.

To optimize sample additives for nanospray, varying concentrations of acetonitrile (ACN), water and the presence of 3% formic acid were tested as 1:1 diluents to a 100 nM d4-ACh standard in aCSF. As shown in Figure 3.2, optimal spray was obtained with a diluent of 1:1 acetonitrile:water containing 3% formic acid.

An issue described previously with ESI of ACh is that endogenous magnesium adducts produced a high background current for the ACh MRM transition[18]. This same

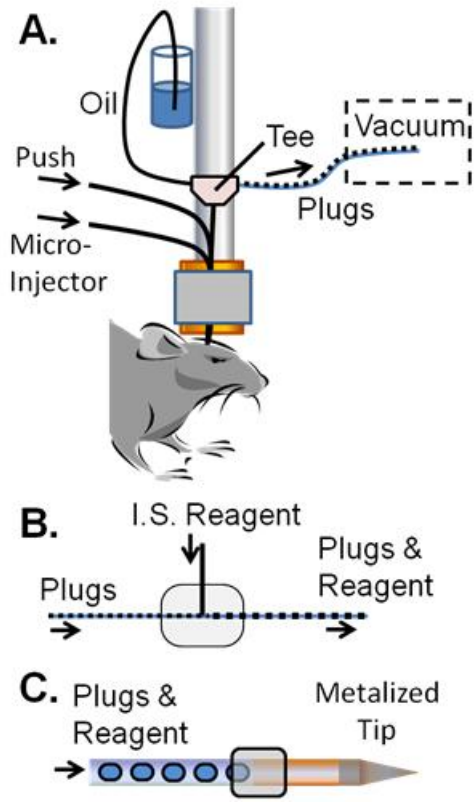

Figure 3.4. Sample collection, processing and analysis were performed in 3 steps. (A) A push-pull perfusion probe was used to fill a Teflon cartridge with up to 20 min of plugs. (B) Plugs from cartridge were infused through a reusable reagent addition tee where a reagent containing d_4-ACh internal standard, EDTA and acetonitrile was added. (C) Plugs containing reagent were infused into a metalized nanospray tip at the MS inlet.

interference was observed with nanospray ionization (not shown). As with conventional electrospray, 3 mM EDTA added to the diluent removed this interference[18]. Though formic acid was used in preliminary optimization experiments, it was later excluded as it interfered with the action of EDTA to remove magnesium adduct interference[18]. This may be due to protonated EDTA having a lower affinity for cationic magnesium ions than the anionic disodium-EDTA salt. Background interference was found to depend on the source temperature of the mass spectrometer. As shown in Figure 3.3, interference was observed when the source temperature was lower than 125°C. No interferences were observed with a source temperature of 140°C and EDTA added to the plugs.

Analysis of Acetylcholine, Choline and Neostigmine

A schematic of the experimental design is shown in Figure 3.4. A commercially available capillary microfluidic tee was used to generate plugs (Figure 3.4A). The small internal geometry (100 μm bore) and gas impermeability make this tee well-suited for 7 s resolution fraction collection by vacuum[14]. By balancing flow resistance of the probe inlet and oil inlet, fractions were collected at a 1:1 aqueous:oil ratio.

A Teflon reagent addition tee was used for adding an internal standard-containing diluent to plugs (Figure 3.4B). As described above, reagent addition to plugs is necessary to improve ion signal and remove interference. The reagent consisted of 50% (vol.) acetonitrile, therefore its low interfacial tension and high viscosity presented a challenge due to plug instability during addition. Comparable flow rates to those used previously for reagent addition (200 nL/min plugs, 100 nL/min reagent) resulted in droplet instability and coalescence within the reagent addition tee. This coalescence was greatly reduced at higher flow rates (600 nL/min reagent, ~1200 nL/min plugs), allowing stable

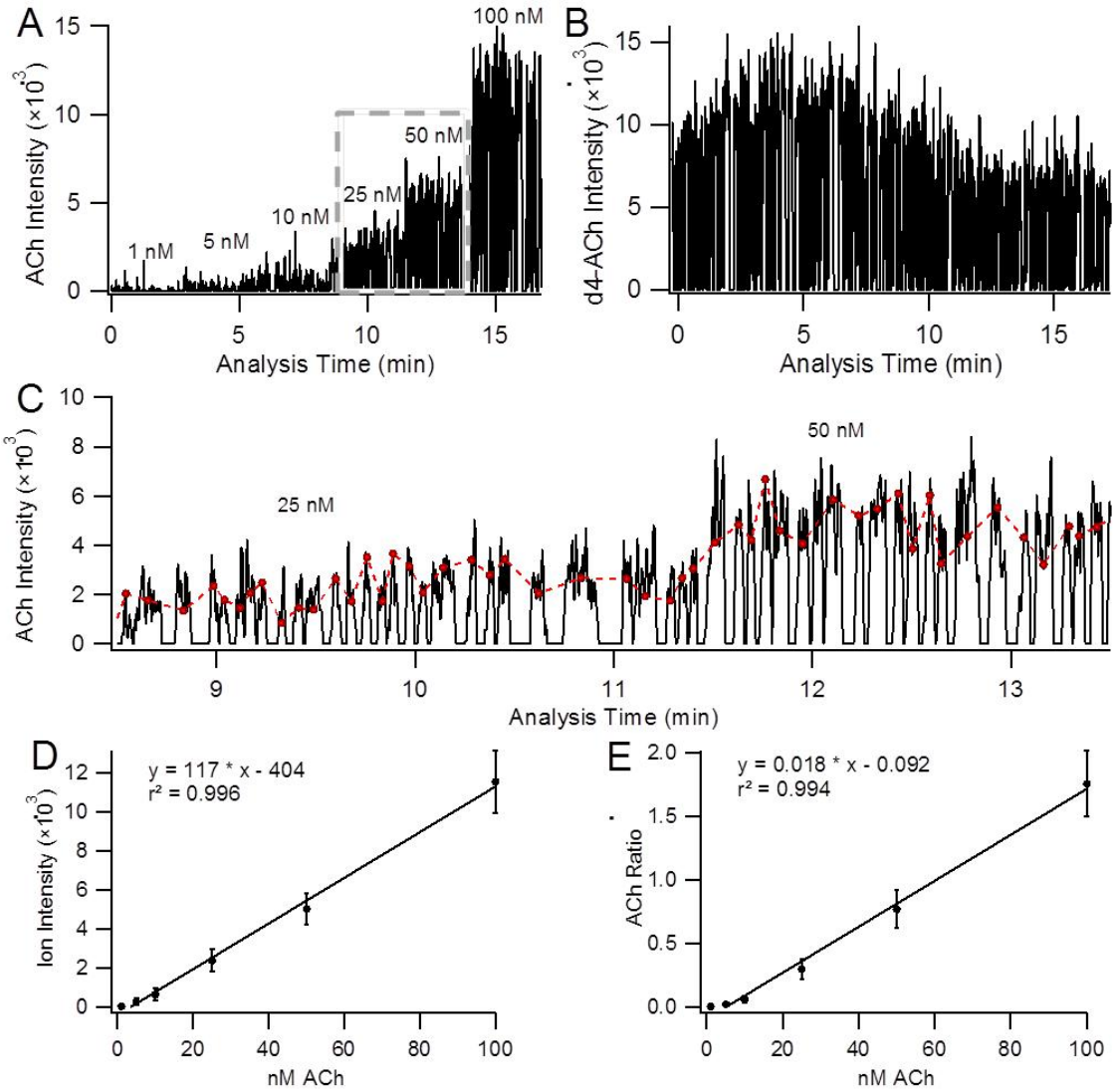

Figure 3.5. (A) Droplet signal trace for a calibration curve of ACh. (B) d_4-ACh internal standard revealed a decrease in ion intensity during the calibration curve. (C) A magnified trace of ACh ion intensity, showing measured peak heights (red). (D) Calibration curve for ACh. (E) Normalized ACh calibration using d4-ACh peak heights.

reagent addition. An advantage of this tee is that it is reusable and durable, minimizing time required for microfabrication and assembly. Only one reagent addition tee was needed for the course of these experiments. A benefit of the plug format is that a second Teflon cartridge tube could be used to transfer plugs following reagent addition without any loss of temporal resolution.

Segmented flow analysis by nanospray provided sensitive and stable analysis of sample plugs[22, 23]. As transfer of samples from Teflon tubing to nanospray capillary requires a simple Teflon union, no coalescence was observed at this connection. Some coalescence did occur spontaneously downstream of the reagent addition tee, most likely due to the acetonitrile reducing interfacial tension, as shown in Figure 3.5C. Coalescence did not affect the measured plug peak height, and therefore height was used as the metric of concentration. A flow rate of 200 nL/min was chosen because it provided stable signal and approximately 15 points per plug maxima (5 scans/s). Plug volumes during analysis were measured by peak width of the internal standard trace and was 14 ± 7 nL (n = 3 animals), which corresponded to an average of 7 nL (8 s resolution) per sampled plug. Of 1031 plugs analyzed from 3 rats, 49% were 11.7 nL or smaller (7 s resolution), 62% were 13 nL or smaller (8 s resolution), and 75% of plugs were 17 nL or smaller (10 s resolution). The greater distribution of sizes of plugs than observed in Chapter II reflects the weaker plug interfacial tension due to an organic reagent additive, and the higher ratio of reagent to sample. The time point of each plug was measured from the center point of the plug during analysis, therefore a coalescenced plug would result in a momentarily slower temporal resolution without affecting the fidelity of subsequent plugs.

Sensitivity and response for each compound was characterized *in vitro*. Limits of detection were calculated from signal to noise for blank plugs. As instrumental noise varied slightly between experiments, calculated limits of detection varied from 2 to 8 nM (typically 5 nM) for ACh, 30 to 90 nM (typically 50 nM) for Ch, and 3 to 8 nM (typically 5 nM) for neostigmine. This corresponds to a 35 amol detection limit of ACh per 7 nL sample.

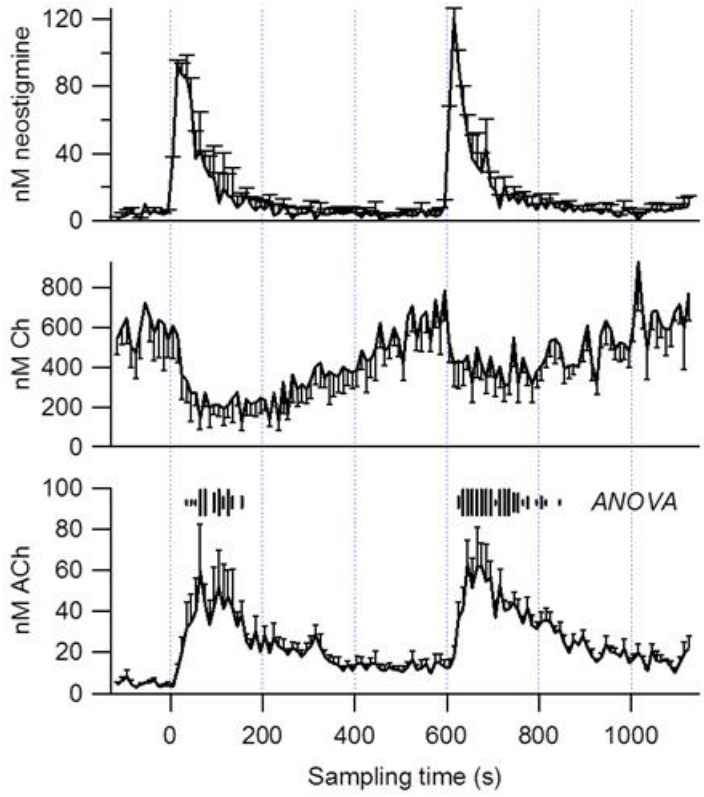

Figure 3.6. High temporal and spatial resolution measurements of neostigmine, ACh and Ch within the anesthetized brain (n = 5 cartridges from 3 rats). Neostigmine was microinjected at t = 0 and 600 s (200 nL in 4 s). Markers indicate significance of ACh increase at each point relative to basal, corresponding (from smallest to largest) to, $p <$ 0.05, 0.01, 0.001, 0.0001 (two-way ANOVA).

ACh ion intensity response was linear with respect to concentration over the physiological range of interest as shown in Figure 3.5D. Though linearity was comparable for absolute response and relative response in Figure 3.5D and 3.5E, ratio of the ACh (also Ch and Neo) to d4-ACh was the metric of choice for determining concentrations. While using ratios did slightly increase variability of measurements (for example, relative standard deviation of 50 nM ACh plugs shown in Figure 3.5D increased from 16% to 19%), it corrected for any signal intensity differences between analysis of *in vivo* sample plugs and standard plugs. This is important as the nanospray

emitter had to be removed and replaced between cartridges of plugs analyzed. Concentrations reported in this paper were not corrected for relative recovery.

In Vivo Measurement of Neurotransmitters

Plugs of neurotransmitters were measured at least 1 h after implantation as previous studies have observed that concentrations of neurotransmitters are unstable within this time[14, 20]. Basal concentrations of ACh and Ch were 5.0 ± 1.9 nM and 490 ± 90 nM (n = 3 rats). These are in agreement with previous measurements using microdialysis, supporting the validity of this assay[24-26].

Concentration dynamics of drug, neurotransmitter and metabolite were measured simultaneously following microinjection. Following a 4 s injection of the acetylcholinesterase inhibitor neostigmine, the neostigmine concentration increased from 10 to 90% of maxima in 14 ± 3 s (n = 10 injections in 3 rats, 2 or 4 injections each). Rise time was limited by plug frequency (typically ~7 s per plug) and could be observed within 1-2 plugs. Rise time of ACh was 35 ± 4 s. ACh exhibited a slower rise time as its concentration continued to accumulate in the extracellular space during the lifetime of the neostigmine. Ch, the metabolite of ACh following acetylcholinesterase action, exhibited a concentration decrease following microinjection. The average 10-90% time to minima in 60 ± 13 s. Figure 3.6 shows averaged traces collected from 3 animals for each analyte.

Average maxima of neostigmine measured within the brain following microinjection were 120 ± 20 nM, reflecting a dilution of the 5 μM drug concentration injected. The average maxima of ACh following microinjection was 65 ± 14 nM. The average minima of Ch following microinjection were 160 ± 40 nM.

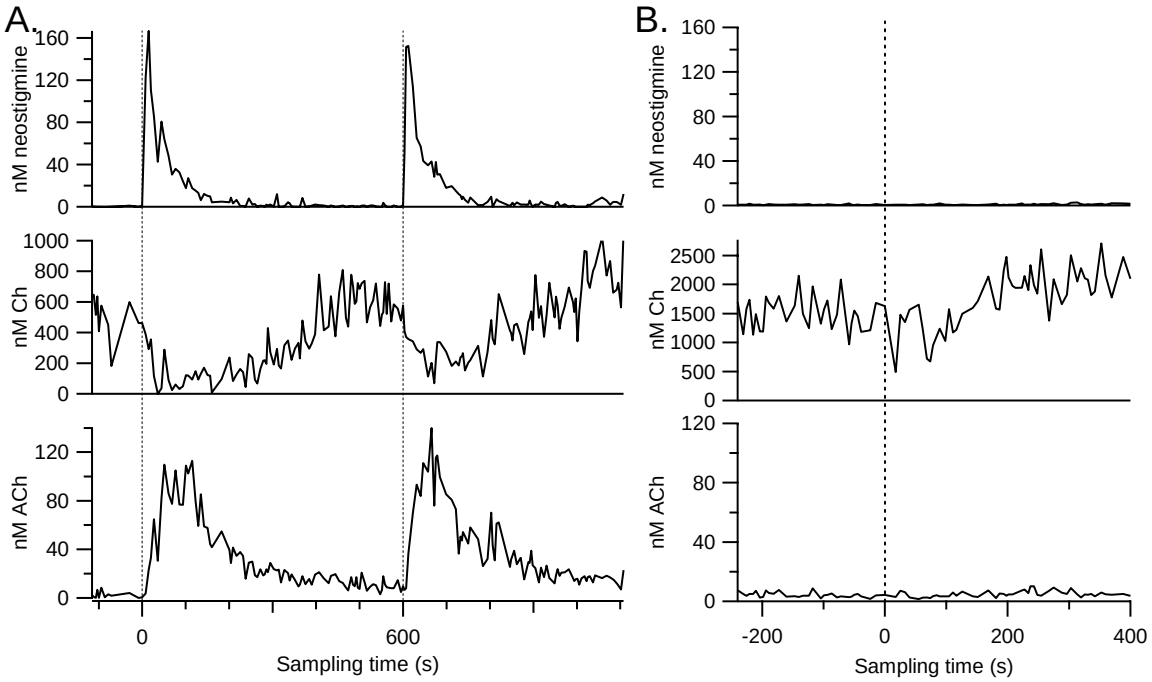

Figure 3.7. Examples of individual traces following 200 nL/4 s microinjections of (A) neostigmine and (B) aCSF.

As a control, microinjections of aCSF were infused and no increase in aCh or decrease in Ch was observed as shown in Figure 3.7B. This confirms that the decrease observed in Ch results from the action of neostigmine and not dilution of extracellular fluid at the tip of the probe. Flow effects of the infused aCSF produced momentary perturbations in basal Ch but did not produce the prolonged decrease to 30% of basal observed with neostigmine (Figures 3.6 and 3.7A).

Future Directions and Potential

The method described presently demonstrates the capability of *in vivo* sampling coupled to mass spectrometry for high spatial and temporal resolution pharmacokinetic studies. Like microdialysis, this method allows the local application of novel drugs to specific regions of the brain to elucidate local effects. This work expands these capabilities to spatial resolution of better than 200 μm. While microelectrodes have

allowed choline or acetylcholine dynamics to be observed within the brain with similar spatial and temporal resolution, sensitivity and selectivity concerns make quantitation difficult[7, 27]. Additionally, the lack of redox activity of drug molecules often precludes electrochemical detection. As a mass spectrometer is a "universal detector" with nM sensitivity, many analytes should be detectable by simply modifying the sample matrix to improve ionization, as demonstrated here. A detection limit of 35 amol was achieved for ACh, demonstrating the high sensitivity of this detector even within biological matrices.

Additional work will include measurements within awake, freely moving animals and improving temporal resolution. We have demonstrated elsewhere that this design of low-flow push-pull probe is compatible with awake, freely moving experiments. High temporal resolution measurements will allow correlation of the drug, neurotransmitter and metabolite transients observed with behavioral responses. Additionally, the simple fluidics of coupling plugs to a nanospray emitter tip makes this method well-suited to measurement of smaller volume plugs. We have previously demonstrated the potential for 200 ms temporal resolution *in vitro* with low-flow push-pull perfusion, and work is ongoing to demonstrate this resolution *in vivo*. A description of how sub-second *in vivo* sampling can be achieved is provided in Chapter VI.

Conclusions

Mass spectrometry with nanospray ionization allows direct, quantitative measurements of neurotransmitters, metabolites and drugs with 7 s temporal resolution when coupled to low-flow push-pull perfusion with segmented flow. This method provides better sensitivity and comparable spatial and temporal resolution to electrochemical measurements without matrix concerns.

References

(1) Westerink, B. H. C.; Timmerman, W. *Anal. Chim. Acta* **1999**, *379*, 263-274.
(2) Castañeda, T. R.; de Prado, B. M.; Prieto, D.; Mora, F. *J. Pineal Res.* **2004**, *36*, 177-185.
(3) Thongkhao-on, K.; Wirtshafter, D.; Shippy, S. A. *Pharmacol. Biochem. Behav.* **2008**, *89*, 591-597.
(4) Robinson, D. L.; Venton, B. J.; Heien, M. L. A. V.; Wightman, R. M. *Clin. Chem.* **2003**, *49*, 1763-1773.
(5) Venton, B. J.; Robinson, T. E.; Kennedy, R. T.; Maren, S. *Eur. J. Neurosci.* **2006**, *23*, 3391-3398.
(6) Aragona, B. J.; Day, J. J.; Roitman, M. F.; Cleaveland, N. A.; Wightman, R. M.; Carelli, R. M. *Eur. J. Neurosci.* **2009**, *30*, 1889-1899.
(7) Parikh, V.; Pomerleau, F.; Huettl, P.; Gerhardt, G. A.; Sarter, M.; Bruno, J. P. *Eur. J. Neurosci.* **2004**, *20*, 1545-1554.
(8) Burmeister, J. J.; Gerhardt, G. A. *Anal. Chem.* **2001**, *73*, 1037-1042.
(9) Kulagina, N. V.; Shankar, L.; Michael, A. C. *Anal. Chem.* **1999**, *71*, 5093-5100.
(10) Oldenziel, W. H.; Dijkstra, G.; Cremers, T. I. F. H.; Westerink, B. H. C. *Brain Res.* **2006**, *1118*, 34-42.
(11) Oldenziel, W. H.; Dijkstra, G.; Cremers, T. I. F. H.; Westerink, B. H. C. *Anal. Chem.* **2006**, *78*, 3366-3378.
(12) Wang, M.; Slaney, T.; Mabrouk, O.; Kennedy, R. T. *J. Neurosci. Methods* **2010**, *190*, 39-48.
(13) Slaney, T. R.; Mabrouk, O. S.; Porter-Stransky, K. A.; Aragona, B. J.; Kennedy, R. T. *ACS Chemical Neuroscience* **2012**, *In Press*.
(14) Slaney, T. R.; Nie, J.; Hershey, N. D.; Thwar, P. K.; Linderman, J.; Burns, M. A.; Kennedy, R. T. *Anal. Chem.* **2011**, *83*, 5207-5213.
(15) Kottegoda, S.; Shaik, I.; Shippy, S. A. *J. Neurosci. Methods* **2002**, *121*, 93-101.
(16) Aris, R. *Proc. R. Soc. London, Ser. A* **1956**, *235*, 67-77.
(17) Wang, M.; Roman, G. T.; Perry, M. L.; Kennedy, R. T. *Anal. Chem.* **2009**, *81*, 9072-9078.
(18) Song, P.; Hershey, N. D.; Mabrouk, O. S.; Slaney, T. R.; Kennedy, R. T. *Anal. Chem.* **2012**, *84*, 4659-4664.
(19) Juraschek, R.; Dülcks, T.; Karas, M. *J. Am. Soc. Mass Spectrom.* **1999**, *10*, 300-308.
(20) Cellar, N. A.; Burns, S. T.; Meiners, J. C.; Chen, H.; Kennedy, R. T. *Anal. Chem.* **2005**, *77*, 7067-7073.
(21) Cellar, N. A.; Kennedy, R. T. *Lab Chip* **2006**, *6*, 1205-1212.
(22) Pei, J.; Li, Q.; Kennedy, R. T. *J. Am. Soc. Mass Spectrom.* **2010**, *21*, 1107-1113.
(23) Pei, J.; Li, Q.; Lee, M. S.; Valaskovic, G. A.; Kennedy, R. T. *Anal. Chem.* **2009**, *81*, 6558-6561.
(24) Uutela, P.; Reinilä, R.; Piepponen, P.; Ketola, R. A.; Kostiainen, R. *Rapid Commun. Mass Spectrom.* **2005**, *19*, 2950-2956.
(25) Zhu, Y.; Wong, P. S. H.; Cregor, M.; Gitzen, J. F.; Coury, L. A.; Kissinger, P. T. *Rapid Commun. Mass Spectrom.* **2000**, *14*, 1695-1700.

(26) Huang, T.; Yang, L.; Gitzen, J.; Kissinger, P. T.; Vreeke, M.; Heller, A. *Journal of Chromatography B: Biomedical Sciences and Applications* **1995**, *670*, 323-327.
(27) Bruno, J. P.; Gash, C.; Martin, B.; Zmarowski, A.; Pomerleau, F.; Burmeister, J.; Huettl, P.; Gerhardt, G. A. *Eur. J. Neurosci.* **2006**, *24*, 2749-2757.

Chapter IV

Chemical Gradients within Brain Extracellular Space Measured using Low-Flow Push-Pull Perfusion Sampling *in Vivo*

Reproduced with permission from Slaney, T.R. et al. ACS Chemical Neuroscience, in press. Copyright 2012 American Chemical Society.

Introduction

A salient feature of the brain is its heterogeneity. Neurons expressing different neurotransmitters are in close proximity and connect together in small nuclei. Neighboring nuclei and sub-nuclei may be involved in distinct processes providing functional significance to heterogeneous distribution. For example, a 1 mm locus of the rat nucleus accumbens (NAc) shell has been implicated in responses to hedonic stimuli[1]. Chemical analysis and histochemical imaging of brain tissue have revealed distribution of neurotransmitters[2, 3], processing enzymes[4, 5], receptors[6, 7], and reuptake proteins[2, 8, 9] that presumably underlie functional heterogeneity in the brain. Although these approaches give an important view of brain organization, they do not provide distribution of neurotransmitters where they are actually active, i.e. in the extracellular space. It would be difficult to predict differences in extracellular concentration because of complex regulation of neurotransmitters by combined effects of synthesis, release, reuptake, and metabolism[10-12]. Direct, spatially resolved measurement of neurotransmitter extracellular concentration is required to address this issue. Such measurements also provide a means

to assess the regulation of a neurotransmitter, its transport through the brain, and its potential for extrasynaptic signaling (i.e., "volume transmission")[13]. In this work we demonstrate a method to measure extracellular concentrations of neurotransmitter and metabolites with 0.004 mm^3 (4 nL) spatial resolution to reveal gradients across the boundary between several nuclei.

Common methods for *in vivo* measurement include microdialysis[14] and microelectrodes[15]. Because microdialysis probes are 200-400 μm diameter with a 1-4 mm long sampling membrane, they provide a relatively gross measure of chemical distributions. Microelectrodes can be made much smaller; however, direct measurement of basal concentration is often confounded by background interference. Nevertheless, differences in dopamine (DA) activity have been detected across ~150 μm distances by electrochemical methods[16-18].

In this work we apply low-flow push-pull perfusion sampling[19] to make spatially resolved measurements in brain extracellular space. This method is similar to classic push-pull perfusion wherein sampling is achieved by infusing physiological buffer and withdrawing sample at equal flow rates through closely spaced capillaries[20]. By using low flow rates (50 nL/min) and smaller capillaries, spatial resolution is enhanced relative to conventional push-pull perfusion[19, 21-23]. Fractions collected from probes in this work are analyzed using a recently developed liquid chromatography-mass spectrometry (LC-MS) method to assay 13 neurotransmitters and metabolites[24].

The method is used to measure extracellular chemical gradients across a few hundred micrometers in three brain regions where DA distributions are expected. We focus on DA because of interest in this neurotransmitter for its role in reward, addiction,

and certain diseases[25, 26]. Also, substantial effort has already been expended in evaluating its extracellular concentration and heterogeneity[17, 27-29] allowing comparison to previous studies.

One set of measurements is made across the corpus callosum at the boundary between cortex and striatum. DA neurons are present in both cortex and striatum, but much richer DA innervation in the striatum than cortex suggests the potential for a sharp concentration gradient[2]. Measurements are also made at the border of ventral tegmental area (VTA) and red nucleus (RN) where a similar gradient is expected based on strong DA innervation of VTA relative to RN[26]. Finally, we collect spatially resolved measurements within the NAc. Functional and morphological heterogeneity within the NAc has implications for addiction and disease pathologies[2, 30, 31]. The dorsolateral accumbens, or core, projects to brain regions associated with motor activity while the ventromedial accumbens, or shell, projects to regions associated with the limbic system[2]. Dopaminergic neurons are found throughout the NAc; but, dopaminergic projections to the core originate within parabrachial VTA and substantia nigra pars compacta, whereas projections to the medial shell originate within paranigral VTA[27, 32]. A consensus on differences in basal concentration of DA within the NAc has not been reached with studies finding higher, equal, or lower concentrations in core versus shell[27]. The variability in microdialysis observations has been attributed to probe placements and angles of implantation[27], emphasizing the significance of spatial resolution.

Although this study centers on detection of likely gradients in DA, the measurement of other neurotransmitters and metabolites provides further insight into

chemical heterogeneity within these regions. Further, the measurements provide a validation of the push-pull method for spatially-resolved chemical measurements.

Materials and Methods

Materials and Reagents

Unless otherwise specified, all reagents were purchased from Sigma Aldrich (St. Louis, MO). Fused silica capillaries were purchased from Polymicro (Phoenix, AZ). Unions for 360 μm outer diameter (OD) capillaries were purchased from Idex Health and Science (P-772, Oak Harbor, WA). Polyimide tubing was purchased from Smallparts.com (Seattle, WA). Thixotropic epoxy was purchased from Epoxy Technology (353ND-T, Billerica, MA). Cyanoacrylate glue was purchased from K & R International (E-Z Bond, Laguna Niguel, CA). Artificial cerebrospinal fluid (aCSF) contained 145 mM NaCl, 2.68 mM KCl, 1.01 mM $MgSO_4$, 1.22 mM $CaCl_2$, 1.55 mM Na_2HPO_4, and 0.45 mM NaH_2PO_4, pH 7.4[22].

Probe Fabrication

For anesthetized experiments, probes were fabricated from two 20 μm inner diameter (ID), 90 μm OD capillaries. These capillaries were coated with thixotropic epoxy and inserted through a 3 cm length of 180 μm ID, 220 μm OD polyimide tubing. Excess epoxy was gently wiped off and the epoxy cured for 1 hour at 50°C and then for 20 minutes at 80°C. The polyimide and capillaries were cut within 3 mm of the end of the polyimide. Adapters consisting of 2 cm lengths of capillary (150 micron ID, 360 micron OD) were glued with cyanoacrylate on both probe capillaries for a probe length of 10 cm. Excess 90 micron OD capillary was cleaved flush with the 360 micron OD adapter using a ceramic capillary cutter.

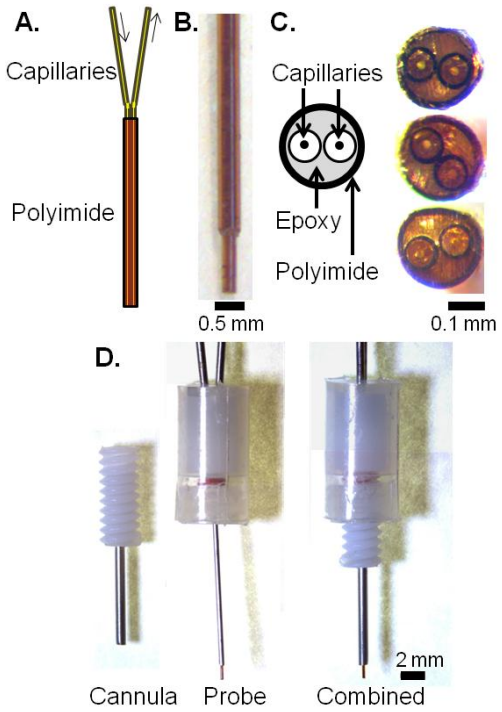

Figure 4.1. (A) Schematic of a polyimide-encased side-by-side capillary probe. The space within the polyimide is filled with epoxy. (B) Side view of a probe used in anesthetized studies, with a 360 µm OD capillary to add rigidity. (C) Polished tips of 3 probes, showing the polished capillaries, epoxy and polyimide. (D) Probe assembly for awake, freely moving studies. When inserted, the probe protrudes 1 mm past the tip of the cannula into the brain.

To polish the probe, each capillary was flushed with 0.5 µL/min of water and the tip was pressed against wet 1500 grain sand paper fixed to a 1 Hz rotating polishing wheel (BV-10, Sutter Instrument Co., Novato, CA). A 2 cm length of 250 µm ID, 360 µm OD capillary was glued over the polyimide to increase rigidity leaving 1 mm exposed at the probe tip. Examples of probes are shown in Figure 4.1A-C.

Probes for awake, freely moving animal experiments were fabricated the same as the anesthetized probes except that they consisted of two 60 cm lengths of 40 µm ID, 100 µm OD capillaries and 200 µm ID, 240 µm OD polyimide tubing. These tubes were threaded through 45 cm of 0.50 mm ID, 1.52 mm OD Tygon tubing (Saint-Gobain, Courbevoie, France), and the tip was inserted through a threaded probe holder

(C312ICP/O/SPC, Plastics One, Roanoke, VA). A 1.2 cm 26 gauge (G) hypodermic tubing (BD, Franklin Lakes, NJ) was placed over the probe and glued 1 mm from the tip with cyanoacrylate. The probe was fixed to the holder by gluing to a ~6 mm length of Tygon placed partially over the metal inlet tube of the probe holder, and the length was chosen to allow 1 mm to protrude from the cannula when inserted. The 26 G tubing did not protrude from the cannula when inserted, as shown in Figure 4.1D. A more detailed fabrication procedure with diagrams can be found in Appendix A.

Surgical Procedures

All surgical procedures were performed according to a protocol approved by the University Committee for the Use and Care of Animals. Male Sprague-Dawley rats weighing between 250 and 300 g were anesthetized using 65 mg/kg ketamine and 0.25 mg/kg dexdomitor i.p. For awake experiments, a stainless steel cannula was inserted to 1 mm dorsal to the region of interest (C312GP/O/SPC – 8 mm, Plastics One, Roanoke, VA). For the VTA and RN experiments, cannulae were implanted at 5.3 mm posterior and 1.0 mm lateral to bregma and to 5.8 or 6.8 mm from dura for the RN or VTA, respectively. For the accumbens, cannulae were implanted at 1.2 or 1.8 mm anterior and 1.4 or 0.8 mm lateral to bregma for the NAc core or shell, respectively. Cannulae were implanted to a depth of 5.8 mm from dura. Three screws were inserted in the skull near the cannula and a cap was fabricated from methyl methacrylate (Teets Cold Cure Denture Material, Co-oral-ite Dental Mfg. CO, Diamond Springs, CA). A small metal clip was also inserted into the cap for attaching the tether. A stylet (C312DC, Plastics One, Roanoke, VA) was inserted into the cannula and the animal was allowed at least 48 h to recover.

For anesthetized experiments, animals were administered ketamine and dexdomitor (as above) with boosters (22 mg/kg ketamine, 0.08 mg/kg dexdomitor) as needed and the probe was fixed to the stereotaxic arm. The animal was placed in an ultra-precise stereotaxic frame (David Kopf, Tujunga, CA). A burr hole was drilled above the region of interest and the probe was slowly lowered (approximately 10 s per mm) while backflushing both capillaries with aCSF at 500 nL/min. When the desired depth was reached, the backflushing was decreased gradually over 30 s to 50 nL per minute per capillary, and was backflushed for 8 minutes prior to starting the "pull" flow. Depths of 2.0, 2.5 and 3.0 mm from bregma were targeted for each animal, and backflushing was used while lowering between depths.

Probe placements were identified by infusing dye through the sampling probe and performing histological analysis of the tissue. After a sampling experiment was complete, 100 nL of either Evans Blue (0.24 mg/mL in aCSF) or a filtered, saturated solution of FastGreen FCF in aCSF were infused at 50 nL/min. FastGreen was preferred because it preferentially labeled the probe track whereas Evans Blue uniformly labeled the entire tissue volume affected by the dye around the probe tip. Brains were fixed in 10% paraformaldehyde containing 2.5% sucrose and 100 mM phosphate buffered saline for at least 24 hours. Brains were then frozen and sliced along the coronal plane to find the probe track. Slicing with a cryostat and manual slicing with a razor were both utilized. Manual slicing provided facile visualization of anatomical features for mapping placements and rapid preparation time. Cryostat slices (60 μm thick) were preferred as they were of better uniformity and reproducibility than manual slices and could be stored on slides for later review (Superfrost Plus, Fisher Scientific, Fairlawn, NJ). Probe

placement was considered to be the point at maximal dye concentration for Evans Blue, or the base of the probe track for FastGreen. Brain regions were identified by reference to the atlas of Paxinos and Watson [33]. Anatomical boundaries and white matter (such as the anterior commissure in the nucleus accumbens, or the mesolateral lemniscus in the VTA) were used as landmarks to aid identification of probe location. Appendix B provides further details and illustrates two examples of histological analysis used to identify probe placement.

Freely Moving Experiments

Following cannulation and recovery, rats were placed in a Raturn (Bioanalytical Systems, West Lafayette, IN) and allowed free access to food and water. To implant the probe, rats were briefly anesthetized with isoflurane vapor and the stylet removed. While backflushing at 500 nL/min through each capillary, probes were gently inserted into the cannula and slowly tightened at ~1 turn per 5 s, making sure to prevent any twisting. Immediately after implanting, the probe backflushing was reduced to 50 nL/min for 8 minutes. Appendix A provides a detailed guide for probe fabrication and use.

Sample collection and analysis

To start "pull" flow, a 13 cm length of 100 µm ID, 360 µm OD capillary was connected to one of the probe capillaries, and sufficient vacuum to fill this tube at 9.4 s/mm (equal to 50 nL/min) was applied. Samples collection was initiated after 1 h of perfusion to allow for tissue recovery[21]. Sampling was conducted for approximately 3 h (~9 fractions) for awake animals, or 1 h (3 fractions) at each depth for anesthetized. Fractions were transferred from 1 µL collection capillaries to low-volume autosampler vials and were immediately derivatized as described previously[24]. The following

reagents were added with intermediate vortexing in rapid succession: 1.5 μL of 100 mM sodium tetraborate, 1.5 μL of benzoyl chloride (2% in acetonitrile), 1.5 μL of ^{13}C-internal standard, and 1 μL of 100 nM d4-ACh in water.

The ^{13}C-internal standard reagent contained 1% (vol) of a ^{13}C-benzoyl chloride derivatized stock solution (described in detail elsewhere[24]), 97% dimethylsulfoxide, and 2% acetic acid. Calibration curves were prepared for each analyte in aCSF with the following concentrations: 0.5, 5, 10, 50 and 100 nM for DA, NM, NE, 5-HT, and ACh; 5, 10, 50, 100, and 1000 nM for DOPAC, HVA, 5-HIAA, Glu, GABA, and Asp; and 50, 100, 500, 1000, and 10000 nM for Gly. Samples were analyzed using a Waters (Milford, MA) NanoAcquity UPLC coupled to either an Agilent (Santa Clara, CA) 6410 mass spectrometer or a Waters Micromass QuattroUltima mass spectrometer. A 5 μL sample plug was injected onto a Waters Acquity T3 1.8 μm C_{18}, 1 mm I.D., 50 mm length column. Mobile phase A was 10 mM ammonium formate with 0.15% (vol.) formic acid, and mobile phase B was acetonitrile. Flow rate of mobile phase was 0.1 mL/min and the gradient used was as follows: initial, 0% B; 0.01 min, 23% B, 2.51 min, 23% B; 3 min, 50% B; 5.2 min, 60% B; 6.46 min, 65% B; 6.47 min, 100% B; 7.3 min, 100% B.

Results and Discussion

Polyimide-encased push-pull probe

A novel push-pull probe design, compatible with commercially available microdialysis cannulae, was used for this work (Figure 4.1). Previous side-by-side push-pull probes housed sampling and infusion capillaries within a hypodermic needle[21, 23]; however, the needle sheath perturbed tissue ventral to the probe inlets and increased probe diameter to approximately twice that of the probe capillaries (400 μm versus 180

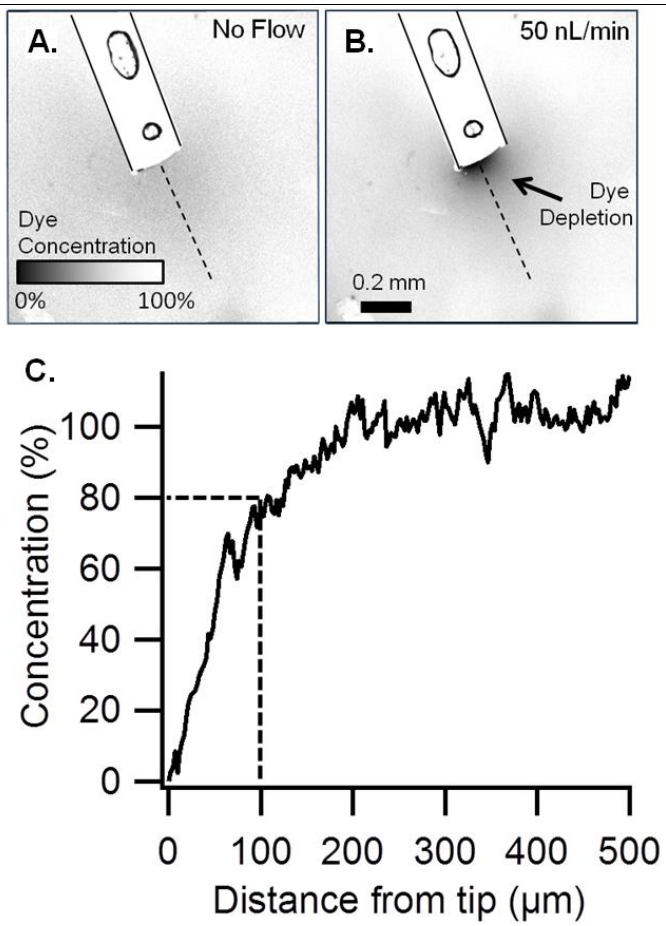

Figure 4.2. Confocal microscopy of a probe (outlined) in agar containing 1 μM resorufin (A) without sampling and (B) push-pull sampling at 50 nL/min. (Circles are air bubbles within the probe epoxy). (C) The relative concentration of resorufin in a linear path (dashes in A,B) from the tip of the probe, measured by the difference in fluorescence. Scale bar is 200 μm.

μm[21]). To avoid these problems, we made probes that consisted of two fused silica capillaries sheathed in polyimide tubing. Polyimide was used because it is biocompatible[34] and available as thin wall (20 μm) tubing. The tip of the probe was polished to provide a smooth surface and unobstructed path between push outlet and pull inlet (Figure 4.1C). The resulting probes are easily made, smaller than previous designs[21], and in principle avoid tissue damage from a protrusion below the sampling zone.

To estimate spatial resolution of sampling (i.e, the volume of tissue sampled by a probe), a probe was inserted into agar gel impregnated with the fluorescent dye resorufin.

Fluorescence imaging of the probe tip during push-pull operation allowed visualization of the sampling field as a localized region of resorufin depletion (Figure 4.2). A plot of fluorescence signal along a line perpendicular to the probe tip (Figure 4.2C) shows that depletion of resorufin extends about 200 μm beyond the tip, but at 100 μm resorufin is about 80% of the bulk concentration. We estimate that the sampled volume is 0.004 mm^3 (4 nL) by assuming a cylindrical sampling field, with radius of 220 μm and height of ~100 μm, centered over the push-pull lumen. Because dilute agar prevents convection, this volume represents spatial resolution for an analyte affected only by diffusion, similar to brain tissue[35-37]. The spatial resolution *in vivo* may be even higher because active processes, such as reuptake and metabolism, may reduce the distance that a molecule could diffuse in the brain space. Thus, a molecule released within the diffusion controlled sampling field may never reach the probe because of these processes[38].

Analysis of Neurotransmitters by LC-MS

Benzoyl chloride derivatization is amenable to analysis of multiple neurotransmitters as it increases sensitivity and retention for chromatographic separation[24]. Figure 4.3 shows representative chromatograms for the 13 neurotransmitters and metabolites monitored. Figure 4.3A shows an example of a fraction collected from within the nucleus accumbens. Stable isotope-labeled internal standard were added to each sample (Figure 4.3B) and the ratio of analyte to internal standard was utilized for measurement of concentrations. Figure 4.3C shows an example of a standard containing all 13 neurotransmitters measured. Blanks of derivatized aCSF were analyzed between sets of samples or standards and showed no significant carry-over (Figure 4.D).

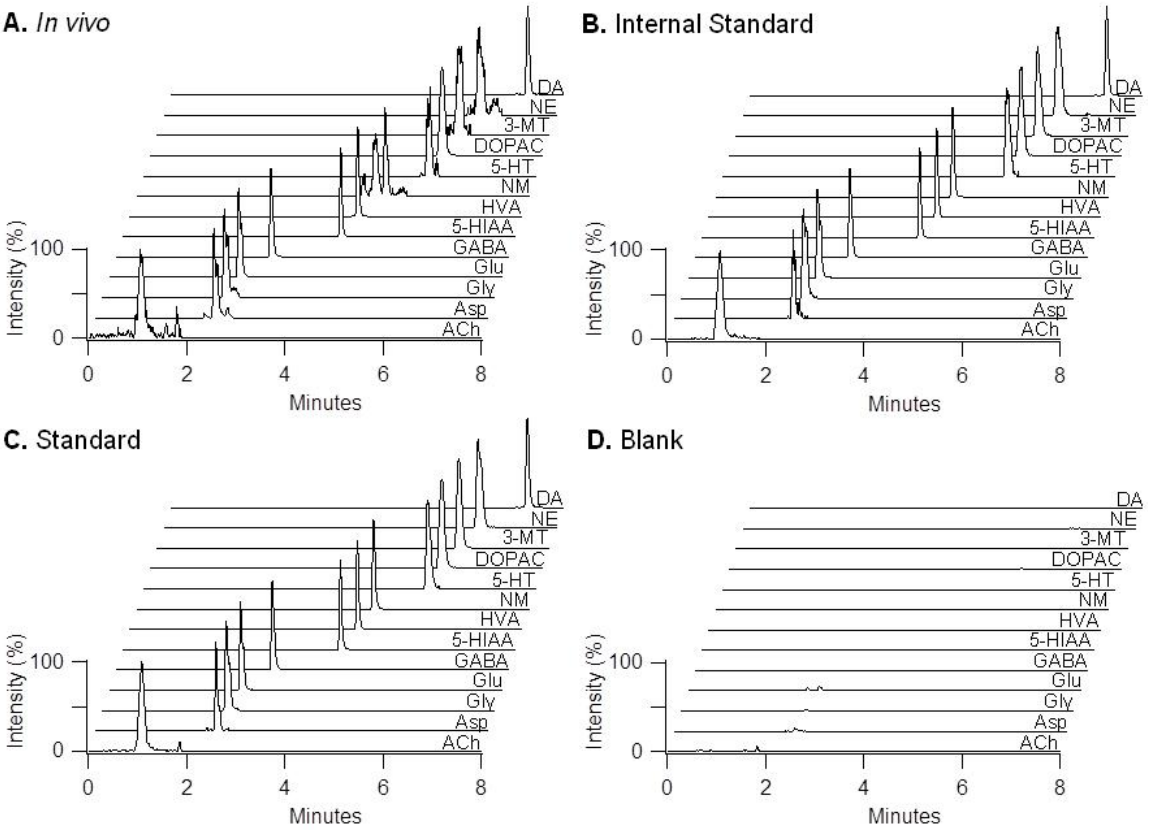

Figure 4.3. Chromatograms of neurochemicals measured (A) *in vivo* from the nucleus accumbens shell and (B) internal standards, (C) a standard containing 100 nM of ACh, NM, 5-HT, 3-MT, NE, and DA; 1000 nM of Asp, Glu, GABA, 5-HIAA, HVA and DOPAC; and 10000 nM of Gly, and (D) an aCSF blank (same scale as C).

Calibration curves were linear over the physiological range of interest. An example of a typical calibration curve is shown in Figure 4.4.

Probe recovery

In vitro recovery at 37 ^{o}C was 93 ± 17 % for Glu and 89 ± 14 % for DA (n = 3) from a stirred vial and 69 ± 4 % for Glu and 51 ± 15% for DA (n = 3) from an unstirred vial. Microdialysis experiments have shown that recovery measurements from a stirred vial more closely emulates the *in vivo* condition[39]. The high recovery is comparable to previously observed values for push-pull perfusion[19, 21, 22] and is a benefit of not having a membrane to limit mass transport (as with microdialysis) and use of low flow rates[35]. Concentrations reported in this chapter are not corrected for relative recovery.

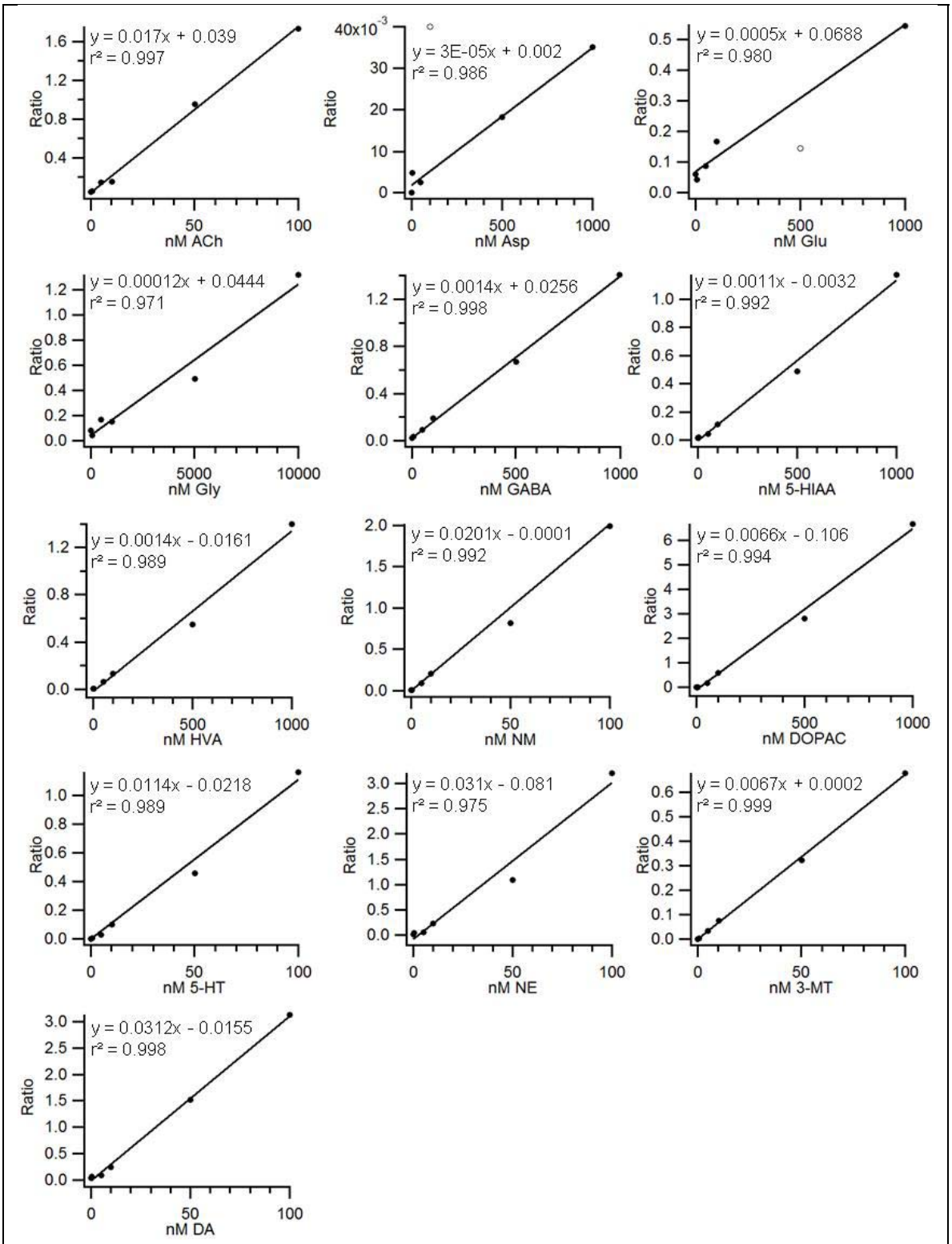

Figure 4.4 Calibration curves for neurotransmitters and metabolites, measured as ratio of analyte to stable isotope-labeled internal standard.

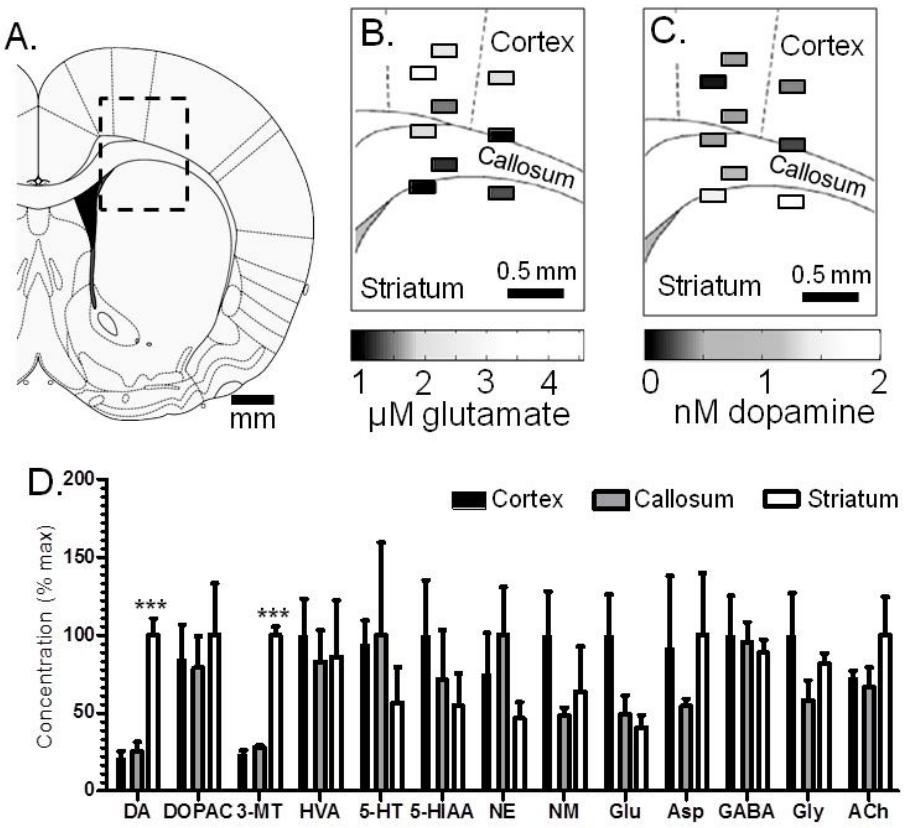

Figure 4.5. A comparison of measurements taken from multiple locations within anesthetized animals. (A) Sampling was conducted at the cortex, corpus callosum, and striatum boundary[33]. The rectangle diameters represent the probe width (220 μm) and a conservative estimate of tissue sampled (100 μm). Probe placements were mapped and concentration measurements at each site are shown for (B) Glu and (C) DA. Vertically aligned fractions represent one animal. (D) Differences in neurotransmitters were observed (*** $p < 0.001$, one-way ANOVA, Tukey's multiple comparisons test).

Measurement of concentration gradients within anesthetized animals

To evaluate a region likely to have DA gradients, samples were collected at 500 μm steps near the border of cortex, corpus callosum, and striatum in 3 animals (Figure 4.5A-C, Table 1). DA concentration changed over short distances and was higher within the dorsal striatum (1.7 ± 0.2 nM) than corpus callosum (0.4 ± 0.2 nM) and cortex (0.4 ± 0.2 nM). The extracellular concentration gradient matches the distribution of DA neurons, which have a much greater population within the striatum than cortex or corpus callosum[2].

Basal Extracellular Concentrations (nM) - Anesthetized			
	Cortex	**Corpus Callosum**	**Striatum**
DA	0.4 ± 0.1	0.4 ± 0.1	1.7 ± 0.2***
DOPAC	47 ± 12	44 ± 11	55 ± 18
3-MT	0.08 ± 0.01	0.10 ± 0.00	0.35 ± 0.02***
HVA	36 ± 8	29 ± 7	31 ± 13
5-HT	0.4 ± 0.1	0.4 ± 0.2	0.2 ± 0.1
5-HIAA	43 ± 15	31 ± 14	24 ± 9
NE	0.8 ± 0.3	1.1 ± 0.3	0.5 ± 0.1
NM	0.2 ± 0.1	0.1 ± 0.0	0.1 ± 0.1
Glu	2600 ± 700	1300 ± 300	1100 ± 200
Asp	590 ± 300	350 ± 30	640 ± 260
GABA	44 ± 11	43 ± 6	39 ± 4
Gly	5400 ± 1500	3200 ± 700	4400 ± 400
Ach	31 ± 2	28 ± 5	42 ± 10

*** $p < 0.001$, one-way ANOVA with Tukey's multiple comparisons test versus both the corpus callosum and cortex.

Table 4.1. Basal measurements of neurotransmitters and metabolites between the cortex and corpus callosum of anesthetized rats ($n = 3$ rats).

As shown in Figure 4.5D and Table 1, no other compounds showed significant differences except the DA metabolite 3-MT which varied from 0.35 ± 0.03 nM to 0.10 ± 0.01 nM to 0.08 ± 0.02 nM for striatum, corpus callosum, and cortex respectively ($p < 0.001$, one-way ANOVA with Tukey's multiple comparisons test). Although DOPAC and HVA were equivalent at different locations, we did find that the ratio of HVA to DOPAC concentration correlated with probe depth (Figure 4.6A). These results are in agreement with previous microdialysis observations from awake rats which found HVA/DOPAC of 1.2 within the cortex and 0.7 within the striatum[40].

Regional differences in DA metabolite concentrations offer insight into not only DA abundance but its turnover and extracellular fate. Among DA metabolites, 3-MT is most correlated with DA release because it is formed only extraneuronally by catechol-*O*-methyltransferase (COMT)[41]. DOPAC is formed primarily within the presynaptic neuron

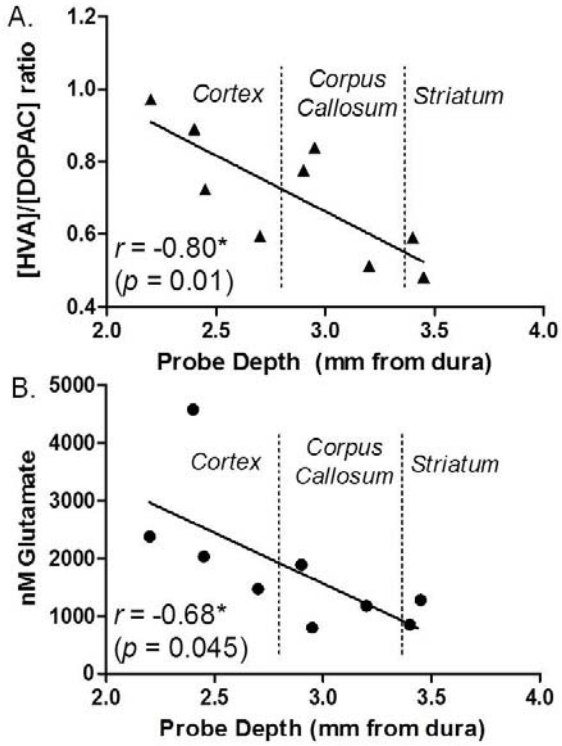

Figure 4.6. (A) HVA/DOPAC ratio (indicative of extraneuronal or intraneuronal DA metabolism) varied across the cortex, corpus callosum and striatum. (B) A gradient of decreasing Glu was also observed as a function of probe depth at this boundary (n = 3 anesthetized rats, 3 measurements per rat).

and is therefore a measure of intraneuronal turnover[42]. As HVA formation requires extraneuronal metabolism by COMT, the ratio of HVA to DOPAC can offer insight to whether extraneuronal metabolism or reuptake is dominant for removal of DA from extracellular space[42, 43]. Because DA reuptake is generally faster than metabolism, the HVA/DOPAC ratio has also been considered an indicator of extracellular DA lifetime. The chemical profile suggests higher release in the striatum (higher 3-MT and DA concentration); but greater intraneuronal turnover within the cortex (as DOPAC concentrations are comparable despite much lower DA in cortex). It is interesting that a gradient of 3-MT is maintained over such a short distance. This result may be a consequence of high monoamine oxidase (MAO) abundance in the corpus callosum[4, 44]. DA and 3-MT are both degraded by MAO with aldehyde dehydrogenase to produce

DOPAC and HVA respectively. In this way, the CC is a barrier to transport of DA and 3-MT from striatum to cortex. This "metabolic wall" may help shield cortex from relatively high DA in the striatum, which may be especially important in view of the low dopamine transporter (DAT) level[45] and high DA lifetime in cortex[46].

Among other compounds, Glu showed some differential distribution. Glu concentration in the cortex was 2.4-fold greater than in the striatum (2.6 ± 0.7 μM versus 1.1 ± 0.2 μM). Although this difference did not reach statistical significance, Glu concentration did have a significant correlation with probe depth (Figure 4.6B, $p < 0.05$, Pearson's $r = 0.678$) suggesting a decreasing concentration gradient passing from cortex to striatum. This observation agrees with previous microdialysis studies which found basal concentrations of Glu to be ~2-fold higher within the cortex than striatum; however, the sizes of the probes used in that work (2-5 mm active length) precluded observations of the gradual gradient across the callosum seen here[47, 48]. Interestingly, the higher concentration of Glu correlates with greater abundance of glial Glu transporters (GLAST and GLT-1) in the cortex relative to the striatum[49]. Because GLAST and GLT-1 remove Glu from extracellular space, these results suggest higher Glu release in cortex to achieve the higher Glu tone.

Gradients in neurochemicals in the dorsal VTA

Gradients of extracellular neurochemicals were examined in the VTA and dorsal of the VTA (RN) of awake, freely moving rats (Figure 4.7). Because these experiments were performed in awake animals, only one probe placement was made per animal. (Micropositioners are available that may allow multiple placements in awake subjects; but for these experiments we used a single position per animal to avoid the complication

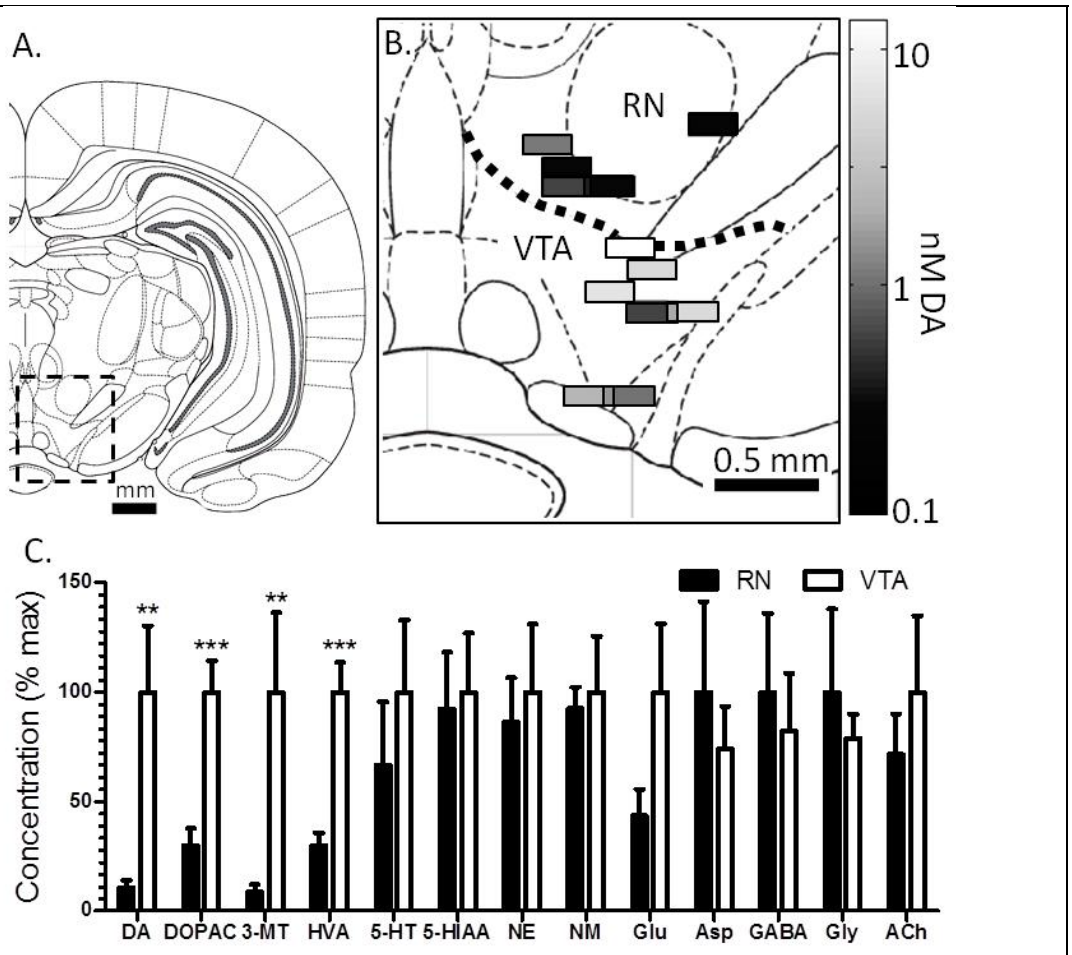

Figure 4.7. (A) A coronal map of the brain showing the location of the VTA and RN and (B) placements of measurements made in the VTA and RN with the DA concentration at each. Samples represent A/P coordinates of 4.80 mm to 5.64 mm posterior to bregma, plotted at 5.28 mm and excluding 1 fraction from the rostral area of the VTA for clarity. (C) Normalized concentrations between the VTA and RN.

of moving a probe in an awake subject.) Experiments grouped as VTA were primarily collected from the parabrachial pigmented nucleus (n = 6) but included one experiment from the parainterfascicular nucleus and one from the rostral part of the ventral tegmental area. Experiments grouped as RN were collected from the red nucleus parvicellular part (n = 3) and the prerubral field (n = 2). No significant differences were observed between sub-nuclei.

Basal Extracellular Concentrations (nM) - Awake, freely moving rats												
	VTA			**RN**			**Core**			**Shell**		
DA	4.8	±	1.5	0.5	±	0.2**	7.2	±	1.2	11	±	4
DOPAC	220	±	30	65	±	17***	1100	±	330	720	±	110
3-MT	3.5	±	1.3	0.30	±	0.11**	0.80	±	0.29	0.66	±	0.12
HVA	150	±	20	44	±	8***	460	±	60	130	±	30***
5-HT	1.6	±	0.5	1.1	±	0.5	1.3	±	0.6	0.6	±	0.2
5-HIAA	430	±	120	400	±	110	720	±	200	220	±	50*
NE	2.5	±	0.8	2.2	±	0.5	2.5	±	1.1	1.0	±	0.3
NM	0.7	±	0.2	0.6	±	0.1	0.4	±	0.1	0.4	±	0.1
Glu	8500	±	2700	3700	±	1000	2400	±	900	930	±	340
Asp	1500	±	400	2000	±	800	1100	±	500	450	±	190
GABA	160	±	50	190	±	70	150	±	110	92	±	48
Gly	7200	±	1000	9200	±	3500	4400	±	1100	2100	±	500
ACh	9.5	±	3.3	6.8	±	1.8	10	±	3	7.3	±	2.1

* $p < 0.05$; ** $p < 0.01$; *** $p < 0.001$ for comparison of VTA to RN or NAc core and shell; Student's T-test of adjacent nuclei.

Table 4.2, Basal extracellular concentrations of neurotransmitters measured within awake, freely moving rats.

Basal concentrations of DA were much higher within the VTA (4.8 ± 1.5 nM, n = 8) than within the RN (0.5 ± 0.2 nM, n = 5) reflecting rich dopaminergic innervation of the mesolimbic system within the VTA relative to RN[26]. As shown in Figure 4.7B, this concentration difference is visible between even the most dorsal region of the VTA and the most ventral of the RN (200 μm apart). The sharp concentration gradient, similar to that seen for cortex-striatum, supports the notion of strong regulation of the diffusion of DA through extracellular space. In contrast to what was observed with the cortex-striatum boundary, all DA metabolites are also significantly more abundant within the VTA than RN (see Table 2): DOPAC was 3-fold higher ($p < 0.001$), 3-MT was 11-fold higher ($p < 0.01$), and HVA was 3-fold higher ($p < 0.001$). These results suggest mechanisms that prevent DA metabolites from diffusing to adjacent nuclei. Such mechanisms may include clearance from extracellular space by neurons, glia, or

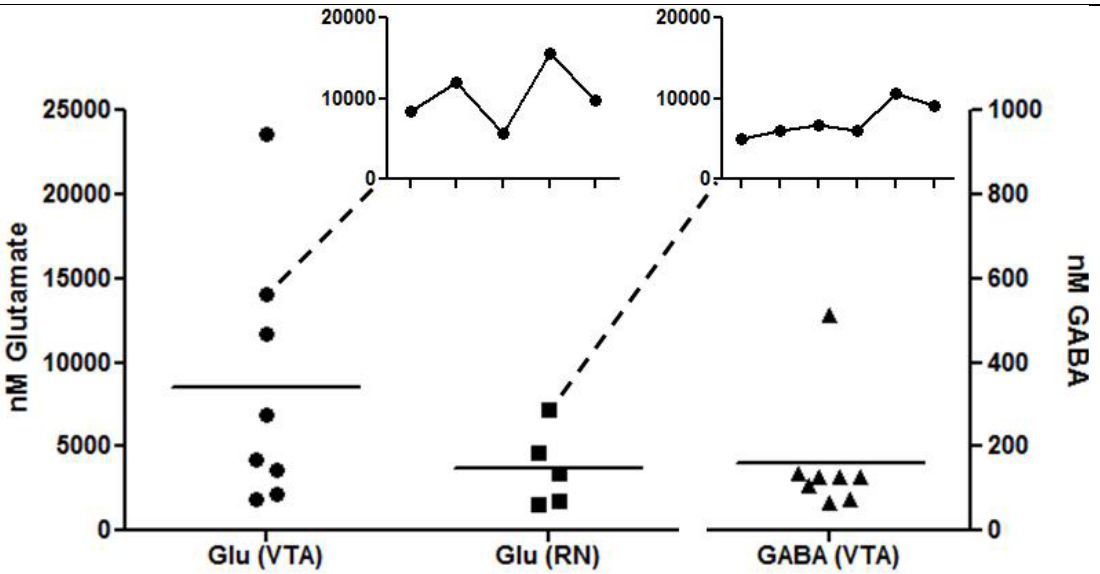

Figure 4.8. Variability of glutamate concentrations within the VTA. Glutamate basal measurements within the VTA demonstrated high variability between animals (markers represent individuals) and within individual animals as opposed to other regions such as the RN, or other neurotransmitters within the VTA (GABA). Insets show sequential fractions analyzed within one individual.

vasculature. The ratio of HVA to DOPAC was not significantly different between the VTA and RN (0.66 ± 0.05 versus 0.75 ± 0.09 respectively), despite differences in DAT distribution[45].

Among other compounds measured, only Glu showed potential spatial heterogeneity of concentration (Figure 4.7C). The basal concentration of Glu was ~2-fold greater within the VTA than the RN; however, this difference did not reach statistical significance because of high variability in the VTA. Glu concentration ranged from 2 and 24 μM (median 5.6 μM) within VTA (n = 8) compared to the 2 to 7 μM (median 3.4 μM) within the RN (n = 5) as shown in Figure 4.8. For comparison, measurements of GABA within the VTA from the same animals are shown in Figure 4.8 and ranged only from 70 to 130 nM (with one outlier of 510 nM). The variance of glutamate measurements was significantly greater in VTA than RN ($p < 0.05$, F-test). We also found that sequential fractions collected within the VTA of a given animal had higher variability than the RN

(examples shown in Figure 4.8), with a relative standard deviation of 65 ± 23 in the VTA as compared to 37 ± 14 in the RN ($p < 0.05$, t-test). The high concentration and variability suggest a high degree of glutamatergic activity with these specific placements. It is unclear if the elevated activity is an individual difference or "hot spots" within the VTA. These data may indicate localized regions of elevated glutamatergic neuronal activity. They may also relate to distribution of non-neuronal sources of Glu such as the cystine-glutamate antiporter, which has been found to cluster in some brain regions[10, 50]. Another possible reason for the variable Glu in the VTA is tissue damage caused by the probe, e.g. disruption of neurons could cause release of intracellular Glu. This explanation is discounted because we have previously observed that Glu concentration in perfusate is elevated immediately after push-pull probe insertion into brain tissue and that it decreases and to a stable level within 0.5 h[22, 23]. Similar findings on microdialysis have been reported[51] and is attributed to the disruption of neurons and subsequent dissipation of the neurotransmitters. Thus, sampling in these experiments has occurred after Glu released by cell disruption has been removed. Further, the variation of Glu was far stronger in the VTA than other brain regions and it seems unlikely that damage associated with the probe would have such disparate effects on different brain regions.

Spatial differences in the nucleus accumbens

Differences in DA concentration between the NAc core and shell is still unsettled because of difficulty of making spatially resolved measurements[27]. To address this issue, we sampled from 11 animals with probe placements in core ($n = 5$) and shell ($n = 6$) as shown in Figure 4.9. The small size of the probes mean that sampling was completely within a specified brain region thus eliminating uncertainty associated with larger probes

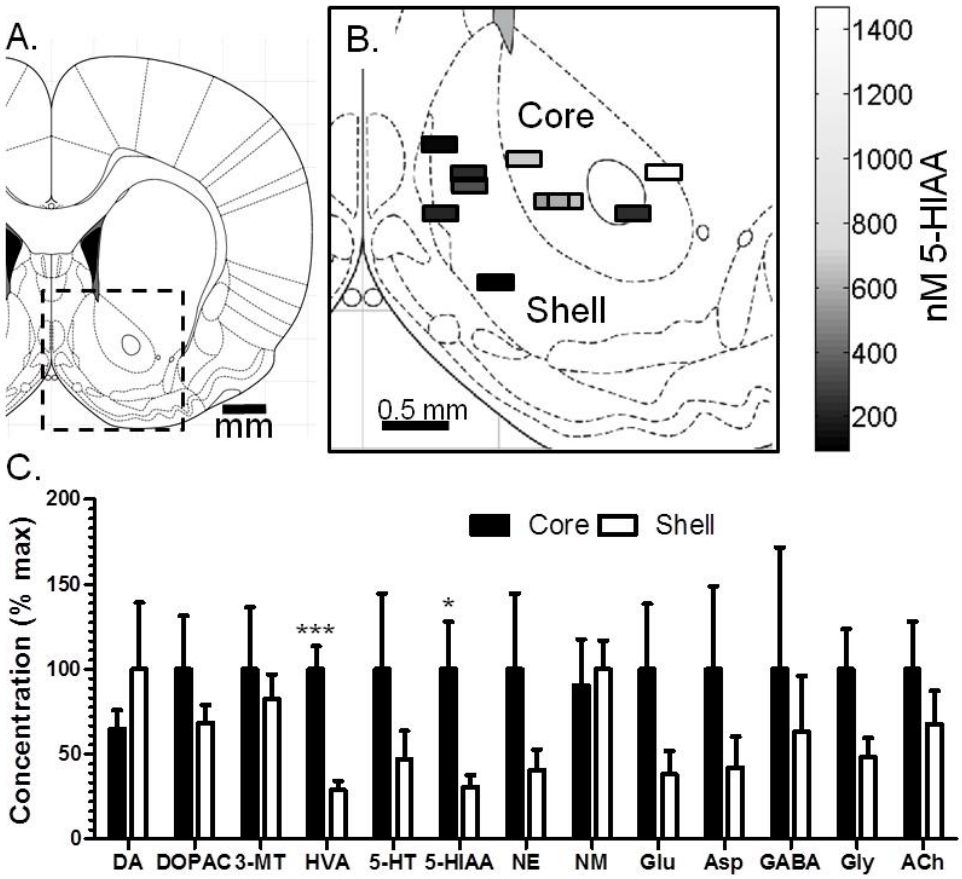

Figure 4.9. (A) A coronal map of the brain showing the nucleus accumbens and (B) placements of 5-HIAA measurements made in the core and shell with the concentration at each. Probes varied from 1.32 to 2.52 mm anterior to bregma but are shown at 1.80 mm anterior to bregma for clarity. (C) Normalized concentrations between the accumbens core and shell.

that may sample from a larger area. Using this method, we found no significant difference between core and shell DA, DOPAC, or 3-MT (Figure 4.6, Table 2); however, HVA concentration was 3-fold higher within core than shell ($p < 0.001$). As a result, the ratio of HVA to DOPAC was lower ($p < 0.01$) within the shell (0.19 ± 0.02) than core (0.53 ± 0.09). The greater HVA within the core suggests greater turnover of DA in the core than shell. The differences in HVA/DOPAC ratio indicate greater intraneuronal than extraneuronal metabolism within the shell and are suggestive of greater DA lifetime in the core[43]. This result is surprising given the higher abundance of DAT within the core

than shell, but has been observed previously by measuring clearance rates of exogenous DA and may relate to regional differences in DAT activity[52]. The shorter extracellular lifetime of DA within the shell may correlate with the much greater behavioral responses observed with local application of DA reuptake inhibitors to the shell than core[29]. Indeed, while these regions are just a few hundred microns apart, voltammetry studies show that their neurochemical activation to cues and drugs varies substantially[30, 31]. We cannot rule out DA hot spots within either nucleus without more extensive mapping as has been suggested by voltammetry studies[53].

The results also suggest greater 5-HT activity in core than shell. 5-HT was 2.2-fold higher in the core; however the concentration difference did not reach statistical significance. Supporting the idea of differences in 5-HT activity, 5-HIAA was 3-fold higher in core ($p < 0.05$). Previous studies have been inconclusive on whether 5-HT activity is different between these two regions. Microdialysis sampling did not find a significant difference in 5-HT concentration between NAc core and shell[29, 54] even though the shell contains a greater number of 5-HT neurons and the core contains more of the 5-HT transporter SERT[2, 3]. In view of the higher 5-HIAA and SERT abundance in the core, it is reasonable to postulate that more 5-HT is released in the core than shell, but greater reuptake and metabolism keep the extracellular concentration similar in the two brain regions. As 5-HT neurons of the core are more vulnerable to drugs of abuse than those of the shell[2], selectively studying 5-HT within the core may provide new insights into addiction.

A significant difference in NE and its metabolite NM between core and shell was not observed, whereas previous microdialysis work observed higher NE concentrations in

Region	Neurotransmitter	"No-Net-Flux" Concentration	Species	Push-Pull Concentration
VTA	DA	5.0 ± 0.5 nM[55]	♀ Indiana "P"	4.8 ± 1.5 nM
	Glu	3.3 ± 0.8 μM, 4.1 ± 0.5 μM[56]	♀ Wistar	8.5 ± 2.7 μM
Accumbens	5-HT	0.7 nM[57]	♂ SD	1.3 ± 0.6 nM (core)
		0.7 ± 0.1 nM[58]	♂ Wistar	0.6 ± 0.2 nM (shell)
		0.6 ± 0.1 nM[59]	♂ Wistar	
	DA	4.7 ± 0.7 nM[60]	♂ Holtzman	7.2 ± 1.2 nM (core)
		5.6 ± 0.4 nM[58]	♂ Wistar	11 ± 4 nM (shell)
		8.3 ± 1.2 nM[59]	♂ Wistar	
	GABA	32.7 ± 4.0 nM[61]	♂ SD	150 ± 110 nM (core) 92 ± 48 nM (shell)
	Glu	1.8 ± 0.4 μM, 2.4 ± 0.5 μM[62]	♂ SD	2.4 ± 0.9 μM (core)
		5.6 ± 1.0 μM[63]	♂ SD	0.93 ± 0.34 μM (shell)
Striatum (anesthetized)	DA	2.5 ± 0.5 nM[64]	♂ SD	1.7 ± 0.2 nM
		6.5 ± 1.1 nM[65]	♂ SD	
	Glu	3.0 ± 0.6 μM[66]	♂ SD	1.1 ± 0.2 μM

Abbreviations: SD = Sprague-Dawley

Table 4.3. Comparison of concentrations measured by microdialysis calibrated by "no-net-flux", and low-flow push-pull perfusion

the shell[27]. This difference may relate to probe placement. Dopamine-β-hydroxylase (DBH) distribution, indicative of NE synthesis, indicates only partial innervation of the shell, favoring the caudal portion, with NE neurons[5]. Examination of results from individual probe placements supports this notion. The lowest concentration of NE (0.1 nM) was observed within the most rostral spot sampled (2.52 mm anterior to bregma), and 2 of the 3 highest concentrations in the most caudal spots sampled (1.4 and 1.2 nM at

1.32 mm anterior to bregma). A more direct study of these differences is required to establish if this trend is statistically significant.

Comparison to microdialysis concentrations

The high recovery by low-flow push-pull perfusion *in vitro* suggests that the recovered concentrations may approximate actual extracellular concentrations. Presently the most accepted method for measuring basal concentrations is by calibrated microdialysis measurements [67, 68]. Recovered concentrations of amine neurotransmitters were similar to those reported previously by microdialysis calibrated by "no-net-flux" (NNF), as shown in Table 3. NNF values for DA were 5.0 nM in the VTA [55], 4.7 to 8.3 nM in NAc (across both core and shell) [58-60], and 2.5 to 6.5 nM in the striatum of anesthetized rats [64, 65], all close to the push-pull values (see Tables 1, 2 and 3). NNF measurements of 5-HT within the accumbens were 0.6 to 0.7 nM [57-59] whereas push-pull measurements averaged 0.9 ± 0.3 nM. In contrast to the good agreement found for amines, amino acids showed more differences. GABA in NAc was ~33 nM by NNF but 3-5 times that (depending on sub-region) by push-pull. Glu concentrations agreed well for NAc core but differed by 5-fold for NAc shell, 3-fold in striatum, and ~2-fold in VTA. Glu concentrations were both higher and lower by NNF, depending on brain region, than by push-pull sampling. Without further study it is difficult to tell if these differences were due to lack of calibration for current method, spatial resolution, differences in probe impact, or other factors.

Probe placement and tissue damage

For all *in vivo* experiments, probe placement was confirmed by injecting dye through the probe and examining coronal brain slices. While this approach has limits, it

does allow confirmation that the probe was positioned within the brain regions and sub-regions reported. The histological images also allow a preliminary evaluation of tissue damage caused by the probes. Two examples of probe tracking are provided along with detailed histology procedures in Appendix B. Substantial tissue disruption is apparent along the cannula track and dorsal of the probe tip; however, around the probe tip no obvious cellular destruction or brain morphology disturbance is apparent. This result is agreement with a previous report[19] and in contrast to observations made with higher flow push-pull perfusion[69]. In view of the potential utility of this sampling method, a detailed study of its effect on tissue is warranted.

Conclusions

Low-flow push-pull perfusion allows high spatial resolution chemical measurements to be made in the brain. When combined with LC-MS the method allows a relatively comprehensive study of chemical gradients in the brain. The results show that gradients in basal concentration of neurotransmitters and metabolites can exist between adjacent brain regions less than 1 mm apart. Gradients appear to be controlled by different mechanisms depending on the brain region. Cortical and striatal DA neurons operate differently with higher release and shorter lifetime in the striatum. A mechanism that prevents transport of DA metabolites from the VTA to adjacent brain regions is active. Among the most intriguing findings is high variability of Glu within the VTA which may indicate hot spots and/or individual differences. High temporal resolution measurements will be useful to further characterize such hot spots and determine their functional significance. Within the NAc, differences in DA and 5-HT activity are apparent, based on the differences in metabolite concentrations despite similar

neurotransmitter concentration, between the core and shell which may explain differences in susceptibility to some drugs. The ability to measure such gradients will help determine their role in highly localized effects of drugs and behavioral control that has been found with other techniques.

References

(1) Peciña, S.; Berridge, K. C. *J. Neurosci.* **2005**, *25*, 11777-11786.
(2) Brown, P.; Molliver, M. E. *J. Neurosci.* **2000**, *20*, 1952-1963.
(3) Van Bockstaele, E. J.; Pickel, V. M. *J. Comp. Neurol.* **1993**, *334*, 603-617.
(4) Willoughby, J.; Glover, V.; Sandler, M. *J. Neural Transm.* **1988**, *74*, 29-42.
(5) Baldo, B. A.; Daniel, R. A.; Berridge, C. W.; Kelley, A. E. *J. Comp. Neurol.* **2003**, *464*, 220-237.
(6) Bubar, M. J.; Stutz, S. J.; Cunningham, K. A. *PLoS ONE* **2011**, *6*, e20508.
(7) Yung, K. K. L.; Bolam, J. P.; Smith, A. D.; Hersch, S. M.; Ciliax, B. J.; Levey, A. I. *Neuroscience* **1995**, *65*, 709-730.
(8) Freed, C.; Revay, R.; Vaughan, R. A.; Kriek, E.; Grant, S.; Uhl, G. R.; Kuhar, M. J. *J. Comp. Neurol.* **1995**, *359*, 340-349.
(9) Miner, L. H.; Schroeter, S.; Blakely, R. D.; Sesack, S. R. *J. Comp. Neurol.* **2003**, *466*, 478-494.
(10) Kalivas, P. W. *Nat. Rev. Neurosci.* **2009**, *10*, 561-572.
(11) Knackstedt, L. A.; LaRowe, S.; Mardikian, P.; Malcolm, R.; Upadhyaya, H.; Hedden, S.; Markou, A.; Kalivas, P. W. *Biol. Psychiatry* **2009**, *65*, 841-845.
(12) Westerink, B. H. C.; Timmerman, W. *Anal. Chim. Acta* **1999**, *379*, 263-274.
(13) Fuxe, K.; Dahlstroem, A. B.; Jonsson, G.; Marcellino, D.; Guescini, M.; Dam, M.; Manger, P.; Agnati, L. *Prog. Neurobiol. (Amsterdam, Neth.)* **2010**, *90*, 82-100.
(14) Nandi, P.; Lunte, S. M. *Anal. Chim. Acta* **2009**, *651*, 1-14.
(15) Robinson, D. L.; Hermans, A.; Seipel, A. T.; Wightman, R. M. *Chem. Rev.* **2008**, *108*, 2554-2584.
(16) Park, J.; Aragona, B. J.; Kile, B. M.; Carelli, R. M.; Wightman, R. M. *Neuroscience* **2010**, *169*, 132-142.
(17) Robinson, D. L.; Howard, E. C.; McConnell, S.; Gonzales, R. A.; Wightman, R. M. *Alcohol.: Clin. Exp. Res.* **2009**, *33*, 1187-1196.
(18) Robinson, D. L.; Venton, B. J.; Heien, M. L. A. V.; Wightman, R. M. *Clin. Chem.* **2003**, *49*, 1763-1773.
(19) Kottegoda, S.; Shaik, I.; Shippy, S. A. *J. Neurosci. Methods* **2002**, *121*, 93-101.
(20) Gaddum, J. H. *J. Physiol. (Lond.)* **1961**, *155*, 1P-2P.
(21) Slaney, T. R.; Nie, J.; Hershey, N. D.; Thwar, P. K.; Linderman, J.; Burns, M. A.; Kennedy, R. T. *Anal. Chem.* **2011**, *83*, 5207-5213.
(22) Cellar, N. A.; Burns, S. T.; Meiners, J. C.; Chen, H.; Kennedy, R. T. *Anal. Chem.* **2005**, *77*, 7067-7073.
(23) Cellar, N. A.; Kennedy, R. T. *Lab Chip* **2006**, *6*, 1205-1212.
(24) Song, P.; Mabrouk, O. S.; Hershey, N. D.; Kennedy, R. T. *Anal. Chem.* **2012**, *84*, 412-419.
(25) Lin, Z.; Canales, J. J.; Bjorgvinsson, T.; Thomsen, M.; Qu, H.; Liu, Q.-R.; Torres, G. E.; Caine, S. B.; Shafiqur, R. *Progress in Molecular Biology and Translational Science* **2011**, *98*, 1-46.

(26) Ikemoto, S. *Neurosci. Biobehav. Rev.* **2010**, *35*, 129-150.
(27) McKittrick, C. R.; Abercrombie, E. D. *J. Neurochem.* **2007**, *100*, 1247-1256.
(28) Owesson-White, C. A.; Roitman, M. F.; Sombers, L. A.; Belle, A. M.; Keithley, R. B.; Peele, J. L.; Carelli, R. M.; Wightman, R. M. *J. Neurochem.* **2012**, *121*, 252-262.
(29) Heidbreder, C.; Feldon, J. *Synapse* **1998**, *29*, 310-322.
(30) Aragona, B. J.; Cleaveland, N. A.; Stuber, G. D.; Day, J. J.; Carelli, R. M.; Wightman, R. M. *J. Neurosci.* **2008**, *28*, 8821-8831.
(31) Aragona, B. J.; Day, J. J.; Roitman, M. F.; Cleaveland, N. A.; Wightman, R. M.; Carelli, R. M. *Eur. J. Neurosci.* **2009**, *30*, 1889-1899.
(32) Lammel, S.; Hetzel, A.; Häckel, O.; Jones, I.; Liss, B.; Roeper, J. *Neuron* **2008**, *57*, 760-773.
(33) Paxinos, G.; Watson, C. *The Rat Brain in Stereotaxic Coordinates*; Academic Press: San Diego, CA, 2008.
(34) Richardson , R. R., Jr.; Miller, J. A.; Reichert, W. M. *Biomaterials* **1993**, *14*, 627-635.
(35) Szerb, J. C. *Can. J. Physiol. Pharmacol.* **1967**, *45*, 613-620.
(36) Nicholson, C.; Phillips, J. M. *J. Physiol. (Lond.)* **1981**, *321*, 225-257.
(37) Höistad, M.; Chen, K. C.; Nicholson, C.; Fuxe, K.; Kehr, J. *J. Neurochem.* **2002**, *81*, 80-93.
(38) Rice, M. E.; Patel, J. C.; Cragg, S. J. *Neuroscience* **2011**, *198*, 112-137.
(39) Tang, A.; Bungay, P. M.; Gonzales, R. A. *J. Neurosci. Methods* **2003**, *126*, 1-11.
(40) Abercrombie, E. D.; Keefe, K. A.; Difrischia, D. S.; Zigmond, M. J. *J. Neurochem.* **1989**, *52*, 1655-1658.
(41) Wood, P. L.; Altar, C. A. *Pharmacol. Rev.* **1988**, *40*, 163-187.
(42) Roffler-Tarlov, S.; Sharman, D. F.; Tegerdine, P. *Br. J. Pharmacol.* **1971**, *42*, 343-351.
(43) Bast, T.; Diekamp, B.; Thiel, C.; Schwarting, R. K. W.; Gunturkun, O. *J. Comp. Neurol.* **2002**, *446*, 58-67.
(44) Hardebo, J. E.; Owman, C. H. *Acta Physiol. Scand.* **1980**, *108*, 223-229.
(45) D'Este, L.; Casini, A.; Puglisi-Allegra, S.; Cabib, S.; Renda, T. G. *J. Chem. Neuroanat.* **2007**, *33*, 67-74.
(46) Yavich, L.; Forsberg, M. M.; Karayiorgou, M.; Gogos, J. A.; Männistö, P. T. *J. Neurosci.* **2007**, *27*, 10196-10209.
(47) Tanahashi, S.; Ueda, Y.; Nakajima, A.; Yamamura, S.; Nagase, H.; Okada, M. *Neuropharmacology* **2012**, *62*, 2057-2067.
(48) Moroni, F.; Cozzi, A.; Carpendo, R.; Cipriani, G.; Veneroni, O.; Izzo, E. *Neuropharmacology* **2005**, *48*, 788-795.
(49) Lehre, K. P.; Levy, L. M.; Ottersen, O. P.; Storm-Mathisen, J.; Danbolt, N. C. *J. Neurosci.* **1995**, *15*, 1835-1853.
(50) Sato, H.; Tamba, M.; Okuno, S.; Sato, K.; Keino-Masu, K.; Masu, M.; Bannai, S. *J. Neurosci.* **2002**, *22*, 8028-8033.
(51) Herrera-Marschitz, M.; You, Z. B.; Goiny, M.; Meana, J. J.; Silveira, R.; Godukhin, O. V.; Chen, Y.; Espinoza, S.; Pettersson, E.; Loidl, C. F.; Lubec, G.; Andersson, K.; Nylander, I.; Terenius, L.; Ungerstedt, U. *J. Neurochem.* **1996**, *66*, 1726-1735.
(52) David, D. J.; Zahniser, N. R.; Hoffer, B. J.; Gerhardt, G. A. *Exp. Neurol.* **1998**, *153*, 277-286.
(53) Wightman, R. M.; Heien, M. L. A. V.; Wassum, K. M.; Sombers, L. A.; Aragona, B. J.; Khan, A. S.; Ariansen, J. L.; Cheer, J. F.; Phillips, P. E. M.; Carelli, R. M. *Eur. J. Neurosci.* **2007**, *26*, 2046-2054.
(54) Valentini, V.; Frau, R.; Bordi, F.; Borsini, F.; Di Chiara, G. *Neuropharmacology* **2011**, *60*, 602-608.
(55) Engleman, E. A.; Keen, E. J.; Tilford, S. S.; Thielen, R. J.; Morzorati, S. L. *Alcohol* **2011**, *45*, 549-557.

(56) Ding, Z.-M.; Engleman, E. A.; Rodd, Z. A.; McBride, W. J. *Alcohol.: Clin. Exp. Res.* **2012**, *36*, 633-640.
(57) Tao, R.; Ma, Z.; Auerbach, S. B. *J. Pharmacol. Exp. Ther.* **2000**, *294*, 571-579.
(58) Smith, A. D.; Weiss, F. *J. Pharmacol. Exp. Ther.* **1999**, *288*, 1223-1228.
(59) Katner, S. N.; Weiss, F. *Alcohol.: Clin. Exp. Res.* **2001**, *25*, 198-205.
(60) Crippens, D.; Camp, D. M.; Robinson, T. E. *Neurosci. Lett.* **1993**, *164*, 145-148.
(61) Xi, Z.-X.; Ramamoorthy, S.; Shen, H.; Lake, R.; Samuvel, D. J.; Kalivas, P. W. *J. Neurosci.* **2003**, *23*, 3498-3505.
(62) Melendez, R. I.; Hicks, M. P.; Cagle, S. S.; Kalivas, P. W. *Alcohol.: Clin. Exp. Res.* **2005**, *29*, 326-333.
(63) Baker, D. A.; McFarland, K.; Lake, R. W.; Shen, H.; Tang, X.-C.; Toda, S.; Kalivas, P. W. *Nat Neurosci* **2003**, *6*, 743-749.
(64) Chen, N. N. H.; Lai, Y.-J.; Pan, W. H. T. *Neurosci. Lett.* **1997**, *225*, 197-200.
(65) Sam, P. M.; Justice, J. B. *Anal. Chem.* **1996**, *68*, 724-728.
(66) Miele, M.; Berners, M.; Boutelle, M. G.; Kusakabe, H.; Fillenz, M. *Brain Res.* **1996**, *707*, 131-133.
(67) Watson, C. J.; Venton, B. J.; Kennedy, R. T. *Anal. Chem.* **2006**, *78*, 1391-1399.
(68) Justice Jr, J. B. *J. Neurosci. Methods* **1993**, *48*, 263-276.
(69) Redgrave, P. *Pharmacol Biochem Behav* **1977**, *6*, 471-474.

Chapter V

Adapting a Plug-based GABA Enzyme Assay and Electrophoresis for 7 s Resolution Neurotransmitter Measurements by Push-Pull Perfusion

Introduction

An inherent advantage of sampling techniques such as microdialysis and low-flow push-pull perfusion is that a variety of different analyses can be utilized for sample analysis. This is beneficial as hundreds of neurotransmitters have been identified[1] and therefore, one assay may be insufficient to observe all chemical signaling implicated in a physiological process. Additionally, processes can occur on the s to ms timescale[2] and may be unique to a brain regions 100s of μm in diameter[3, 4]. Therefore, sampling techniques able to match this spatial and temporal resolution may offer new insights towards understanding neurophysiology.

Currently, most high spatiotemporal resolution measurements within the brain are made with microelectrodes by either amperometry or fast-scan cyclic voltammetry[5]. While able to resolve ms transients within sub-mm regions of the brain[2], electrodes for relatively few analytes have been developed. Additionally, quantitative measurement of neurotransmitters is difficult given the high background of biological matrices[6, 7]. Segmented flow-coupled low-flow push-pull perfusion is an attractive technique for high spatiotemporal resolution monitoring of neurotransmitters[8]. In particular, segmented flow

can be used to store nL "plug" fractions of neurotransmitters in an immiscible oil carrier to preserve temporal resolution, allowing samples to be analyzed offline[8, 9]. This facilitates analysis via a number of assays with which it might otherwise be challenging to integrate a vacuum source. Additionally, it allows multiple processing steps to be utilized independently, such as a reagent addition step and a detection step. Segmented flow analysis techniques include enzyme assays[8, 10], immunoassays[11], microchip capillary electrophoresis[12, 13], and mass spectrometry[14, 15]. As plugs in an immiscible oil carrier are discrete, they can be stored and transported without cross-contamination[16].

Fluorogenic enzyme assays are attractive for analysis of nL samples as they have μM to nM sensitivity[8, 10]. A commercially available fluorogenic enzyme assay for glutamate has previously been used with push-pull perfusion, providing 7 s resolution and a 300 nM limit of detection[8]. Other analytes which are potentially amenable to fluorogenic enzyme assays include GABA[17], acetycholine and choline[18], and lactate[19].

GABA is a universal inhibitory neurotransmitter found ubiquitously in brain tissue, and it is implicated in many physiological processes[20, 21]. While many studies have measured GABA both with and without high temporal resolution using microdialysis[21-23], no sensors are currently available for high spatial and temporal resolution measurements. As low-flow push-pull perfusion is amenable to fluorogenic enzyme assays with 7s resolution[8], adapting an enzyme assay for GABA to plugs would provide a method to obtain both high spatial and temporal resolution measurements within the brain[17].

Microchip electrophoresis is another potential method for rapid, high temporal resolution measurements of neurotransmitters. Push-pull perfusion has previously been demonstrated to be compatible with capillary electrophoresis using microfabricated

polydimethylsiloxane microchips[24, 25]. However, the continuous flow utilized by these devices made temporal resolutions of better than 45 s difficult[24, 25]. More recently, segmented flow has been utilized to preserve temporal resolution of plug samples for CE analysis[10, 12, 13, 26]. In these devices, segmentation is preserved until just prior to injection onto a separation channel. By using electroosmotic flow to gate the injection of plugs into the electrophoresis channel, injection reproducibility and separation efficiency is greatly improved over previous, passively gated designs[13, 26].

In this work, two assays were adapted to the offline analysis of 6 nL plugs collected using low-flow push-pull perfusion. A novel plug-based enzyme assay was developed for the analysis of the neurotransmitter γ-aminobutyric acid (GABA) with 7 s resolution. A previously described capillary electrophoresis chip was utilized following fluorescent derivatization of amine neurotransmitters with naphthelene-2,3-dicarboxaldehyde (NDA) in an offline format. Both assays were evaluated *in vitro* and the capillary electrophoresis was demonstrated *in vivo* for high temporal resolution neurotransmitter analysis.

Materials and Methods

Reagents and Materials

Unless otherwise specified, all reagents were purchased from Fisher Scientific (Fairlawn, NJ) and were certified ACS reagent grade or better. GABase, nicotinamide adenine dinucleotide phosphate (NADP+), reduced NADP+ (NADPH), β-mercaptoethanol(β-ME), (2-hydroxypropyl)-β-cyclodextrin (β-CD) and 1H,1H,2H,2H-perfluoro-1-octanol (PFO) were purchased from Sigma Aldrich (St. Louis, MO). Naphthelene-2,3-dicarboxaldehyde was purchased from Invitrogen (Carlsbad, CA).

Perfluorodecalin (PFD) was purchased from Acros (Fairlawn, NJ). Artificial cerebrospinal fluid (aCSF) contained 145 mM NaCl, 2.68 mM KCl, 1.01 mM $MgSO_4$, 1.22 mM $CaCl_2$, 1.55 mM Na_2HPO_4, and 0.45 mM NaH_2PO_4, pH 7.4[25]. High-K^+ aCSF was the same composition as aCSF but with 145 mM KCl and 2.68 mM NaCl.

Probe Fabrication and Operation

Polyimide-encased push-pull probes were fabricated as described in Chapter III. Probes consisted of 20 μm inner diameter (ID), 90 μm outer diameter (OD) fused silica capillaries of 10 cm length (Polymicro, Phoenix, AZ). These capillaries were glued with thixotropic epoxy (353ND-T, Epotek, Billerica, MA) within a 180 μm ID, 220 μm OD polyimide sheath (Amazon Supply, Seattle, WA). To adapt to 360 μm fittings, 2 cm lengths of 150 μm ID, 360 μm OD capillary were glued at the ends of the fused silica capillaries. Probe tips were polished smooth while backflushing, as described in Chapter III. Microinjectors consisting of 20 cm lengths of 40 μm ID, 100 μm fused silica capillary were attached to probe side (~100 μm from the probe tip) using cyanoacrylate. To stimulate neurotransmitter release, 100 nL of high-K^+ aCSF was microinjected over 1 s. A picospritzer was used at 41 psi for microinjections (General Valve, Fairfield, NJ).

Probe infusion or "push" flow of aCSF were achieved at 50 nL/min using a syringe pump (Fusion 400, Chemyx, Stafford, TX). Withdrawal or "pull" flow was supplied by applying 145 mm Hg of vacuum to a Teflon plug collection tubing as described previously[8]. This Teflon tubing (150 μm ID, 360 μm OD from IDEX, Oak Harbor, WA) was connected to a commercially available tee (C360QTPK4, Valco, Houston, TX). A balanced flow resistance oil inlet was placed in the other tee inlet

consisting of 20 cm of 40 μm ID, 360 μm OD capillary and placed into an oil reservoir attached to the probe holder. Oil consisted of a 50:1 (vol) solution of PFD and PFO.

Surgical procedures

All animal procedures were performed according to a protocol approved by the University Committee for the Use and Care of Animals. Male Sprague-Dawley rats were anesthetized by i.p. injection of ketamine (75 mg/kg) and dexmedetomidine (0.25 mg/kg). Boosters of 25 mg/kg ketamine and 0.08 mg/kg dexmedetomidine were administered as needed. A burr hole was drilled at 1.0 mm anterior and ±2.6 mm lateral to bregma. Probes were implanted to a depth of 5.0 mm from dura, and perfusion was conducted for 1 hr prior to sample collection. During implantation, probe capillaries were backflushed to prevent occlusion[8].

GABA Plug-based assay

An offline enzyme assay of plug fractions collected was analyzed by continuous enzyme reagent addition, incubation, and detection by laser-induced fluorescence (LIF) with a photomultiplier tube (PMT), as described previously[8] and shown in Figure 5.1. A Teflon-based reagent addition tee was used to add the reagent to each plug. Fabrication of this tee is described in detail in Chapter II. Following collection, plugs within a Teflon cartridge were coupled to the inlet of this reagent addition tee. The outlet of the tee was coupled to a 60 cm length of Teflon reaction tubing. The end of this reaction tubing was placed vertically in a capillary mount, and aligned using a micropositioner with a 60× microscope objective fixed to a PMT enclosure[27]. A 355 nM laser was focused on the capillary orthogonal to the PMT for excitation (DPSS Lasers, Santa Clara, CA).

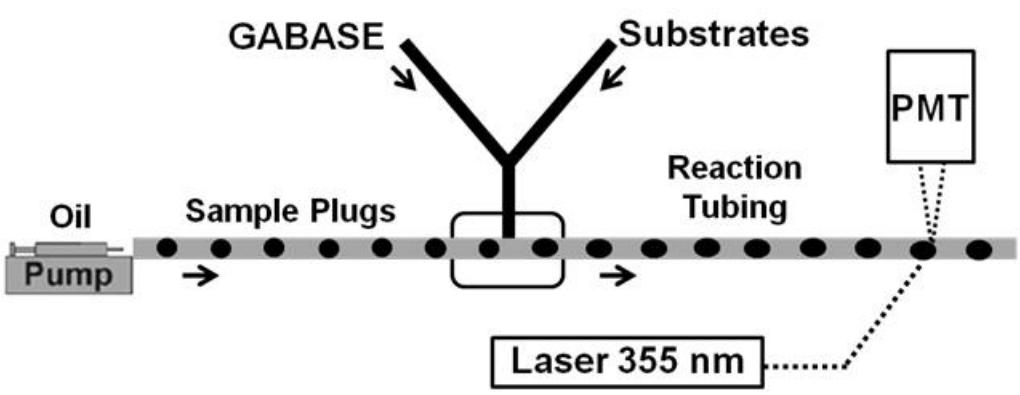

Figure 5.1 Schematic of a plug-based GABA enzyme assay. To analyze push-pull perfusate samples, plugs were pumped into a Teflon reagent addition tee. The enzyme GABASE and its substrates NADP+ and α-ketoglutarate were added at a 1:2 reagent:sample ratio. Each plug then traveled through a uniform length of reaction tubing where fluorescence was detected by laser and PMT.

Plugs were pumped into the reagent addition tee at 200 nL/min and reagent was added at 50 nL/min (1:2 reagent:sample vol.). Reagent consisted of10 mM β-ME, 15 mM α-KG, 3.75 mM $NADP^+$, and 0.3 U/mL of GABASE in 100 mM sodium pyrophosphate, pH 8.6[28]. GABASE was first prepared as a stock solution of 15 U/mL in 75 mM potassium phosphate, pH 7.2 with 25% (vol) glycerol. (This was adapted from an assay protocol by Sigma Aldrich, St. Louis, MO). Enzyme activity and concentrations were optimized using a 384-well plate reader (Perkin Elmer, Shelton, CT).

Microchip Capillary Electrophoresis of Plugs

Analysis of plugs by electrophoresis with LIF detection required derivatization of plugs with NDA. To fluorescently tag amine neurotransmitters, NDA and potassium cyanide (KCN) were added using a reagent addition tee (described in Chapter II). KCN and NDA were each prepared in 50% acetonitrile and 10 mM sodium tetraborate pH 10 and mixed online during reagent addition (shown in Figure 5.2A). At the outlet of the tee was a Teflon transfer cartridge. The reagent addition tee and transfer cartridge were shielded from light.

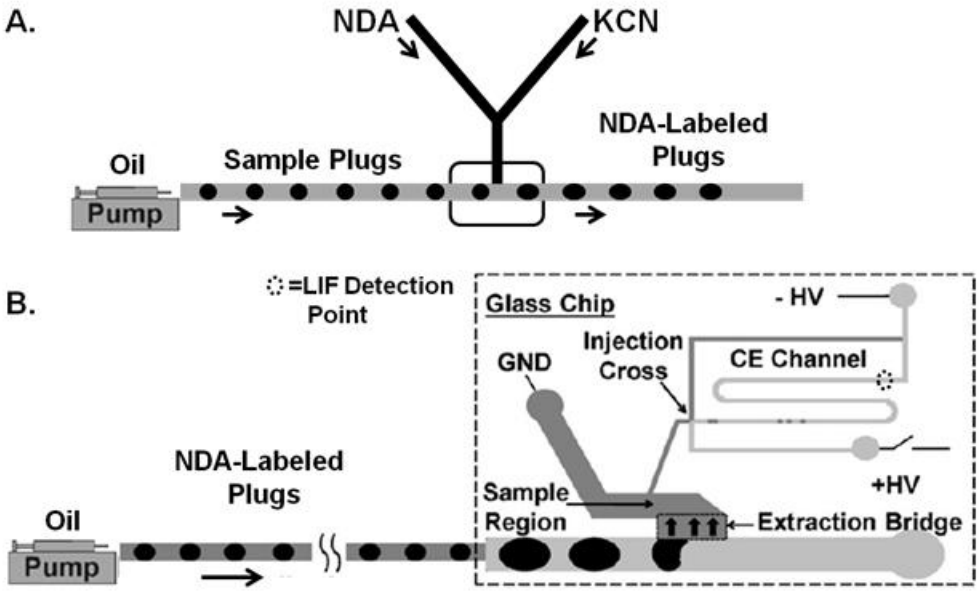

Figure 5.2. Analysis of push-pull sample plugs by microchip CE. (A) After collection, plugs are fluorescently tagged by pumping through a reagent addition tee in which NDA and KCN are added at a 1:2 reagent:sample ratio. (B) For analysis, plugs were infused onto a glass CE microchip. A hydrophilic bridge extracts aqueous plugs from oil. Immediately after extraction, samples are drawn by electroosmotic flow to an injection cross, where an injection into the CE channel for each plug is made by momentarily pausing the electroosmotic flow of separation buffer. Adapted with permission from [12], copyright 2010 Elsevier.

Fabrication of the glass capillary microchip device is described in detail elsewhere[12, 26]. The design of this device is shown in Figure 5.2B. Briefly, channels were masked by photolithography, and etched using hydrofluoric acid. The plug channel was 120 μm wide by 50 μm deep. The extraction bridge was 300 μm wide, 300 μm long and 6 μm deep, and separation channels were 6 μm deep[26]. The plug channels were derivatized hydrophobic using octadecyltrichlorosilane, while the extraction bridge and separation channels remained hydrophilic[26].

To analyze each NDA-derivatized plug, plugs were pumped from the Teflon tubing into the glass microchip (shown in Figure 5.1B). The aqueous plugs were extracted from oil by the hydrophilic extraction bridge, then were immediately drawn by

EOF towards the injection cross. Operation of this chip is described in detail elsewhere[26]. Separation timing and plug frequency entering the chip were matched to achieve 1 injection per plug. Separation buffer was 10 mM sodium tetraborate containing 1 mM β-CD. Fluorescence was detected on the separation channel by a 440 nm laser at 490 nm emission using an epifluorescent optics stage described previously[26].

Results and Discussion

Evaluation of a Plug-based GABA Enzyme Assay

The amino acid neurotransmitter GABA is not natively fluorescent; therefore, enzymatic methods were used to convert it to a readily detectable molecule. GABASE consists of two enzymes prepared by extraction from cultured *pseudomonas fluorescens*[28, 29]. These enzymes are GABA-glutamate transaminase (GABA-T) and succinic semialdehyde dehydrogenase (SSDH). In the presence of α-ketoglutarate and NADP+, these enzymes react with GABA to yield NADPH and glutamate. NADPH is

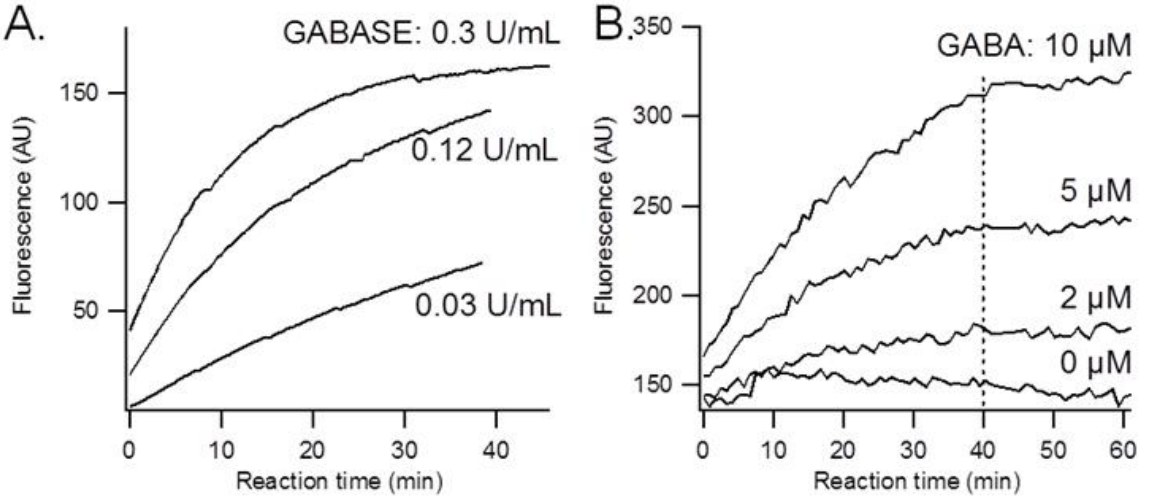

Figure 5.3. Optimization of enzyme concentration and reaction time. Reagents were prepared as described above, except (A) enzyme concentration was varied (60 µM GABA) or (B) GABA concentration was varied (0.3 U/mL GABASE). Reaction was fastest with 0.3 U/mL GABASE and neared equilibrium at 40 minutes.

highly fluorescent and a common target for enzyme assays[17, 30]. This reaction is shown below.

$$GABA + \ \alpha\text{-}Ketoglutamarate \xrightarrow[GABA-T]{} L\text{-}Glutamate + Succinic\ Semialdehyde$$

$$Succinic\ Semialdehyde + NADP^{+} \xrightarrow[SSDH]{} Succinate + NADPH$$

As this assay is compatible with a single reagent-addition step, it is readily amenable to droplet-based enzyme assays[8, 10].

To optimize reaction parameters, reaction progress was monitored by fluorescence of evolved NADPH using a plate reader. Enzyme concentration was varied to measure the effect on reaction rate. As shown in Figure 5.2A, 0.3 U/mL provided the fastest reaction velocity evaluated (higher was not tested due to practical limitations of the quantity of GABASE available). Optimal reaction time was measured by incubating different concentrations of GABA across the physiological range of interest. As shown in Figure 5.2B, 40 minutes achieved equilibrium across the physiological range of interest for GABA (0 to 10 μM). Therefore, Teflon tubing length (60 cm) was chosen to match this reaction time (40 min at 250 nL/min).

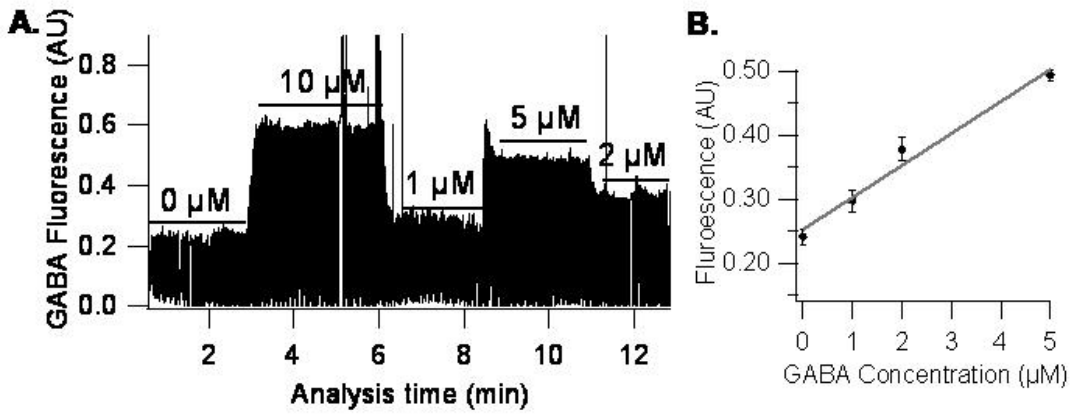

Figure 5.4. (A) Fluorescence trace of GABA standard plugs analyzed by enzyme assay. (B) Calibration of the assay was linear over the physiological range of interest (0 to 5 μM).

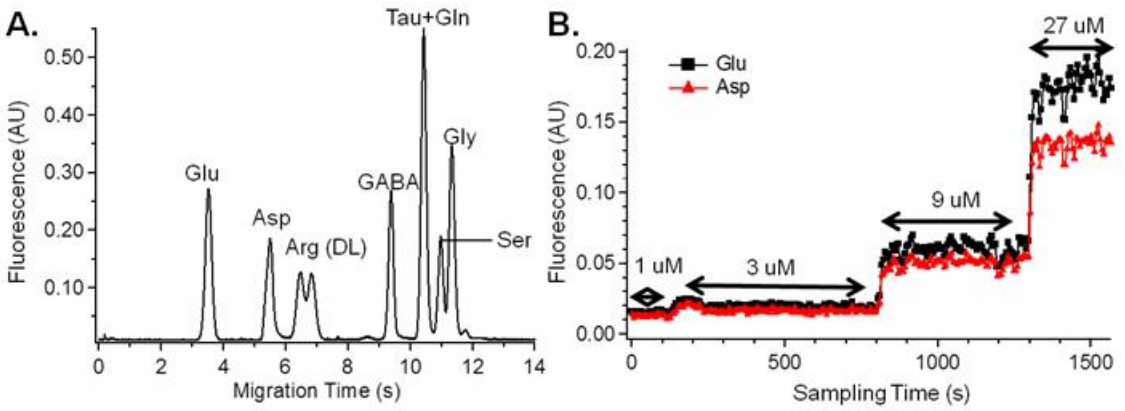

Figure 5.5. NDA-labeled neurotransmitters within plugs were analyzed by microchip CE. (A) An overlapped electropherogram for glutamate(Glu), aspartate(Asp), arginine (Arg), GABA, taurine (Tau), glutamine (Gln), glycine (Gly) and serine (Ser), where separation length was 6.5 cm and 650 V/cm applied. (B) Rapid analysis of Glu and Asp with 6 s separations, 1 separation per plug (1.5 cm channel length at 690 V/cm).

As mentioned above, this reaction required only one reagent addition step, facilitating adaptation to a plug-based enzyme. Unlike Amplex Red assays utilized previously[8, 10], fluorescence did not increase over time within the blank (Figure 5.3B) and therefore the enzyme was mixed with its co-substrates within one syringe, simplifying fluidics. An example of a calibration curve from plug standards is shown in Figure 5.4. Limit of detection of this assay was 0.7 μM. This corresponds to a 4×10^{-15} mol detection limit for a 6 nL plug, improving upon the 1×10^{-11} mol detection limit demonstrated previously[17].

Monitoring of Multiple Neurotransmitters by Capillary Electrophoresis

To assess the potential for capillary electrophoresis for analyzing plugs with high temporal resolution, standards of 6 amino acid neurotransmitters were collected from a stirred vial. An example eletropherogram is shown in Figure 5.5A. An advantage of this design is that if a faster separation is desired, the detection point can be easily varied to change the effective channel length. Figure 5.5A shows separation of 8 amino acid neurotransmitters within 14 s in 6.5 cm of channel. By using a shorter channel length,

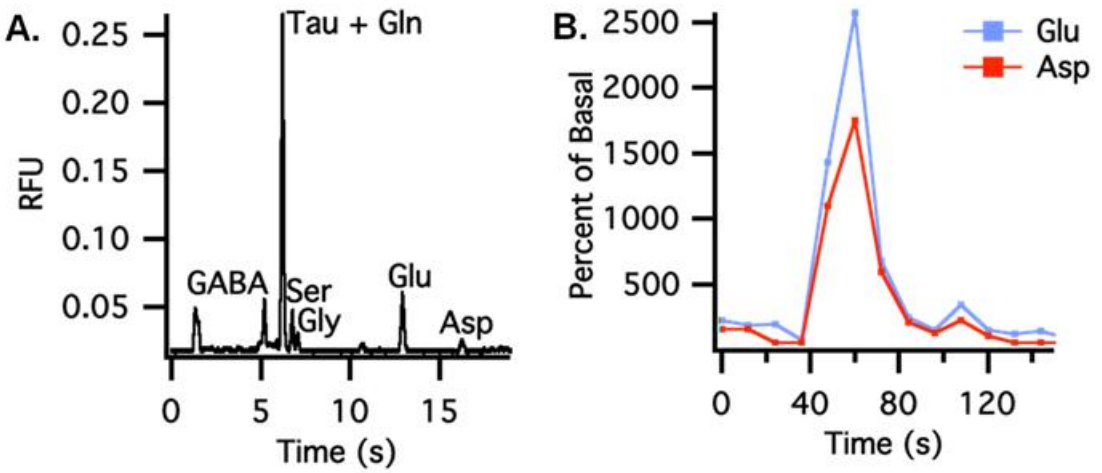

Figure 5.6. (A) Potassium microinjection increased Glu, Asp and GABA (second peak) concentrations. (B) Microinjection of potassium at 40 s produced large increases in Glu and Asp.

glutamate and aspartate can be analyzed within 6 seconds allowing for high throughput (600 samples/hr) analysis of plugs (Figure 5.5B).

Step changes can be resolved within 1 to 2 plugs (Figure 5.5B), meaning temporal resolution is preserved through this microchip. This is expected as the volume of each plug (~9 nL following reagent addition) is sufficient to wash the previous plug from the EOF inlet on the chip (Figure 5.2B)[26].

In Vivo Measurement of Rapid Neurotransmitter Dynamics

Electrophoresis allows rapid separation and detection of NDA-labeled glutamate and aspartate even within the matrix of the brain (Figure 5.6). Microinjections of potassium produced a large increase in extracellular glutamate and aspartate, as shown in Figure 5.6B. This was a 26-fold increase in glutamate and 18-fold increase in aspartate. GABA also is clearly visible with potassium microinjection, however at basal concentrations it was not resolved from co-eluting compounds. In this preliminary experiment, one of every two plugs was injected for 12 s temporal resolution (plugs were

collected at 6 s intervals), however, this method is currently capable of 6 s resolution, as was demonstrated *in vitro.*

Future Directions and Potential

Both a GABA enzyme assay and on-chip CE have potential for *in vivo* measurement of neurotransmitters. The GABA assay is capable of higher throughput than electrophoresis as the analysis time per plug (excluding 40 minute reaction incubation) is limited by the flow rate of the plugs through the LIF detector and ms plug analysis times have been demonstrated previously[11]. The detection limit was insufficient to reliably detect basal GABA, which ranges from ~0.7 μM[25] to ~0.1 μM (described in Chapter IV). This detection limit can be improved by better control of fluorescence background as the PFO within the oil and other reagents contained contaminants resulting in a background equivalent to 5 μM of GABA. An alternative is to chemically convert NADPH to a secondary fluorophore of longer wavelength such as resorufin; however, care must be taken to find an NADPH assay which is unaffected by the enzyme reagents needed for GABASE, including β-ME and $NADP^+$, both of which can increase background[31].

As shown above, the CE microchip has potential to detect GABA *in vivo* as well as simultaneously measuring glutamate, aspartate and other neurotransmitters. As push-pull is high spatial resolution, this provides the potential for rapid, multianalyte neurochemical monitoring selectively within smaller regions of the brain. Work is ongoing to improve the reliability of plug extraction while achieving faster and more efficient separations.

Conclusions

The potential of segmented flow-coupled low-flow push-pull perfusion for other plug-based enzyme assays and separations-based analyses without sacrificing temporal resolution was demonstrated. A novel plug-based enzyme assay was developed and demonstrated for the neurotransmitter GABA. This assay has a 4 fmol detection limit and is compatible with high-throughput analysis. Further optimization of assay parameters, particularly careful exclusion of fluorescence contamination from reagents, should allow facile measurement of basal GABA within the brain.

Electrophoresis allows highly sensitive detection of multiple analytes collected *in vivo*. This allows measurement of glutamate and aspartate with high throughput (6 s to 12 s/plug depending on efficiency desired) and this work presents the highest temporal resolution measurements yet demonstrated for aspartate within the brain with 200 μm spatial resolution.

References

(1) Greengard, P. *Science* **2001**, *294*, 1024-1030.
(2) Robinson, D. L.; Venton, B. J.; Heien, M. L. A. V.; Wightman, R. M. *Clin. Chem.* **2003**, *49*, 1763-1773.
(3) Robinson, D. L.; Howard, E. C.; McConnell, S.; Gonzales, R. A.; Wightman, R. M. *Alcohol.: Clin. Exp. Res.* **2009**, *33*, 1187-1196.
(4) Peciña, S.; Berridge, K. C. *J. Neurosci.* **2005**, *25*, 11777-11786.
(5) Robinson, D. L.; Hermans, A.; Seipel, A. T.; Wightman, R. M. *Chem. Rev.* **2008**, *108*, 2554-2584.
(6) Oldenziel, W. H.; Dijkstra, G.; Cremers, T. I. F. H.; Westerink, B. H. C. *Anal. Chem.* **2006**, *78*, 3366-3378.
(7) Heien, M. L. A. V.; Khan, A. S.; Ariansen, J. L.; Cheer, J. F.; Phillips, P. E. M.; Wassum, K. M.; Wightman, R. M. *Proceedings of the National Academy of Sciences of the United States of America* **2005**, *102*, 10023-10028.
(8) Slaney, T. R.; Nie, J.; Hershey, N. D.; Thwar, P. K.; Linderman, J.; Burns, M. A.; Kennedy, R. T. *Anal. Chem.* **2011**, *83*, 5207-5213.

(9) Song, H.; Chen, D. L.; Ismagilov, R. F. *Angew. Chem. Int. Ed.* **2006**, *45*, 7336-7356.
(10) Wang, M.; Roman, G. T.; Schultz, K.; Jennings, C.; Kennedy, R. T. *Anal. Chem.* **2008**, *80*, 5607-5615.
(11) Chen, D.; Du, W.; Liu, Y.; Liu, W.; Kuznetsov, A.; Mendez, F. E.; Philipson, L. H.; Ismagilov, R. F. *Proc. Natl. Acad. Sci. USA* **2008**, *105*, 16843-16848.
(12) Wang, M.; Slaney, T.; Mabrouk, O.; Kennedy, R. T. *J. Neurosci. Methods* **2010**, *190*, 39-48.
(13) Roman, G. T.; Wang, M.; Shultz, K. N.; Jennings, C.; Kennedy, R. T. *Anal. Chem.* **2008**, *80*, 8231-8238.
(14) Hatakeyama, T.; Chen, D. L.; Ismagilov, R. F. *J. Am. Chem. Soc.* **2006**, *128*, 2518-2519.
(15) Pei, J.; Li, Q.; Lee, M. S.; Valaskovic, G. A.; Kennedy, R. T. *Anal. Chem.* **2009**, *81*, 6558-6561.
(16) Wang, M.; Hershey, N.; Mabrouk, O.; Kennedy, R. *Anal. Bioanal. Chem.* **2011**, *400*, 2013-2023.
(17) Graham, L. T.; Aprison, M. H. *Anal. Biochem.* **1966**, *15*, 487-497.
(18) Browning, E. T. *Anal. Biochem.* **1972**, *46*, 624-638.
(19) Lloyd, B.; Burrin, J.; Smythe, P.; Alberti, K. G. *Clin. Chem.* **1978**, *24*, 1724-1729.
(20) Castañeda, T. R.; de Prado, B. M.; Prieto, D.; Mora, F. *J. Pineal Res.* **2004**, *36*, 177-185.
(21) Del, A. A.; Segovia, G.; Fuxe, K.; Mora, F. *J. Neurochem.* **2003**, *85*, 23-33.
(22) Venton, B. J.; Robinson, T. E.; Kennedy, R. T. *J. Neurochem.* **2006**, *96*, 236-246.
(23) François, W.; Nicolas, B.; Annie, P.; Nadia, U.; Guy, C.; Claude, F.; Marc, S. *Eur. J. Neurosci.* **2000**, *12*, 4141-4146.
(24) Cellar, N. A.; Kennedy, R. T. *Lab Chip* **2006**, *6*, 1205-1212.
(25) Cellar, N. A.; Burns, S. T.; Meiners, J. C.; Chen, H.; Kennedy, R. T. *Anal. Chem.* **2005**, *77*, 7067-7073.
(26) Wang, M.; Roman, G. T.; Perry, M. L.; Kennedy, R. T. *Anal. Chem.* **2009**, *81*, 9072-9078.
(27) Bowser, M. T.; Kennedy, R. T. *Electrophoresis* **2001**, *22*, 3668-3676.
(28) Jakoby, W. B.; Sidney, P. C.; Nathan, O. K. In *Methods Enzymol.*; Academic Press, 1962; Vol. Volume 5, pp 765-778.
(29) Scott, E.; Jakoby, W. *The Journal of biological chemistry* **1959**, *234*, 932-936.
(30) Lowry, O. H.; Roberts, N. R.; Kapphahn, J. I. *J. Biol. Chem.* **1957**, *224*, 1047-1064.
(31) Castillo, G. M.; Thibert, R. J. *Microchem. J.* **1988**, *38*, 191-205.

Chapter VI

Future Directions

Introduction

In this work, the potential of using low-flow push-pull perfusion for monitoring different neurotransmitters with high temporal and spatial resolution within the brain has been demonstrated. By coupling probes to microfluidic plug-generating tees, samples were analyzed with various single and multi-analyte assays while maintaining 7 s temporal resolution (with the potential for 200 ms resolution). This technique was first utilized with an enzyme assay for the neurotransmitter glutamate, then with nanospray mass spectrometry for simultaneous monitoring of acetylcholine, its metabolite choline, and the drug neostigmine *in vivo*. A new design of miniaturized push-pull probe was characterized and used to identify differences in neurotransmitter abundance and metabolism with 200 μm resolution. Lastly, amenability of this sampling method to other assays was demonstrated by coupling sampling to a plug-based GABA assay, and microchip capillary electrophoresis. These probes have comparable spatial and temporal resolution to microelectrodes[1] while providing better selectivity, nM sensitivity, and multianalyte measurements. There remain several avenues to further expand this methodology, and to utilize it for performing *in vivo* neurochemical experiments.

In Vivo Demonstration of Millisecond Temporal Resolution

Using low-flow push-pull perfusion for sub-second temporal resolution chemical measurements would be a significant technological advance as this method provides the potential to measure many analytes not presently observable at that resolution. Low-flow push-pull perfusion is capable of 200 ms resolution sampling, provided an inlet with minimal dispersion is utilized and plug frequency is sufficient to store these dynamics. In Chapter II, collection and storage of 200 ms (100 pL) plugs was accomplished by using a narrow, 50 μm inner diameter (ID) Teflon capillary to maintain the plug geometry. A number of challenges resulted from this small tubing, such as high flow resistance limiting the number of plugs which could be collected to ~1 min. Other experiments indicated that plugs in 50 μm ID tubing are unstable after reagent addition, rapidly coalescing due to differences in velocities between consecutive plugs.

A strategy to collect trains of sub-second plugs for extended periods of time is to increase volume of plugs generated and store within larger (100 μm) inner diameter (ID) Teflon tubing. This should be achievable by one or both of the following strategies: addition of a makeup flow to the aqueous phase before segmentation, and increasing the flow rate of push-pull perfusion. Increasing flow rate of push-pull perfusion has the added benefit of allowing larger ID probe inlets to be utilized with less dispersion, reducing backpressure.

Using a Makeup Flow to Increase Plug Frequency

Addition of a makeup flow to collected perfusate at the point of plug generation would allow storage of higher frequency plugs in larger diameter tubing. One method to couple this diluent flow to a push-pull probe outlet is to replace the plug generating tee

with a cross. For example, the commercially available 100 μm ID tee utilized in Chapters II and III (C360QTPKG, Valco, Houston, TX) is also available as a 100 μm ID cross (C360QXPK4). By placing the aqueous inlets side-by-side, these phases should mix as plugs are generated.

Many bioanalytical assays necessitate the addition of a reagent to samples prior to analysis, such as enzymes (Chapters II and V), internal standard (Chapter III) or a derivatization reagent (Chapter V); therefore it may be possible to utilize this reagent as the makeup flow. The internal standard for acetylcholine analysis described in Chapter III is well-suited as a makeup flow in offline analysis as it is chemically stable, and the assay is not time-sensitive. Fluorogenic enzyme reagents (Chapters II and V) could potentially be utilized for makeup flow in online analyses as the Teflon collection tubing of the push-pull probe could be connected directly to a laser-induced fluorescence detector with vacuum applied at the detector outlet.

Increasing Perfusion Flow Rates

Increasing the flow rate of low-flow push-pull perfusion allows higher frequency plug generation, but also reduces dispersion within the probe inlet. Calculations and descriptions of the effects of probe dimensions on temporal resolution are described in detail in Chapter II. While 10 μm ID capillary allows high temporal resolution, it greatly increases flow resistance, risking air bubble formation or leaking from higher vacuum and allowing only a very short inlet to be used (≤ 1 cm). Achieving ms temporal resolution with 20 μm ID probe inlets would avoid the practical difficulties of narrower capillaries. The benefits of reducing inlet length from 10 cm (Chapters II and III) to 5

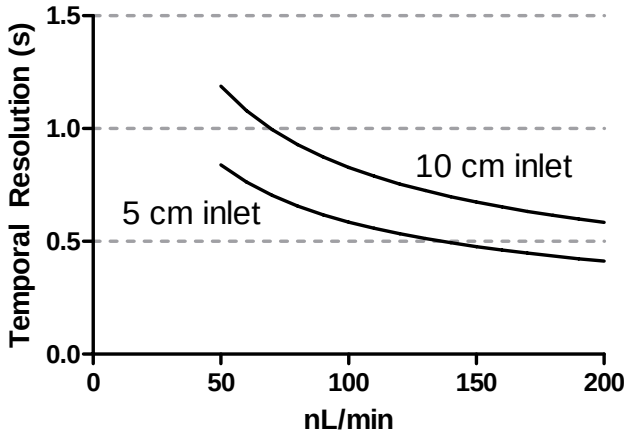

Figure 6.1. Calculated temporal resolution (10 to 90% rise time for a concentration step change) for 20 μm bore probe capillary inlets as a function of flow rate for both a 5 cm inlet and a 10 cm inlet.

cm, and increasing perfusion flow rate from 50 to 100 or 200 nL/min is shown in Figure 6.1.

One concern of increased flow rates is how fast tissue can be perfused without occluding the probe or causing tissue trauma. The flow rate limit of 50 nL/min for low-flow push-pull perfusion was chosen based on one account of probe reliability, and the effects of different flow rates on tissue at these nL/min rates is not established[2]. Immunohistochemical labeling can be used to characterize the effects of different perfusion flow rates on tissue[3]. To test the feasibility of higher rates, a polyimide encased push-pull probe (described in chapters III and IV) was used to sample from the striatum with a flow rate of 100 nL/min. In this experiment, 1.7 nL plug fractions were collected at 1 s intervals in 100 μm ID Teflon tubing for 10 minutes, with the potential for greater lengths of time. This was accomplished utilizing a 100 μm ID plug-generating tee and a 10 cm length, 20 μm ID capillary probe as described in Chapter IV. To attain this flow rate, -300 mm Hg vacuum was applied to the collection tubing (instead of -150 mm Hg used with this same probe assembly for 50 nL/min).

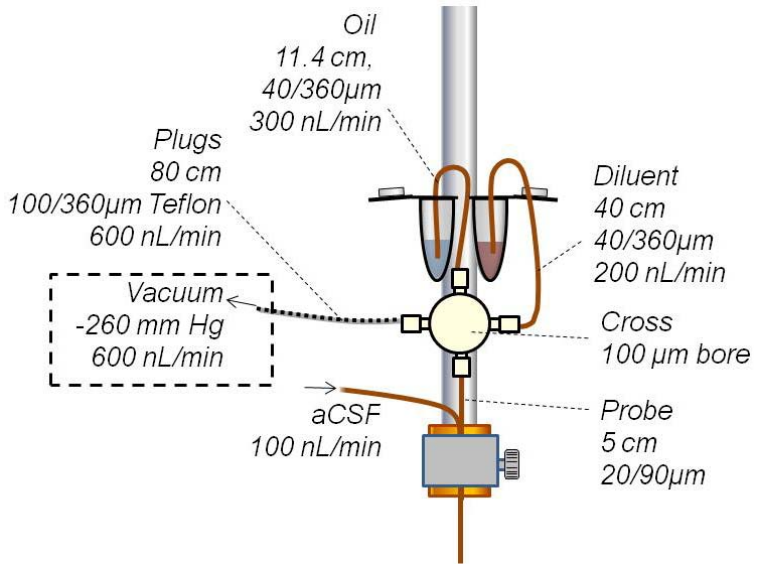

Figure 6.2. Probe assembly for millisecond temporal resolution sampling. A 5 cm probe constructed of 20 µm inner diameter, 90 µm outer diameter (20/90 µm) is fixed to a stereotaxic probe holder (1770, David Kopf, Tujunga, CA). The probe outlet is connected to the cross. Water and oil are placed in vial reservoirs affixed to the holder and feeding via capillaries as shown to the cross. Capillary dimensions are written as ID/OD.

Proposed Probe Assembly for Sub-Second Temporal Resolution Sampling

The specifications for a proposed probe capable of sub-second temporal resolution is shown in Figure 6.2. This assembly utilizes a reduced probe length and a higher sampling flow rate (100 nL/min) than previously utilized (Chapter II and III), as well as a water diluent. The probe is a polyimide-encased design is constructed of 20 µm bore, 90 µm outer diameter capillaries (as described in Chapter III and IV) with a length of 5 cm. The probe inlet is connected to a syringe pump to supply "push" flow, whereas the outlet is connected to a 100 µm bore cross (C360QXPK4, Valco, Houston, TX). Connected to the cross is a diluent inlet capillary (40 cm, 40 µm ID) which will supply water from a reservoir at 200 nL/min. The oil inlet to the cross consists of 11.4 cm of 40 µm bore capillary placed in a reservoir of 50:1 (vol:vol) perfluorodecalin:1,1,2,2-perfluoro-1-octanol ("oil"). The outlet of the cross is 80 cm of 100 µm bore Teflon

tubing, which will store 10 min of ~1.7 nL plugs collected at 3 Hz. Required vacuum will be approximately -260 mm Hg (plugs may exhibit additional flow resistance and exact vacuum will be determined empirically).

Temporal resolution of this probe is predicted to be 0.6 s, corresponding to 2 plugs. This rise time is limited by inlet dispersion, as shown in Figure 6.1. By replacing the water diluent with a reagent, plugs collected can be adapted to different assays. This requires a simple calculation to adjust the flow resistance of the reagent inlet. For example, a 1:1 (vol:vol) acetonitrile:water diluent containing a stable isotope internal standard for mass spectrometry (Chapter III) has a lower viscosity than water (0.77 cP instead of 0.89 cP at 25°C), therefore an inlet length of 46 cm could be used instead of 40 cm to provide the 200 nL/min makeup flow.

Silicon Microfabricated Push-Pull Probes

A method for improving spatial resolution and reducing tissue trauma of low-flow push-pull perfusion is to utilize silicon microfabricated probes. Silicon is an attractive substrate for fabrication as a variety of lithographic processes have been developed for its processing and shaping[4, 5]. Recently, a method utilizing deep reactive ion etching (DRIE) of silicon-over-insulator (SOI) wafers was developed to form channels within silicon probes. This was demonstrated as a viable way to fabricate low-flow push-pull probes.

Briefly, a series of holes were etched to the desired channel depth within the silicon neural probe by DRIE. Isotropic reactive ion etching was utilized to widen the bottom of the holes until they connected into a channel (~20 μm ID), and the top of the probe was sealed using polysilicon. These probes were 11 mm long and, within 5 mm of the tip, only 80 μm in diameter as shown in Figure 6.3.

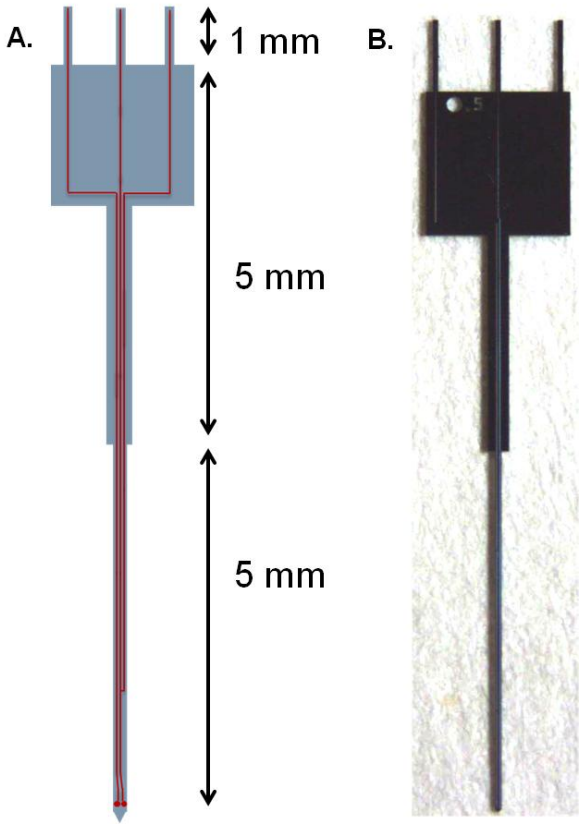

Figure 6.3. Probes were microfabricated to a total length of 11 mm. This design incorporates a third channel for generation of plug samples within the probe (A) for high temporal resolution. (B) Photograph of a microfabricated low-flow push-pull probe.

Preliminary experiments have demonstrated successful probe operation within the striatum of anesthetized rats. Fractions collected at 20 min intervals were analyzed using benzoyl chloride derivatization and liquid chromatography-mass spectrometry, measuring 17 analytes[6] with approximately 100 μm spatial resolution. Details of probe fabrication, use and operation, and *in vivo* measurements results are provided in Appendix C. To improve on the operation of these probes, microfabrication allows a number of modifications including within-probe droplet generation (shown in Figure 6.3A) and addition of multiple push-pull orifices.

Incorporation of segmented flow within the microfabricated tee greatly reduces within-probe dispersion. This is because the probe inlet length pre-segmentation can be as small as a few hundred μm. For example, if the distance between the inlet and plug generating tee was 1 mm and the channel was 20 μm ID, flow would experience only 100 ms of dispersion within this inlet. As discussed above, strategies will need to be employed to facilitate manipulation of sub-second plugs. An example of a strategy would be to etch plug channels to a wider diameter (for example, 40 μm) after the plug generating tee in order to facilitate plug transport, and incorporate a diluent channel to add a makeup flow to plugs just prior to exiting the probe.

Microfabricated probes would be beneficial as a tool for mapping concentration gradients between small brain nuclei, as described in Chapter IV. Whereas experiments in Chapter IV only sampled one region at a time per animal, microfabricated probes could incorporate additional push-pull orifices at different depths. These can be fabricated by using lithography to insert two additional channels and two additional connectors at the top of the probe. While some neurotransmitters were observed to be significantly different at basal levels between 200 μm distances, such as within the ventral tegmental area (VTA) and above the VTA, it is likely these regions respond differently when an animal is administered a drug or conducts a behavior. Simultaneous monitoring of a rat both within the VTA and above the VTA during presentation of a food stimulus would provide a validation of this strategy as unexpected appetitive events are known to produce dopamine release within the VTA[7]. Additionally, high temporal resolution measurements of glutamate (Chapter II) by droplet-based methods would indicate if the large glutamate variability in the VTA (Chapter IV) correlates with

behaviors. Other features which could be incorporated on a Si microfabricated probe include microinjector channels for local application of drugs and microfabricated electrodes for local stimulation of neuronal release.

Improved Temporal Resolution of Benzoyl Chloride-Labeled Samples

In Chapter IV, the utility of benzoyl chloride derivatized samples for mapping multiple neurotrasnmitters with high spatial resolution was demonstrated with 13 analytes quantified simultaneously. Though a slower time resolution than enzyme assays or CE, the multianalyte capability of this technique makes measurements highly informative. Despite the small sample volume utilized (1 μL), pM concentrations of neurotransmitters could be quantified within the brain, an advantage of the high sensitivity of the LC-MS method utilized[6]. Temporal resolution could be enhanced by further reducing sample volumes. For example, 2 minute temporal resolution could be accomplished by collecting and storing 100 nL fractions, which could then be derivatized and analyzed. These small sample volumes may be collected and transferred using narrow bore capillaries as before (for example, 4.6 cm of 75 μm bore capillary), but microfluidic techniques may facilitate handling and prevent evaporation.

Microfluidic plugs of ~100 nL volume collected at the probe outlet would be a potential way of handling these small fractions. Previous work has demonstrated 160 nL plug collection and storage with microdialysis effluent (~ 3 minute resolution) using 250 μm bore Teflon tubing[8], indicating the utility of large plugs. Plugs could be derivatized using a reagent addition tee, which can be fabricated within Teflon tubing of these large sizes in a similar fashion to that described in Chapter II. Following derivatization with benzoyl chloride, a syringe pump could be used to transfer plugs into vials prior to

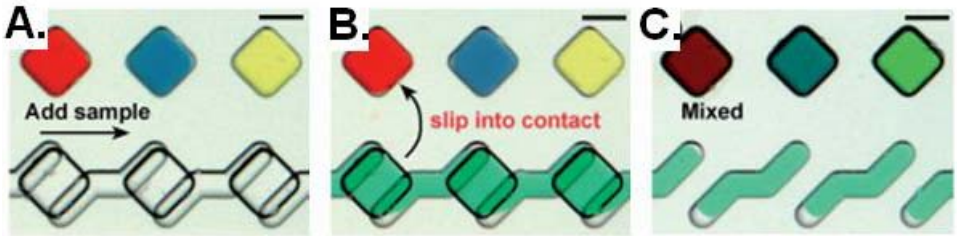

Figure 6.4. Operation of a Slip Chip for collection and derivatization of nL samples. (A) Sample is loaded into microwells. (B) Sample microwells are slid into contact with reagent wells. (C) Reagent wells are isolated, containing discrete fractions. Scale bar is 250 μm. (Adapted from [9] with permission of the Royal Society of Chemistry).

injection on the mass spectrometer, or plugs could be injected via an injection valve directly into a chromatography column for LC-MS analysis.

One concern is the presence of oil and whether it would interfere with retention of analytes on a chromatography column. A benefit of benzoyl chloride derivatized neurotransmitters is their chemical stability[6]. Should this problem present, plug samples could be transferred to vials, dried to remove oil, then redissolved in sample solvent[6].

Another possibility for collecting, storing and derivatizing 100 nL fractions is a microchip known as a "Slip Chip"[9, 10]. This device utilizes microchannels etched onto glass slides to store sample fractions in etched wells, and these fractions can be addressed by sliding the unbonded layers of the chip[9]. As glass microchips are non-gas permeable, this is an attractive substrate for a vacuum-based push-pull system and may provide more facile manipulation. Figure 6.4A-C illustrates how a Slip Chip is operated. Push-pull perfusate could be pulled through a chip of 200 nL wells until all are filled, and the chip "slipped" to add benzoyl chloride reagent to each well. A design modification with one vertical sample channel could allow sample wells to be individually filled by slipping the chip horizontally, which may be advantageous for preventing Taylor dispersion.

Following derivatization, an individually addressable transfer channel could be utilized to transfer each sample to an autosampler vial, or directly into an LC instrument.

While the microbore (1 mm diameter) chromatography column utilized for the experiments within Chapter IV provided nM to pM sensitivity for analytes[6], switching to a capillary LC column may further enhance sensitivity. The inner volume of a capillary column is much smaller; therefore, well-retained analytes can be pre-concentrated by injecting high sample volumes relative to column volume. This could provide excellent sensitivity for monoamine and catecholamine neurotransmitters, despite sub-μL sample volumes.

Pharmacological Studies of Metabolism with 200 μm Resolution

Multianalyte monitoring with low-flow push-pull perfusion revealed differences in metabolite and neurotransmitter concentrations on the sub-mm scale, as discussed within Chapter IV. Though this provided indirect evidence of different metabolic routes for dopamine within different brain regions[11, 12], these differences cannot be well-established without identifying the specific transporters and enzymes involved. Researchers have identified the norepinephrine transporter as a major source of dopamine uptake within the cortex and accumbens shell[13]. It is unclear as to what the fate of dopamine is following this reuptake, whether dopamine is metabolized, released, or converted to norepinephrine[13].

Low-flow push-pull perfusion is well suited to elucidating these questions. Discrete areas of the accumbens shell can be monitored as within Chapter IV, but while infusing ^{13}C-dopamine. The metabolic fate of ^{13}C-dopamine can be examined by measuring its ^{13}C-metabolites, as well as^{13}C-norepinephrine and the ^{13}C-metabolites of

norepinephrine (normetanephrine and 3-methoxy-4-hydroxyphenyglycol). As norepinephrine transporter inhibitors are effective antidepressants, this may provide insight as to their mechanism[13, 14]. Norepinephrine reuptake inhibitors such as desipramine or nisoxetine would be co-infused to examine their effects on dopamine metabolism[15].

Conclusions

The capabilities of low-flow push-pull perfusion measurements at fast temporal and fine spatial resolution can be further developed, and probes can be used for novel studies not possible by other techniques. By optimizing probe segmented flow geometries, probe flow rates, and adding a makeup flow, collection and storage of ms temporal resolution plugs can be readily achieved. Silicon microfabricated probes are a viable way to reduce inlet dispersion, probe size, and integrate features such as multi-depth sampling, microinjectors and electrodes. As the benzoyl chloride LC-MS assay provides excellent multianalyte capabilities, its temporal resolution can be reduced 10-fold by improved sample handling, and this assay could be utilized for differences in dopamine uptake and metabolism on the sub-mm scale using ^{13}C-labeled dopamine.

References

(1) Robinson, D. L.; Hermans, A.; Seipel, A. T.; Wightman, R. M. *Chem. Rev.* **2008**, *108*, 2554-2584.
(2) Kottegoda, S.; Shaik, I.; Shippy, S. A. *J. Neurosci. Methods* **2002**, *121*, 93-101.
(3) Polikov, V. S.; Tresco, P. A.; Reichert, W. M. *J. Neurosci. Methods* **2005**, *148*, 1-18.
(4) Prem, P.; Kazuo, S.; Sudhir, C. *Journal of Micromechanics and Microengineering* **2007**, *17*, R111.
(5) Wise, K. D. *Sensors and Actuators A: Physical* **2007**, *136*, 39-50.
(6) Song, P.; Mabrouk, O. S.; Hershey, N. D.; Kennedy, R. T. *Anal. Chem.* **2012**, *84*, 412-419.

(7) Horvitz, J. C. *Neuroscience* **2000**, *96*, 651-656.
(8) Song, P.; Hershey, N. D.; Mabrouk, O. S.; Slaney, T. R.; Kennedy, R. T. *Anal. Chem.* **2012**, *84*, 4659-4664.
(9) Du, W.; Li, L.; Nichols, K. P.; Ismagilov, R. F. *Lab Chip* **2009**, *9*, 2286-2292.
(10) Liu, W.; Chen, D.; Du, W.; Nichols, K. P.; Ismagilov, R. F. *Anal. Chem.* **2010**, *82*, 3276-3282.
(11) Bast, T.; Diekamp, B.; Thiel, C.; Schwarting, R. K. W.; Gunturkun, O. *J. Comp. Neurol.* **2002**, *446*, 58-67.
(12) Roffler-Tarlov, S.; Sharman, D. F.; Tegerdine, P. *Br. J. Pharmacol.* **1971**, *42*, 343-351.
(13) Carboni, E.; Silvagni, A. **2004**, *16*, 121-128.
(14) Lin, Z.; Canales, J. J.; Bjorgvinsson, T.; Thomsen, M.; Qu, H.; Liu, Q.-R.; Torres, G. E.; Caine, S. B.; Shafiqur, R. *Progress in Molecular Biology and Translational Science* **2011**, *98*, 1-46.
(15) Li, M.-Y.; Yan, Q.-S.; Coffey, L. L.; Reith, M. E. A. *J. Neurochem.* **1996**, *66*, 559-568.

Appendices

Appendix A

Practical Considerations for Experimental Designs for Low-Flow Push-Pull Perfusion Sampling

Introduction

Since the first demonstration of low-flow push-pull perfusion in 2002, several systems and methods for performing such experiments have been described[1-9]. These records include descriptions of the protocols necessary to successfully implant and operate these probes. Similar accounts have been provided in Chapters II, III and IV of this work. A number of salient details of techniques that were employed to improve reliability of results, but which did not fit readily into these chapters, have been included in this section. The objective of this appendix is to document in detail probe fabrication, experimental procedures, as well as some methodological considerations and apparatus to aid future researchers to use low-flow push-pull perfusion. In addition, troubleshooting aspects will be discussed.

Considerations of Probe Designs

In the experiments described in this work, it was observed that bleeding at the tip of the probe correlated with the probe becoming occluded while sampling. Therefore, probes were designed to reduce tissue disruption. In the course of these experiments, two different probe designs were used: the first consisting of two side-by-side capillaries encased in a 27 gauge needle and the second of two capillaries encased in a polyimide

sheath. Inserting a pointed needle into tissue was found to improve reliability relative to an equal size, blunt probe (N. Cellar, personal communication). Conversely, polyimide-encased push-pull probes had a blunt tip by design, but reduced risk of tissue trauma and bleeding by maintaining a diameter of only 220-240 μm (versus 400-450 μm[1, 7, 8]).

Designs which further minimize probe size while maintaining a pointed geometry may prove beneficial. For example, four out of four attempts to sample with silicon-microfabricated probes of 80 μm diameter and a pointed tip (described in Appendix C) were successful, with no clogging or bleeding during implantation.

Tools for Probe Fabrication

Probe fabrication required being able to grip capillaries for two purposes: precise manipulation, and applying tensile and compressive force. Tapered extra-fine stainless steel forceps (5669A32, McMaster-Carr, Santa Fe Springs, CA) were suitable for gripping and manipulating capillaries with microscopic precision, such as threading a 90 μm outer diameter (OD) capillary into a 150 μm inner diameter (ID) capillary lumen. Any imperfections in the forceps which may interfere with holding capillaries can be corrected by slightly polishing the clasped tips of the forceps with a rotary tool (Dremel, Mount Prospect, IL). Applying force to capillaries was challenging as these forceps could easily damage 90 μm OD capillaries. Therefore, larger general purpose forceps (such as 7379A21, McMaster-Carr) with a layer of labeling tape padding on the tips (Fisherbrand 0.75 inch width, Fairlawn, NJ) were utilized for applying force.

Working with probes necessitated careful observation during fabrication and use. A binocular microscope was utilized during fabrication (SMZ745, Nikon Instruments, Melville, NY). During sampling experiments, a microscope was impractical due to size

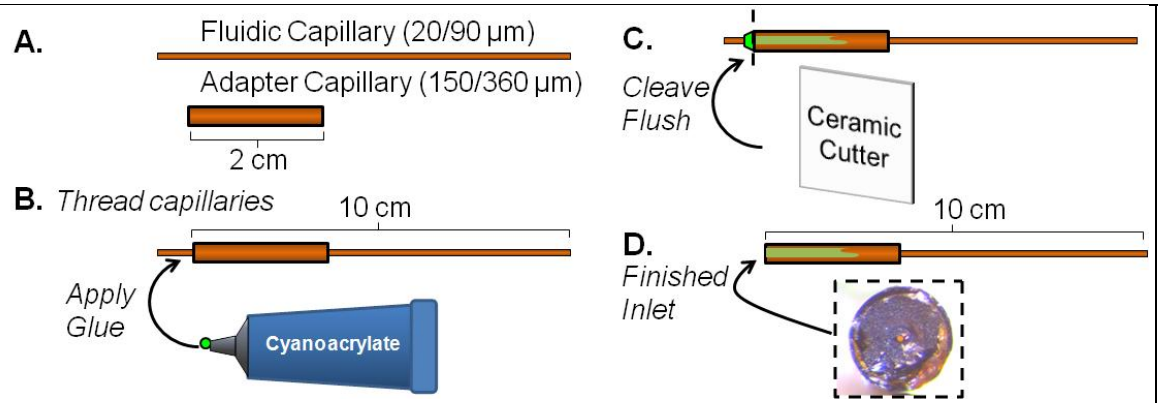

Figure A.1. Inlet capillary fabrication for needle-encased probes. (A) Capillaries were cut for probe inlets (~15 cm for 20/90 µm capillary). (B) The 20/90 µm capillary was inserted through the adapter capillary, with ~1 cm protruding from one side. Cyanoacrylate was applied to fill the space between the capillaries without coating the sides of the adapter capillary, and length was cut to 10 cm as shown. (C) A ceramic cutter was then used to cleave the inner capillary and excess cyanoacrylate from the end of the adapter capillary. (D) After cleaving, the surface of the adapted capillary end was flat, with cyanoacrylate filling the gap between inner and outer capillaries.

constraints; hence a jeweler's loupe magnifying glass (10× or 20× magnification) was used.

Probe Fabrication –Needle-Encased Probes

For purposes of temporal resolution and backpressure (discussed in Chapter II), 20 µm ID, 90 µm OD (abbreviated 20/90 µm) capillaries were utilized for probe fabrication. These capillaries were adapted for commercially available 360 µm fittings by gluing a 2 cm 150/360 µm capillary over one end, as shown in Figure A.1. Cyanoacrylate glue (E-Z Bond, Laguna Niguel, CA) was used to both fasten the adapter in place and fill the space between the inner and outer capillaries. A ceramic cutter allowed both the cyanoacrylate and inner capillary to be cut flush with the adapter capillary, as shown in Figure A.1D. The flat side of the capillary cutter was rubbed against the tip to smooth any protruding material not removed by cutting.

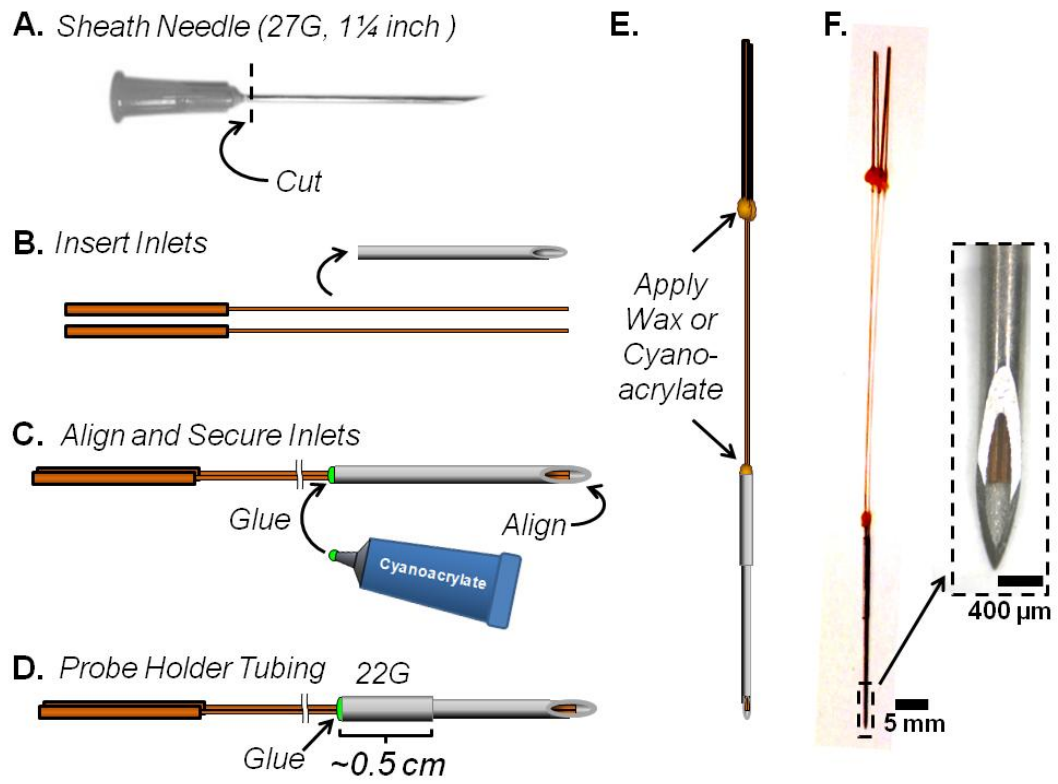

Figure A.2. Fabrication of needle-encased probes. (A) Sheath needles were prepared by removing the hub from commercial hypodermic needles. (B) Two probe inlet capillaries (with adapters) were inserted into the needle sheath. (C) Probe capillaries were aligned and fixed in place with cyanoacrylate. (D) To facilitate mounting to the stereotax probe holder, a 0.5 cm length of hypodermic tubing was slid over the needle sheath as shown, and fixed with cyanoacrylate. (E) Wax or cyanoacrylate was applied to protect inner capillaries from damage where they enter outer capillaries or needles. (F) Photograph of completed probe, showing alignment of probe capillaries.

Probes were fabricated using 27 gauge hypodermic needles (1¼ inch, BD, East Rutherford, NJ). These needles were cut using a rotary tool to remove the hub (Figure A.2A). Inner edges of the cut needles were opened and deburred using the tip of another needle. Two capillaries with adapters were then inserted through the needle (Figure A.2B) and aligned with each other and the center of the needle bevel (Figure A.2C). Cyanoacrylate was applied to fix capillaries to the needle (Figure A.2C). For facilitating the attachment of probes to the stereotaxic holder (1770, David Kopf, Tujunga, CA), a 5 mm length of 22 gauge hypodermic tubing (Amazon Supply, Seattle, WA) was placed

over the hypodermic tubing and secured with cyanoacrylate (Figure A.2D). The 22 gauge tubing was at least 1 cm from the probe tip and therefore did not enter the tissue on implantation.

One practical limitation of capillary-based sampling probes is that the inner capillary is easily broken where it concentrically enters another capillary or a hypodermic tubing. This problem was corrected by applying a small amount of wax (Sticky Wax, Kerr, Orange, CA) or cyanoacrylate to these junction points (Figure A.2E). A completed probe is shown in Figure A.2F.

Probe Fabrication – Polyimide-Encased Probes

A second style of probe was developed to reduce probe size and to be compatible with cannulae for awake animal experiments. These probes utilized 20/90 μm capillaries like the needle-encased probes, but replaced the needle sheath with polyimide tubing (180 μm ID, 220 μm OD, Amazon Supply, Seattle, WA). The fabrication procedure is outlined in Figure A.3. First, the polyimide tubing was cut to length (3 cm) using a razor blade, and the probe capillaries (~15 cm of 20/90 μm capillary) were cut with a ceramic cutter. These capillaries were then threaded through the polyimide tubing (Figure A.3B). To facilitate inserting the capillaries through the polyimide, the polyimide was gently squeezed with forceps to make its shape slightly oval. The polyimide was centered over the fused silica capillaries, and thixotropic epoxy (353NDT, Epoxy Technology, Billerica, MA) applied to the end of the capillaries to be covered with the polyimide (Figure A.3C). The polyimide was then slid over the epoxy (Figure A.3D). This thixotropic epoxy was selected based on its non-flowing properties: the epoxy remained

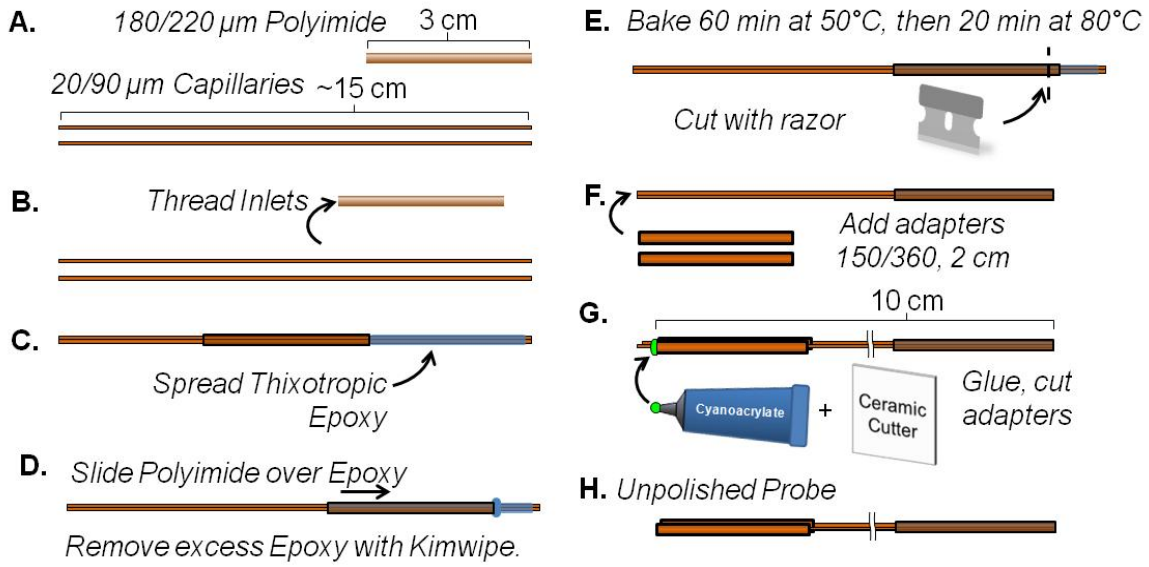

Figure A.3. Fabrication of a polyimide-encased push-pull probe**.** (A) A 3 cm length of polyimide was cut to length with a razor, and two probe capillaries (without adapters) were prepared. (B) Probe capillaries were threaded through the polyimide. (C) Thixotropic epoxy was coated on the probe capillaries, and (D) the polyimide was carefully slid over the epoxy. Excess epoxy was gently wiped from the outside of the polyimide, and (E) the capillary was baked at low temperature until the epoxy was cured. A razor was then used to cut flush the capillaries, epoxy and polyimide. (F) Capillary adapters were next applied to the probe capillaries and aligned to a total probe length of 10 cm. (G) These were glued with cyanoacrylate and cleaved with a ceramic cutter (as in Figure A.1) to yield an unpolished, bare polyimide probe (H).

within the space between the capillaries and polyimide during curing and would not clog the probe capillaries.

When removing excess epoxy from the surface of the polyimide, a Kimwipe tissue (Kimberly Clark, Roswell, GA) was very gently passed over the polyimide surface. It was important not to apply any pressure to the sides of the polyimide as this would create long air pockets, which would become orifices in the surface of the probe tip. The probe was cured at a relatively low temperature (60 min at 50°C, then 20 min at 80°C). If the probe epoxy was heated too quickly, it was found that air bubbles in the epoxy would expand, creating voids. A razor blade was then used to cut flush the capillaries, polyimide and epoxy to form the probe tip (Figure A.3E). Small air bubbles did not

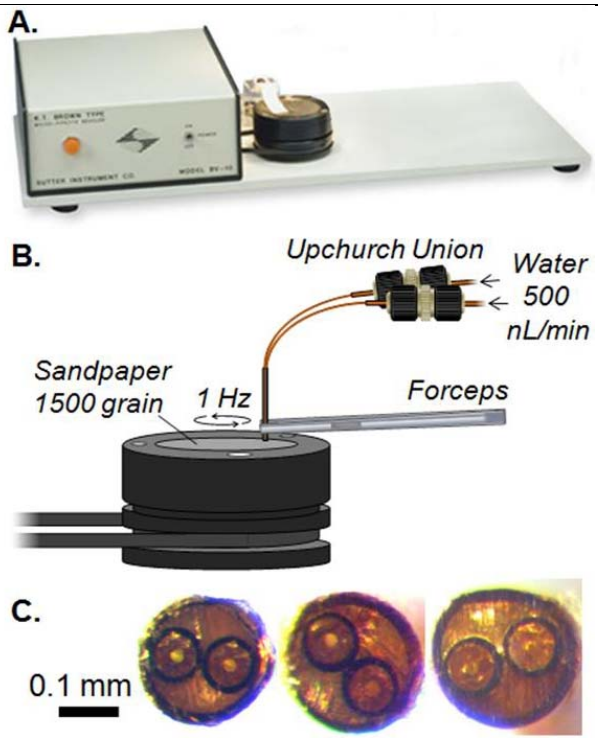

Figure A.4. Polishing polyimide-encased probes. (A) 1500-grain wet sandpaper was applied to a capillary beveler for polishing. (B) The sandpaper was pre-wetted with water and the probe backflushed with water at 500 nL/min. Forceps were used to gently hold the polyimide-encased probe tip to the rotating sandpaper surface. (C) Examples of polished probe tips.

affect the probe if they were not at the surface of the tip of the probe, therefore the location of the cut was selected to avoid any air bubbles.

Adapters (2 cm, 150/360 μm) were added to the probe capillaries after cutting the probe tip (Figure A.3F). Probe length was measured (10 cm, Figure A.3G) and the adapters glued with cyanoacrylate and cut as in Figure A.1. As with the needle-encased probes (Figure A.2E), wax or cyanoacrylate was applied to prevent the probe capillaries from breaking.

Probes were polished to create a smooth, uniform sampling tip. For polishing, a BV-10 electrode beveler (Sutter Instruments, Novato, CA) was utilized, as shown in Figure A.4A. 1500-grain sandpaper was placed on the polishing surface of the beveler and was pre-wetted with water. To prevent clogging, the probe was backflushed with

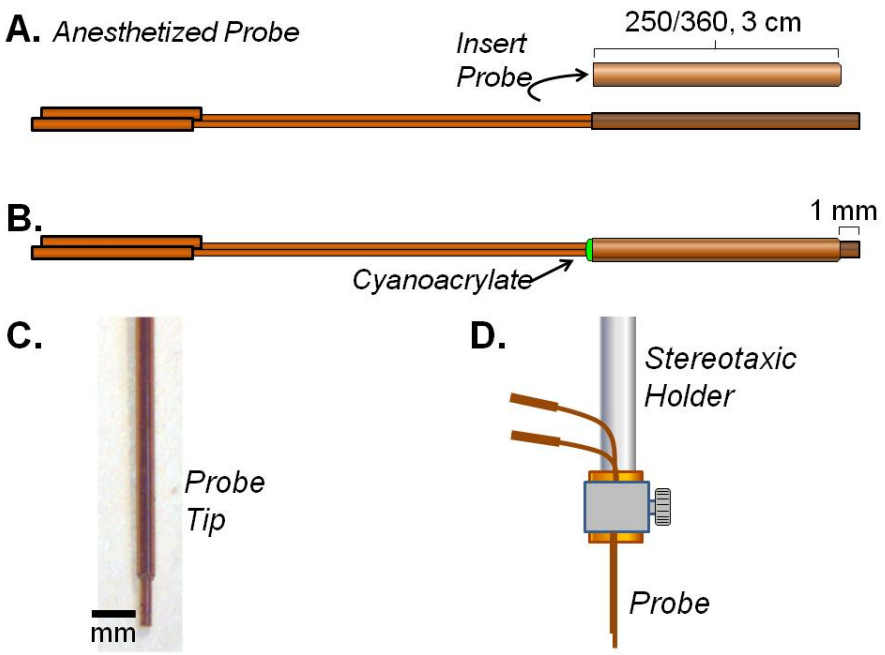

Figure A.5. Preparing polyimide-encased probes for anesthetized animals. (A) The probe was inserted through a 3 cm length of 250/360µm capillary to provide stiffness, and (B) this capillary was glued to leave 1 mm of probe protruding from this capillary, as shown in (C). (D) The probe was fixed vertically to the mounting block (tan color) of the stereotaxic holder first with an ~1 cm piece of labeling tape (not shown), then with the metal holder ring.

water at 500 nL/min through each capillary using a syringe pump. To polish, forceps were used to gently hold the probe tip to the sandpaper while the sandpaper rotated at 1 Hz (Figure A.4B). Probes were polished to achieve a flat surface. Excess polyimide was removed by placing the probe on a glass surface under a microscope and trimming with a razor blade. Examples of polished probe tips are shown in Figure A.4C.

Polyimide-Encased Probes for Anesthetized Experiments

Polyimide-encased probes were flexible and therefore required reinforcement before implantation to the brain. For anesthetized experiments, polyimide-encased probes were threaded concentrically through a 3 cm length of 250/360 µm capillary (Figure A.5A). A 1 mm length of probe protruded from the tip of this fused silica capillary as shown in Figure A.5B. This length was selected to minimize tissue

disruption near the sampling site while avoiding probe deflection. The capillary was cemented in place with cyanoacrylate. The finished probe tip is shown in Figure A.5C. These probes were placed in a stereotaxic holder (1770, David Kopf, Tujunga, CA) as shown in Figure A.5D. To facilitate mounting and prevent the probe from sliding, an ~1 cm piece of labeling tape (not shown) was used to affix the probe to the holder before fastening the metal ring.

Polyimide-Encased Probes for Awake Experiments

Probes utilized for awake experiments were fabricated by the same procedure as the anesthetized polyimide-encased probes (Figure A.3), but with different tubing geometries. Instead of 20/90 μm capillaries, 40/100 μm capillaries were utilized. The probe capillaries were initially cut to ~65 cm length and a 3 cm, 200/240 μm polyimide sheath applied to one end of the capillaries (Figure A.3A-D). After filling with epoxy, curing and cutting as before, the capillary adapters were added to provide a probe length of 60 cm (Figure A.3G). Because of the larger ID of the probe capillaries, a backflushing flow rate of 2 μL/min, rather than 500 nL/min, was utilized during polishing (Figure A.4).

For awake experiments, cannulae were used so as to allow probes to be acutely implanted in awake, freely moving rats. The flexibility of polyimide-encased probes made them compatible with commercially available cannula systems (Plastics One, Roanoke, VA). The probe holders utilized were model C312ICP/O/SPC with no internal hypodermic tubing. Cannulae were model C312GP/O/SPC (21 gauge) with 8 mm length. Stylets (or obturators) were model C312DC. Before use, stylets were inserted through a cannula and cut flush with the tip of the cannula using wire cutters.

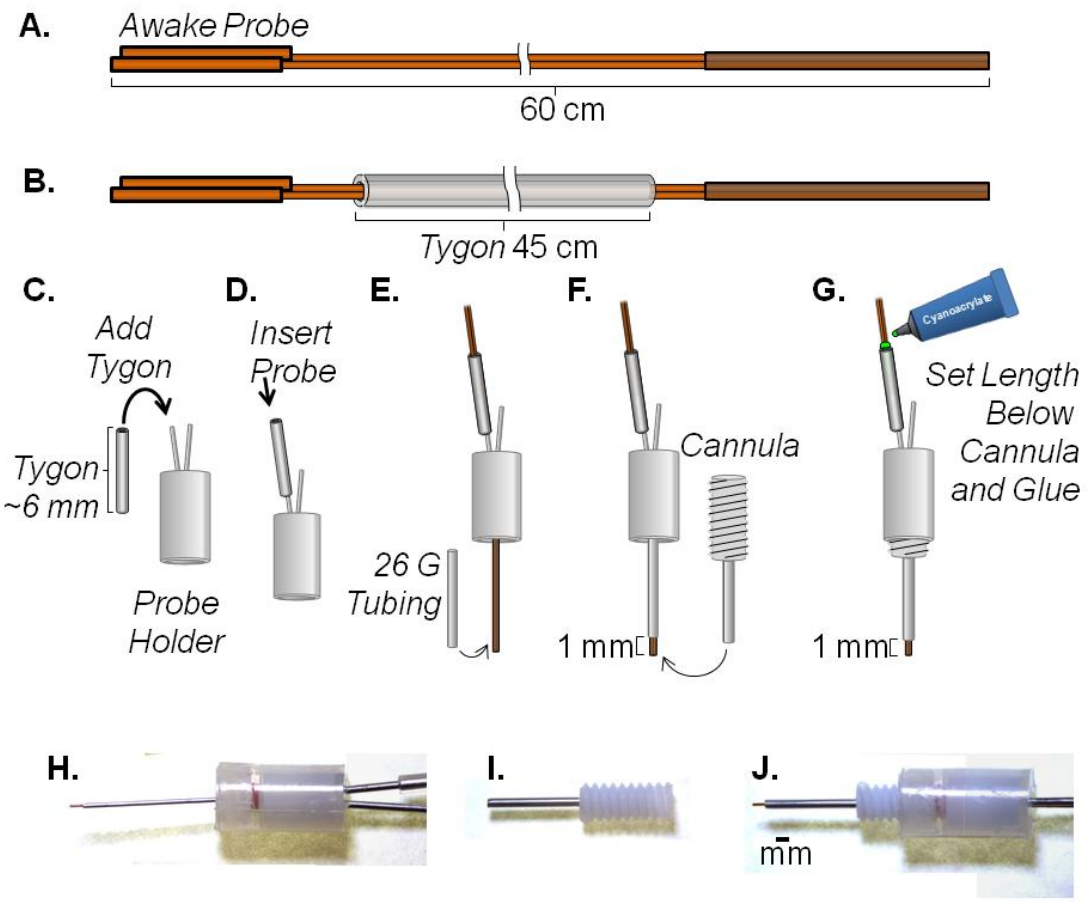

Figure A.6. Assembly of polyimide-encased probes for awake animals. (A) A polished probe was fabricated as in figures A.3 and A.4 but using 40/100 µm capillaries to a length of 60 cm, and 200/240 µm polyimide. (B) The probe was threaded through 45 cm of Tygon tubing. (C) An ~6 mm piece of Tygon was applied to an inlet of the probe holder and (D) the probe was inserted through this tygon. (E) 26G hypodermic tubing was threaded over the probe tip and carefully glued, leaving 1 mm of probe protruding. This was carefully secured with cyanoacrylate (not shown). (F) The cannula was connected to the probe holder and (G) the probe was glued to the Tygon tubing above the probe holder at a length where 1 mm of probe (and no 26G tubing) protruded from the cannula. Micrographs show examples of (H) completed probes, (I) a cannula, and (J) an assembled probe and cannula.

A detailed protocol for assembling the cannula system for awake *in vivo* sampling is shown in Figure A.6. After fabricating a push-pull probe, it was threaded (Figure A.6B) through a 45 cm length of 0.50/1.52 mm Tygon tubing (St. Gobain, Akron, OH). An ~6 mm piece of the Tygon tubing was placed over one of the connector inlets of the probe holder and the probe threaded through this inlet (Figure A.6C-D).

To fill the space between the probe and stylet during insertion (minimizing deflection), a 26 gauge hypodermic needle (1/2 inch, Precision Glide, BD, East Rutherford, NJ) was placed over the tip of the probe (Figure A.6E). This needle was prepared by removing the hub with a rotary tool, as in Figure A.2A. The blunt end of this needle faced the tip of the probe, and was glued with cyanoacrylate to allow 1 mm of probe to protrude past the needle (Figure A.6F). The probe was then threaded through a cannula (Figure A.6F). After fastening the cannula, the length of the probe was set to 1 mm past the tip of the cannula with none of the 26 gauge needle protruding, and it was secured to the ~6 mm length of polyimide with cyanoacrylate (Figure A.6G). An example of a completed probe is shown in Figure A.6H. A cannula is shown in A.6I and the assembled probe and cannula in A.6J.

Segmented Flow Sampling of Neurotransmitters

For high-temporal resolution experiments with either needle-encased (Chapter II) or polyimide-encased (Chapter III) probes, segmented flow-based samples were collected. To generate these samples, commercially available 100 μm bore tees (C360QTPKG, Valco, Houston, TX) were utilized. These tees were selected because they were practical (50 μm bore tees clogged frequently) and did not compromise temporal resolution at 50 nL/min flow rates (unlike 150 μm bore tees).

To place the droplet-generating tee in close proximity to the brain and provide a stable mounting point, the tee was fixed to the probe holder just above the probe. A diagram of the placements of sampling hardware is shown in Figure A.7. The oil (50:1 vol:vol of perfluorodecalin:1H,1H,2H,2H-perfluoro-1-octanol) was placed in a vial and was attached to the probe holder just above the tee. The vial and the base of the tee were

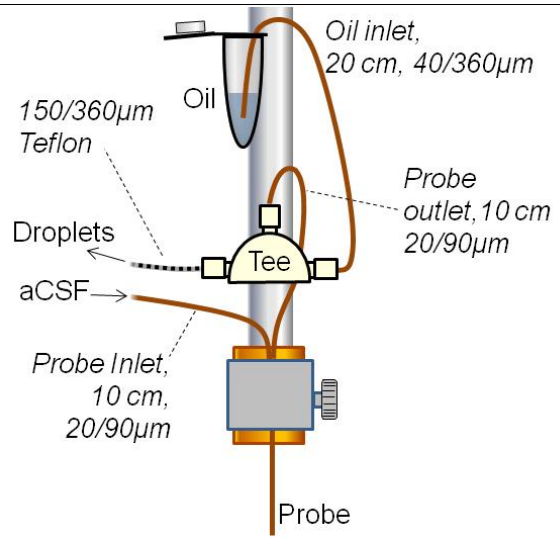

Figure A.7. Assembly of probes for collecting segmented flow samples. Anesthetized probes were attached to a stereotaxic probe holder. The droplet-generating tee (100 µm ID) and oil reservoir vial were connected to the holder above the probe using tape (not shown). The probe outlet, oil inlet and droplet outlet were connected to the tee as shown, and vacuum applied to the Teflon (-150 mm Hg) to provide pull flow.

secured to the holder using tape (not shown). To balance flow rates of aqueous and oil phases (nominally 50 nL/min aqueous, 70 nL/min oil), a 20 cm length of 40/360 µm capillary was used for oil, and a 10 cm length of 20/90 µm capillary for aqueous (the probe capillary). Chapter II describes the temporal resolution and backpressure tradeoffs of different probe inlet geometries.

Plug geometry was evaluated before probe implantation by sampling a vial of aCSF. Sampling was started by applying vacuum (-150 mm Hg) to the Teflon tubing. Plugs should be capsules (non-spherical) and uniform in size. At 50 nL per minute, plugs formed nominally at 7 s intervals. It is important to monitor the segmented flow generated during sampling to quickly identify and fix any problems that could occur. Descriptions of droplet appearances during normal and problematic conditions are described below, along with troubleshooting suggestions to obtain or restore stable segmented flow.

Surgical Procedures for Anesthetized Sampling

All animal procedures were performed according to a protocol approved by the University Committee for the Use and Care of Animals of the University of Michigan. The anesthetic utilized was ketamine (65 mg/kg) with dexmedetomidine (0.25 mg/kg) administered by intraperitoneal (IP) injection. Boosters of one-third the dose of each were administered as needed. The rat brain atlas of Paxinos and Watson[10] provides instructions for how to place an animal in a stereotaxic frame, how to level the head, and where bregma and lambda are located on the surface of the skull. Bregma was used as reference for anterior/posterior and lateral measurements, and the dura (at the surface of the brain) was reference for dorsal/ventral measurements during implantation.

After first shaving, sterilizing and incising the scalp, the surface of the cranium was cleaned with a number 10 scalpel blade, revealing the suture lines. A burr hole was drilled using a 30,000 RPM rotary tool (Dremel, Mount Prospect, IL) above the sampling site. To avoid damaging the probe during implantation, an incision was made in the dura using a 27 gauge hypodermic needle (BD, East Rutherford, NJ).

Probe Implantation

During implantation, the probe inlet was disconnected from the tee and connected to the syringe pump for backflushing. Unions for connecting to the syringe pump were also taped to the probe holder at approximately the same height as the oil reservoir. The unions employed were commercially available 360 μm capillary fittings from either IDEX Health and Science (P-772, Oak Harbor, WA) or Valco (C360UPK4 or C360UPK6, Houston, TX). IDEX unions were larger and more difficult to fasten when attached to a probe holder, but were less prone to clogging than the Valco fittings.

Probes were backflushed at a high flow rate while lowering the probe (500 nL/min per capillary) to prevent occlusion, then decreased to 50 nL/min for 8 minutes of backflushing. With needle probes, the flow rate was reduced over ~40 s as described previously[9], whereas with polyimide probes, it was decreased immediately upon reaching the final depth. As probe size was minimized, backflushing was reduced to match the decrease in probe trauma (for example, with silicon microfabricated probes described in Appendix C, only 200 nL/min was used).

After 8 min of 50 nL/min backflushing, the "pull" capillary was reconnected to the plug-generating tee and vacuum applied to the Teflon tubing. In most instances, flow immediately commenced with plugs comparable to when the probe was tested in aCSF. Troubleshooting instructions for *in vivo* sampling with segmented flow are provided below.

Sampling from Awake, Freely Moving Animals

Surgical Protocol for Cannulation

As outlined above, a cannula system (Figure A.6) was utilized to allow sampling of neurotransmitters from awake, freely moving animals. A Plastics One cannula holder was purchased (1966, David Kopf, Tujunga, CA), fixed to one arm of the stereotax and a cannulae placed within this holder. As above, the rat was anesthetized and mounted into a stereotaxic frame. A burr hole was drilled above the region of interest, and was located by using bregma as a reference. Three burr holes for screws were drilled around the sampling burr hole. Three stainless steel screws were inserted into the skull, leaving the screw heads ~1 mm above the surface of the skull (0-80 x 3/32, Plastics One, Roanoke,

VA). The dura was incised as above, and the cannula was implanted to a depth of 1 mm above the target within the brain.

A mounting clip for the tether of a Raturn (Bioanalytical Systems, West Lafayette, IN) was fabricated by bending a stainless steel wound clip (340555, Harvard Apparatus, Holliston, MA) to 90° and placing it on the skull next to the cannula with one end protruding vertically. Methyl methacrylate (Teets Cold Cure Denture Material, Co-oral-ite Dental Mfg. Co., Diamond Springs, CA) was applied to the skull until the entire wound, the screws, ~1 mm of the cannula threads, and the base of the clip were covered. Care was taken to sculpt a smooth skull cap having no sharp edges and a rounded lip at the skin around the wound. After the cap cured, the cannula holder was released and a stylet secured within the cannula.

Following surgery, animals were monitored carefully, maintaining body temperature, until fully ambulatory. Atipamezole was given by IP injection (0.75 mg) as a reversal agent for dexmedetomidine, and gentamicin was given to prevent infection (0.03 mL at 100 mg/mL IP). Carpofen (5 mg/kg subcutaneous) was administered prior to surgery and 24 h after surgery for analgesia during recovery.

Probe Implantation

Immediately prior to implantation, probes were backflushed with a syringe pump to verify capillaries were not occluded, and "pull" flow was tested by connecting a 1 μL (13 cm, 100/360 μm) capillary to the probe. Fluidic connections to the probe were made with 360 μm unions from IDEX (P-772, Oak Harbor, WA) as these were the most reliable fittings tested for 360 μm connections. Flow rate was monitored by measuring

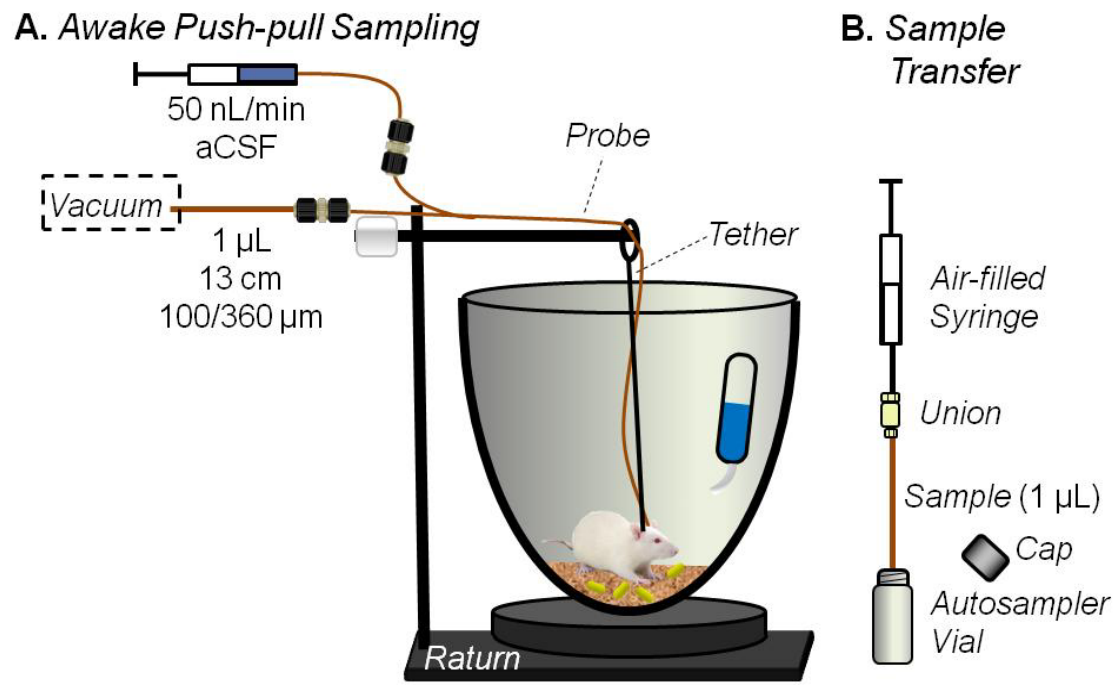

Figure A.8. Sampling from awake animals. (A) Animals were placed within a Raturn, and connections made using IDEX unions on the Raturn arm. Push flow was supplied with a syringe pump, whereas pull flow with vacuum on the outlet of a 1 µL capillary. (B) After collecting 1 µL (20 min), the collection capillary was replaced with a fresh capillary, and a syringe filled with air was used to push the sample into a conical autosampler vial.

the fill rate of the 1 µL capillary (9.4 s/mm corresponded to 50 nL/min) and vacuum was adjusted to achieve this flow rate (nominally -50 mm Hg). After testing vacuum, the "pull" capillary of the probe was connected to a backflushing syringe for implantation.

Sampling was performed by placing a cannulated rat in a Raturn, allowing free movement without tangling probe capillaries (Figure A.8). For implantation, rats were briefly anesthetized with isoflurane. The stylet was removed and cannula cleaned by applying a few drops of sterile saline and carefully reinserting and removing the stylet.

While backflushing the probe (500 nL/min aCSF per capillary) it was tightened over ~30 s. Care was taken to ensure the probe did not rotate during implantation. After tightening, backflushing flow rate was immediately reduced to 50 nL/min. The Raturn tether was connected by an alligator clip to the clip in the dental cement cap. A small

piece of duct tape was wrapped around the probe and tether clip, taking care to avoid contact with the skin or fur. After 8 minutes of backflushing, a 1 μL capillary was connected to the "pull" capillary of the probe and vacuum applied. Flow rate was monitored and vacuum adjusted as needed to maintain 50 nL/min. Fractions collected within one hour of implantation were discarded as previous work has suggested basal concentrations are unstable for the first ~30 min of sampling[1, 8].

Experimental Considerations and Troubleshooting for nL/min Fluidic Systems

Syringe Pumps and "Push" Flow

Crucial to collecting perfusate at 50 nL/min is maintaining reliable flow rates throughout the infusion (or "push") fluidics. Though such considerations may seem trivial, unstable "push" flow to the probe was found in several instances where the probe appeared to become or became occluded. Maintaining these low infusion flow rates is not difficult to achieve with commercially available components, but the system must be properly designed and assembled.

Previous work utilized microfluidic pumps to provide stable flow rates[7, 8], but our experiments utilized syringe pumps. Choice of syringe pump was not critical; Chemyx Fusion 400 (Stafford, TX), CMA 402 (Holliston, MA), or Harvard PHD 2000 (Holliston, MA) have all been used successfully, but pump stability can decrease with wear. To avoid pulsatility, 25 μL syringes (Gastight, Hamilton, Reno, NV) were employed.

Different fittings were utilized successfully during these experiments to couple syringes to capillary (360 μm OD) tubing. The most critical features of making fluidic connections were to utilize fittings with minimal internal volume (150 μm bore or smaller) and to prevent air entrapment during assembly. Stainless steel, 1/16", 150 μm

bore fittings were found to be robust and reliable for this purpose (ZU1XC, Valco, Houston, TX). Stainless steel ferrules and 1/16" OD polymeric sleeves were used within these fittings to adapt to syringes and capillary (IDEX, Oak Harbor, WA).

Choice of capillary dimensions for 50 nL/min flow rates was critical to ensure a low system volume with reasonable linear velocities through the capillaries. For example, if a 50 cm capillary length was used to connect a syringe to a probe, a 75 μm bore capillary would require 2.2 μL, corresponding to 45 minutes, to flush. A 40 μm bore capillary would require only 0.6 μL and 12 minutes to flush. For these experiments, ~50 cm lengths of 40 μm bore, 360 μm outer diameter were used reliably.

A critical step in ensuring flow stability was the complete degassing of all liquids stored cold (such as aCSF) before infusion. This was achieved by placing vials of these liquids into a 37°C bath for ~10 minutes to accelerate the warming process, or by using a sonicator. Also, incubating at room temperature for 30 minutes prior to use was likewise sufficient. Failure to do so resulted in air bubbles being generated within syringes, which were detrimental to flow stability.

A useful tool in this research for validating flow rates and stability within a system was a microfluidic flow meter. This device, used periodically to ensure system flow stability during troubleshooting (SLG1430-025, Sensirion, Zurich), revealed such non-trivial issues as defective syringe pumps and damaged fittings.

Troubleshooting in Vivo Sampling

Before implantation of any probe, both "push" and "pull" flow should be verified *in vitro* to ensure that no occlusion had occurred during probe fabrication. In the course of experiments, probe occlusion was occasionally observed. A benefit of the side-by-side

capillary probe design related to occlusion was that the push-pull capillaries were interchangeable. By switching these capillaries, flow could often be immediately resumed. In cases where alternating the capillaries did not restore flow, three causes were identified as most suspect: trapped air, syringe pump flow, and tissue trauma.

The presence of trapped air at any point within in the microfluidic system presented an occlusion risk. This was because the high air/water interfacial tension within small bore (20-40 μm) capillaries presented a significant pressure boundary. Care in making connections and degassing liquids was found to prevent this problem. However, if it occurred, fittings were flushed with aCSF to fix this issue mid-experiment.

In the event of an occlusion, verification of the syringe pump operation, as well as the lack of air bubbles within the syringes should be conducted. In our research, this problem was unlikely when aCSF was properly degassed and the connections carefully made (as described above). Since this pump was essential to continuous, reliable flow rates during an experiment, it should be considered.

The third source of occlusion, and one which could not be fixed after implantation was tissue trauma and bleeding within the brain. Care and precision was necessary when inserting probes within the brain. By minimizing probe size (described above) and inserting probes at a steady but slow rate, the likelihood of bleeding was greatly reduced. It was found to be helpful, even in unsuccessful experiments, to perform histology as this can indicate if bleeding occurred along the probe track. If bleeding was found, more care during implantation or modification of probe design should be considered.

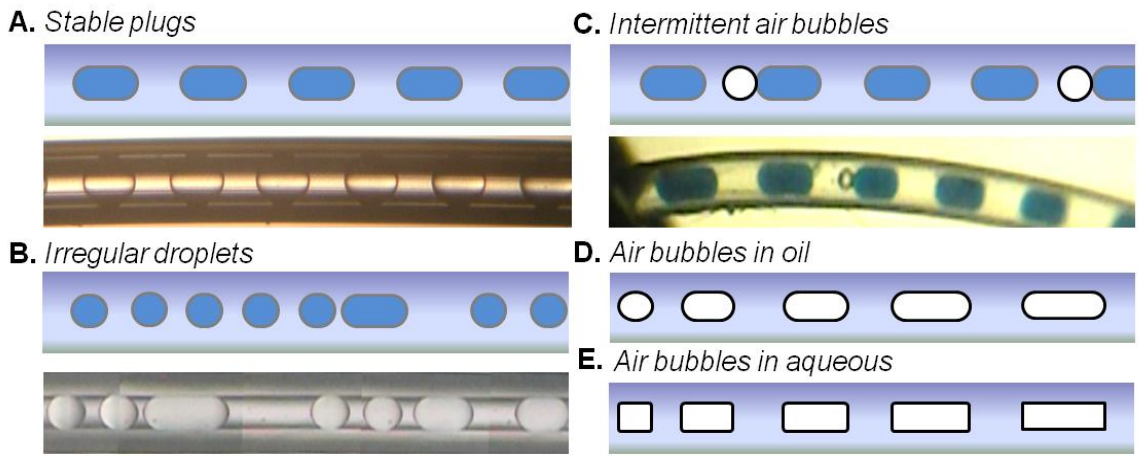

Figure A.9 Examples of segmented flow streams that are (A) optimal and (B-D) problematic. (B) Plugs which have broken into irregular droplets. (C) Air bubbles intermittently during sampling (blue dye is aqueous). (D) Air bubbles within oil (no aqueous flow). (E) Air bubbles in aqueous (no oil flow).

Evaluating and Troubleshooting Segmented Flow Sampling

Prior to implantation within an animal, it was helpful to identify and fix any problems that were occurring with segmented flow generation. Therefore, probes placed in aCSF should be tested before use. Figure A.9A illustrates an example of typical segmented flow during sampling: a reproducible train of capsule-shaped plugs. When connections issues or clogs occurred, the observable plugs may resemble the illustrations in Figures A.9B-E).

Figure A.9B demonstrates an example of unstable plug geometry that could occur during sampling. Plugs could be unstable if the Teflon tubing was poorly cut or damaged, or if the ferrule on the Teflon capillary was too tight or too loose. To remedy, the Teflon tubing was disconnected, inspected for damage (pinches or kinks) and replaced if necessary. The Teflon tubing was recut with an unused razor blade on a clean glass surface (such as a microscope slide) to obtain a smooth, flat, perpendicular end. Filling the tee with aCSF removed any trapped air, and the Teflon tubing was replaced (ensuring it protruded at least 1 mm through the ferrule before tightening). The fitting

was tightened and gentle tension applied to the Teflon to ensure it was held in place. The flow was then restarted and the ferrule slowly tightened until stable plugs were obtained. If this did not resolve the issue, the tee was replaced.

Plugs were also be monitored to ensure no air bubbles have been generated. Air bubbles interfere with sampling in a number of ways: causing plugs to coalesce, increasing backpressure (reducing flow rates), and produce unstable analyte signal during analysis. Air bubbles were distinguished from aqueous plugs by their easily visible interfaces. However, aqueous plugs in oil were less defined and required a collimated light source to observe. It was found that air bubbles might occur intermittently during sampling, as shown in Figure A.9C, or in a train of bubbles as in Figures A.9D-E. If a slow air leak happened, but otherwise sampling appeared normal (Figure A.9D), it could often be fixed by gently tightening the fittings on the Valco tee. If tightening was not effective, the Teflon tubing could be recut (as above) and the capillaries and probe replaced. If these efforts were unsuccessful, the tee could be replaced also.

In the event that only a stream of air bubbles was observed (Figure A.9D-E), determining if they are air-oil or air-aqueous bubbles was important for troubleshooting. Air-oil bubbles were noted to be capsule-shaped (Figure A.9D), whereas air-aqueous bubbles had perpendicular interfaces to the Teflon tubing walls (Figure A.9E). The presence of air-aqueous bubbles indicated that the oil capillary was still priming (when the air and aqueous segments were close to the same size). Air-oil plugs indicated a clogged or broken probe, a loose connection on the Valco tee, or a damaged Valco tee.

The last problematic condition which might be observed when testing the segmented flow was one-phase (or “continuous”) flow. If the phase was aqueous

(determined from the phase boundary at the start of the flow), the oil capillary was diagnosed as clogged or the tee damaged. A determination that the flow was oil indicated that the probe capillary was clogged or the tee damaged.

To summarize, loose fittings at the tee or clogged capillaries were most often the source of problems in segmented flow streams and could be easily adjusted to remedy these issues. However, when all else failed, a replacement tee fixed segmented flow in almost every situation. As segmented flow was in most cases optimized before implantation, plug stability issues and air bubbles seldom arose during the *in vivo* experiment.

Troubleshooting Segmented Flow in Vivo

While the troubleshooting steps outlined in the previous section described how to fix issues occurring before probe implantation, problems could also occur after implantation. For any of the scenarios described above and as shown in Figure A.9, the same troubleshooting steps would apply.

Following implantation, probe occlusion, indicated by the aqueous plugs becoming widely spaced or stopping, could occur. To fix this, the "push" syringe and its fittings were inspected for stable flow. The second backflushing syringe could also be used for "push" flow. When resetting the "push" flow did not mitigate this problem, switching the probe "push" and "pull" capillaries was helpful. With recurrent issues, backflushing the probe or increasing the "push" flow rate to 100-200 nL/min briefly (less than 30 s) could be tested cautiously. However, if stable sampling was not achieved quickly, this might indicate bleeding within the tissue, or a clogged and damaged probe. In the event of critical probe failures such as these, having backup probes which could be

implanted in the same nuclei of the other brain hemisphere (if the experimental design permitted) was beneficial. A second probe was a viable way to ensure that the animal could be used successfully for the experiment. As mentioned previously, an examination of histology (described in Appendix B) could reveal whether bleeding occurred within the tissue, which could be an indicator of any systematic issues (i.e. probe shape, or implantation rate) that require modification in the experimental design.

Conclusions

Push-pull perfusion offers the potential for widespread use as a sampling technique. Hardware and assembly requirements are no more challenging or costly than a conventional microdialysis experiment, but the nature of nanoliter per minute flow rates may present difficulties to those unaccustomed to utilizing microfluidics. With careful choice of hardware, assembly, and probe implantation procedures, researchers from different fields and expertise can realize the benefits of high spatial resolution sampling by low-flow push-pull perfusion.

References

(1) Slaney, T. R.; Nie, J.; Hershey, N. D.; Thwar, P. K.; Linderman, J.; Burns, M. A.; Kennedy, R. T. *Anal. Chem.* **2011**, *83*, 5207-5213.
(2) Slaney, T. R.; Mabrouk, O. S.; Porter-Stransky, K. A.; Aragona, B. J.; Kennedy, R. T. *ACS Chemical Neuroscience* **2012**, *In Press*.
(3) Patterson, E. E., II; Pritchett, J. S.; Shippy, S. A. *Analyst* **2009**, *134*, 401-406.
(4) Thongkhao-on, K.; Wirtshafter, D.; Shippy, S. A. *Pharmacol. Biochem. Behav.* **2008**, *89*, 591-597.
(5) Pritchett, J. S.; Pulido, J. S.; Shippy, S. A. *Anal. Chem.* **2008**.
(6) Kottegoda, S.; Pulido, J. S.; Thongkhao-on, K.; Shippy, S. A. *Molecular Vision* **2007**, *13*, 2073-2082.
(7) Cellar, N. A.; Kennedy, R. T. *Lab Chip* **2006**, *6*, 1205-1212.
(8) Cellar, N. A.; Burns, S. T.; Meiners, J. C.; Chen, H.; Kennedy, R. T. *Anal. Chem.* **2005**, *77*, 7067-7073.
(9) Kottegoda, S.; Shaik, I.; Shippy, S. A. *J. Neurosci. Methods* **2002**, *121*, 93-101.

(10) Paxinos, G.; Watson, C. *The Rat Brain in Stereotaxic Coordinates*; Academic Press: San Diego, CA, 2008.

Appendix B

Histology for Identification of Probe Placements

Reproduced with permission from Slaney, T.R. et al. ACS Chemical Neuroscience, Accepted for publication November 12, 2012. Copyright 2012 American Chemical Society.

Introduction

Histology is an important tool for neurochemical measurements. Histology allows both the probe placement to be precisely identified, and the tissue at the sampling site of the probe to be examined. This technique was extensively utilized in Chapter IV as mapped placements revealed chemical gradients in the brain extracellular compartment. In small animals such as rodents, these regions can be difficult to accurately target, making verification of placements for smaller nuclei essential. In troubleshooting, histology also revealed if tissue trauma was the source of sampling issues. The goal of this appendix is to provide a detailed description of the two histology techniques that were utilized, and how placements were identified.

Materials and Methods

Reagents and Materials

Unless otherwise specified, all reagents were purchased from Sigma Aldrich (St. Lous, MO). The paraformaldehyde solution contained 10% (wt.) of paraformaldehyde, 2.5% (wt.) sucrose and 100 mM sodium phosphate, pH 7.4. To facilitate dilution of the

paraformaldehyde, the solution was stirred overnight while heating to approximately 58°C (not exceeding 60°C). Fast Green FCF and Evans Blue were purchased from Fisher (Fair Lawn, NJ). Artificial cerebrospinal fluid (aCSF) contained 145 mM NaCl, 2.68 mM KCl, 1.01 mM $MgSO_4$, 1.22 mM $CaCl_2$, 1.55 mM Na_2HPO_4, and 0.45 mM NaH_2PO_4, pH 7.4[1].

Necropsy Procedures

All animal use was performed according to a protocol approved by the University Committee for the Use and Care of Animals. Male Sprague-Dawley rats (typically 250-350 g) were purchased from Harlan (Indianapolis, IN). At the conclusion of a sampling experiment, animals were sacrificed by barbiturate overdose (0.3 mL of 390 mg/mL sodium pentobarbital). To label the probe track, 100 nL of dye was infused at 50 nL/min using a syringe pump. The dye used was either 0.24 mg/mL Evans Blue in aCSF or a filtered, saturated Fast Green FCF solution in aCSF. The probe was then removed and the brain excised, first by decapitation, then removal of the skull. The brain was carefully placed in 10 to 15 mL of paraformaldehyde solution. Brains were then stored at ~4°C for at least 24 h before slicing.

Sucrose was sometimes used as a cryoprotectant for tissue before slicing. After fixing a brain in paraformaldehyde for at least 24 h, it was transferred to 10-15 mL of a 25% sucrose solution containing 100 mM sodium phosphate, pH 7.4. Brains were stored at least 24 h at 4°C before slicing. Sucrose was not typically used as it did not significantly affect slice quality for purposes of probe tracking.

Cryostat Tissue Slicing

Histology was performed utilizing a Leica cryostat set to -20°C (Buffalo Grove, IL). Brains were first frozen using dry ice and then mounted to a stainless steel chuck. The brain and chuck were placed in the cryostat for several minutes until completely frozen, and then were placed into the microtome within the cryostat. Disposable microtome blades were utilized (Fisherbrand, Fisher Scientific, Fair Lawn, NJ). The slice thickness was set to 60 μm, and at least every other slice was collected near the probe placement. Slices were carefully placed on tissue adherent microscope slides (Superfrost Plus, Fisherbrand, Fisher Scientific, Fair Lawn, NJ).

Manual Tissue Slicing

Another technique that was utilized for slicing was manual slicing. A fixed brain was carefully wrapped in aluminum foil and placed in a -80°C freezer for at least 5 min until frozen. This frozen brain was then placed on a large microscope slide and a razor blade was used to make coronal slices through the sampling site. Slices were approximately 0.5 mm thick, but could vary in size. Slices were not stored but were imaged immediately.

Imaging of Slices

To identify placements, brain slices were imaged using an optical microscope (SMZ745, Nikon Instruments, Melville, NY). Imaging cryostat slices required careful adjustment of slide illumination and camera settings. Best imaging of slice features were obtained using a fiber optic light for moderate intensity, off-angle illumination of the slice. As cryostat slices were translucent, black felt was placed approximately 1 cm

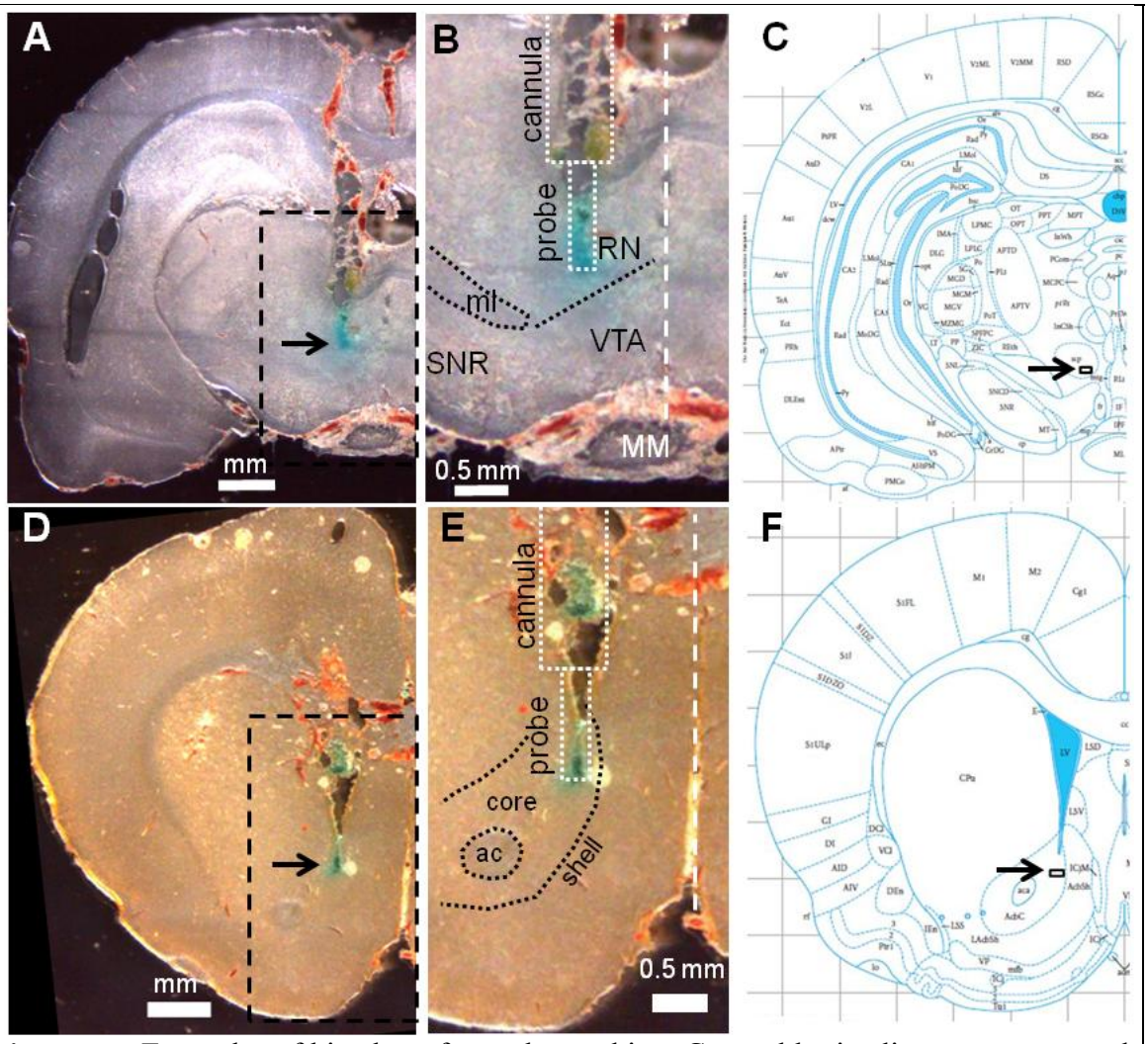

Figure B.1 Examples of histology for probe tracking. Coronal brain slices were mounted to microscope slides (A, D). Fast Green FCF stained the probe track a blue color, whereas the cannula track was inherently visible by displaced tissue (A, B, D, E). Anatomical features including white matter, ventricles, and regional boundaries provided references for identifying placements (B, E). Probe tip placements were then mapped on diagrams of coronal slices (C, F). Panels B and E include overlays of the probe and cannula locations (drawn to scale), the medial line (white), and visible features. Arrows indicate sampling sites (A, C, D, F). Abbreviations: SNR – substantia nigra reticulata; ml – medial lemniscus; MM – medial mammillary nucleus; ac – anterior commissure; RN – red nucleus; VTA – ventral tegmental area.

below the slice to remove any background light. Manual slices were imaged using the same microscope, but the greater thickness allowed flexibility in lighting as brain features were easily visible compared to cryostat slices.

Discussion

Identification of Brain Nuclei

Following slicing, tissue was imaged using a microscope. As shown in Figure B.1, white matter, lobe boundaries and ventricles were used as references to identify probe placements in the brain atlas of Paxinos and Watson[2]. The probe distance anterior or posterior to bregma was measured by determining the coronal diagram which best matched the slice of the probe placement. As a cryostat provides known slice thicknesses, anterior or posterior placement could be verified by the number of slices from a distinct feature, such as the union point of the two hemispheres of the corpus callosum (1.6 mm anterior to bregma). After nuclei were identified, measurements could be grouped by placement.

Figure B.1 reveals tissue damage dorsal of the probe tip due to the larger cannula; however, it provides verification of no bleeding or significant disruption at the sampling site (arrows). In experiments where a sampling probe became occluded, blood was occasionally observed at the tip of the probe. This information was valuable in understanding tissue damage and refining probe designs and methods. For example, with a microfabricated probe of 80 μm diameter, no bleeding or tissue displacement was visible along the entire probe track (see Appendix C).

Conclusions

In vivo measurements within small brain nuclei can vary significantly from surrounding tissue due to discrete neuronal populations. Additionally, visible signs of tissue disruption such as bleeding can be informative when diagnosing performance

issues with a direct sampling method such as low-flow push-pull perfusion. For these reasons, histology is a valuable tool for *in vivo* neurochemical measurements.

References

(1) Cellar, N. A.; Burns, S. T.; Meiners, J. C.; Chen, H.; Kennedy, R. T. *Anal. Chem.* **2005**, *77*, 7067-7073.

(2) Paxinos, G.; Watson, C. *The Rat Brain in Stereotaxic Coordinates*; Academic Press: San Diego, CA, 2008.

Appendix C

Silicon Microfabricated Push-Pull Probes for Neurochemical Sampling

Woong Hee Lee, Thomas R. Slaney, and Robert T. Kennedy, manuscript to be submitted.

Introduction

A desirable trait for neural implants for chemical measurements is a small device size. Benefits of reduced device size are two-fold: a reduction in tissue trauma[1] and enhancement of spatial resolution[2, 3]. The benefits of spatial resolution are readily apparent: "hot spots" of neurotransmitter activity can be identified as have been within the nucleus accumbens, and regional differences in activity can be discerned by spatially resolved measurements[2, 3]. Furthermore, local basal concentrations of neurotransmitters can vary on the 100s of μm scale, as demonstrated in Chapter IV. Reduction of tissue trauma is important to ensure measurements reflect the normal physiology of neural tissue.

A technique with the potential for greatly reduced probe size is low-flow push-pull perfusion[4]. While the probe diameter of microdialysis probes is limited by the diameters of available dialysis fibers, low-flow push-pull perfusion probes are only constrained to the sizes of the sampling tubing and orifices. Initial probe designs utilized hypodermic tubings relatively large in size (400-450 μm)[5, 6]; however, substitution of fused silica capillaries has greatly reduced device sizes (as in Chapter IV) to ~200 μm[7].

Microfabrication of neural implants from silicon has been well-established as a way to minimize size. Silicon microelectrodes are commercially available[8, 9] and allow integration of different functionalities within a compact device. Silicon microneedles have been fabricated and can be mm in length[10]. Despite these capabilities, silicon probes have not to date been utilized for sampling methods such as low-flow push-pull perfusion.

In this work, silicon low-flow push-pull perfusion probes were constructed from silicon-over-insulator (SOI) wafers by incorporation of two fluidic channels. Connections were made to the base of these silicon probes utilizing fused silica capillaries as intermediate flow paths. To demonstrate sampling and examine basal concentrations of neurotransmitters, microliter fractions were collected, derivatized with benzoyl chloride, and analyzed utilizing liquid chromatography-mass spectrometry.

Materials and Methods

Reagents and Materials

Silicon wafers were purchased from Silicon Valley Microelectronics (Santa Clara, CA), Wafer World (West Palm Beach, FL), or University Wafer (South Boston, MA). Fused silica capillaries were purchased from Molex (Phoenix, AZ). Epoxy was purchased from Loctite (5-Minute Epoxy, Westlake, OH). Crystalbond Adhesive was purchased from Structure Probe (West Chester, PA). Unless otherwise specified, all reagents for sampling and sample analysis were purchased from Fisher Scientific (Fairlawn, NJ) and were Certified ACS grade or better. Artificial cerebrospinal fluid (aCSF) contained 145 mM NaCl, 2.68 mM KCl, 1.01 mM $MgSO_4$, 1.22 mM $CaCl_2$, 1.55 mM Na_2HPO_4, and 0.45 mM NaH_2PO_4, pH 7.4.[11]

Microfabrication Facilities

Microfabrication of low-flow push-pull probes was performed within a class 1000 cleanroom (Lurie Nanofabrication Facility at the University of Michigan, Ann Arbor, MI). A Karl Suss ACS 200 instrument was utilized for photoresist coating, baking and development (Garching, Germany). A Karl Suss MA-6 mask aligner was used for exposure of resist. Etching of silicon dioxide (SiO_2) and C_4F_8 was performed using a LAM 9400 plasma etcher (LAM Research Corporation, Fremont, CA). For deep reactive ion etching (DRIE) and reactive ion etching (RIE), an STS Pegasus 4 etcher was utilized (SPTS, Newport, UK). Low pressure chemical vapor deposition (LPCVD) of polysilicon was accomplished by use of a Tempress 6604 D3 furnace tube (Vaassen, Netherlands).

Silicon Probe Fabrication

Probes were fabricated from N-type SOI wafers of 100 mm diameter with a thickness of 525 μm. RCA cleaning was performed to remove any organic or inorganic contaminants[12]. A process schematic of the probe fabrication is shown in Figure C.1. Silicon dioxide was grown within a furnace to a thickness of 1 μm. Fluidic channels were masked in 3 μm thick SPR 220 photoresist (Dow, Midland, MI) by patterning a series of 3 μm diameter holes 17 μm apart along the channel length. Oxide was removed from beneath the resist utilizing plasma etching. Holes were extended to the channel depth (27 μm) by DRIE. Channels were formed by widening the base of these holes via RIE to a width of 20 μm and plasma etching was repeated to remove C_4F_8 that was deposited during DRIE. Photoresist was then removed, the wafer rinsed, and then RCA cleaned. Following cleaning, LPCVD was utilized to seal the channels by depositing 3 μm of polysilicon.

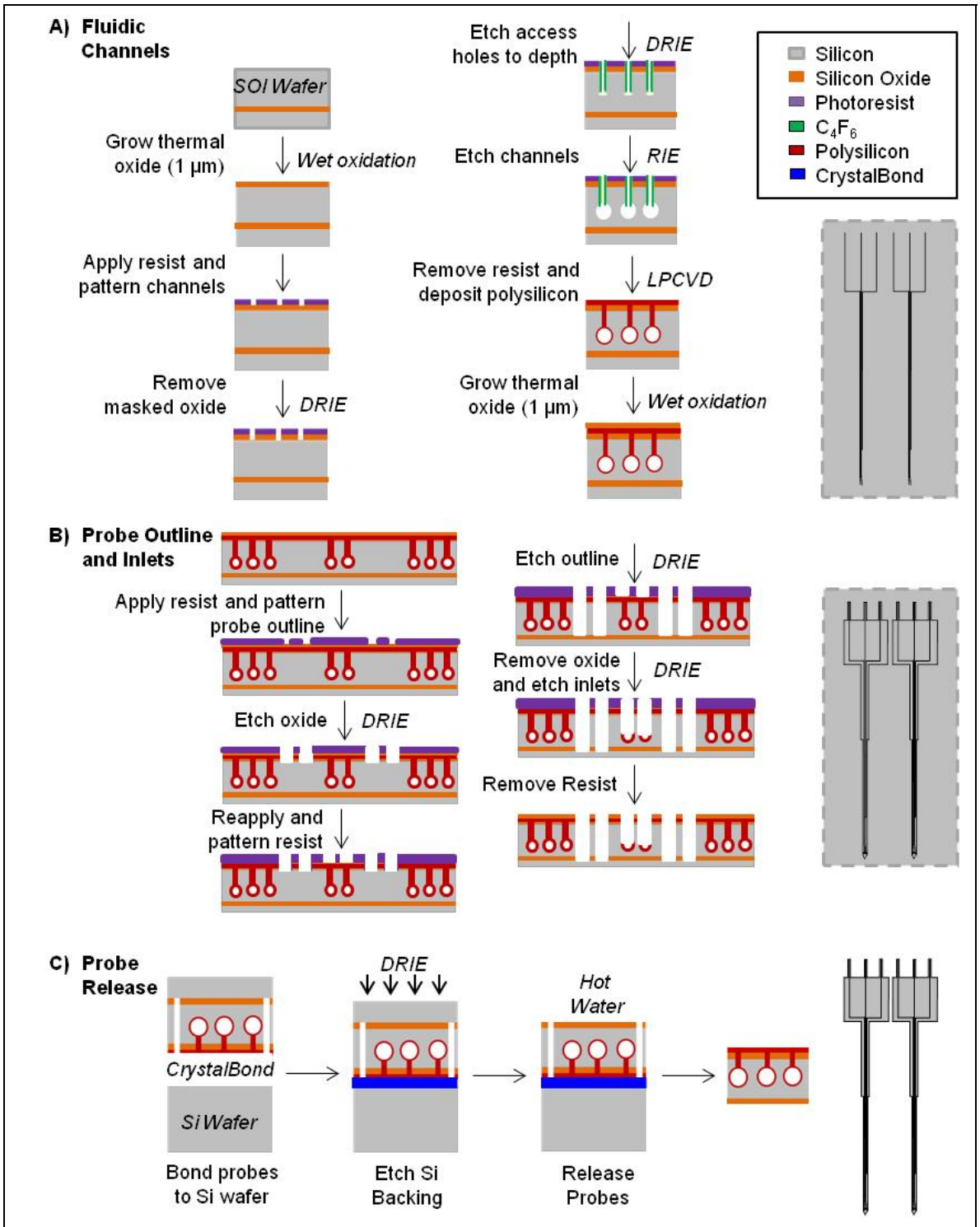

Figure C.1 Microfabrication procedure for silicon probes. (A) Probe channels were fabricated by reactive ion etching. (B) Deep reactive ion etching was then used to cut probe shapes and sampling inlets. (C) CrystalBond adhesive was used to fix probes to a silicon support. DRIE was then utilized to thin the probe backing, and hot water to release individual probes. Top views shown on right.

Following channel fabrication, wafers were placed into an oven to grow a 1 μm layer of SiO_2. A 3 μm layer of SPR 220 photoresist was deposited, the probe outlines masked and developed, and SiO_2 and polysilicon removed by DRIE. A coating of AZ 9260 photoresist was then applied to the wafer (AZ Electronic Materials, Branchburg, NJ), masked and developed to expose the probe outlines and sampling inlets (20 μm by 20 μm). Probe outlines were etched using DRIE until the probe silicon is traversed, while the oxide and polysilicon layers retarded etching of the probe inlet holes. By continuing DRIE, the oxide and polysilicon above the inlet holes was removed and etching continued until the channel depth was reached (25 μm).

Releasing probes from the SOI wafers was accomplished by etching to remove the backside silicon. This was accomplished by first utilizing Crystalbond adhesive to fix the top surface of the SOI wafer to a second silicon wafer substrate. DRIE was then utilized to remove the silicon backing of the SOI wafer. To release probes from the support wafer, the wafer was placed into warm water, dissolving the adhesive.

Probe Designs

Silicon push-pull probes were fabricated as above to provide a total device length of 11 mm (as shown in Figure C.2). Posts for fluidic connections (described below) were 1 mm in length. The extracranial portion of the probe connecting the posts to the implanted portion was a 2 mm by 2 mm. The ventral portion of the implanted probe was 200 μm diameter and 5 mm long. The ventral portion of the probe was 5 mm long and 84 μm in width. Inlets of the probe were at the ventral-most tip of the probe, and beneath the inlets, the probe outline tapered at 45° angles to a 90° point.

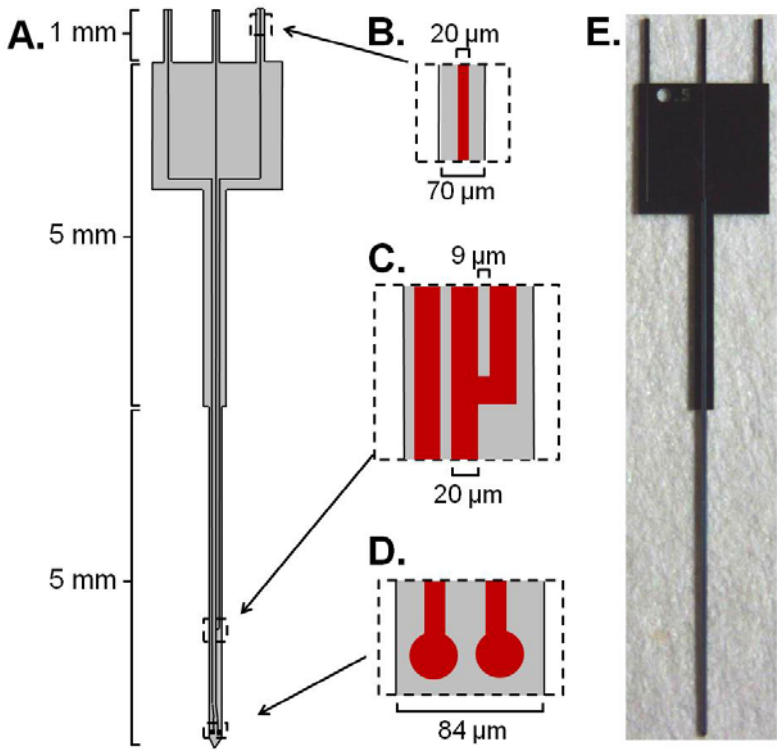

Figure C.2. Design of silicon push-pull probes. (A) An overview of probe shape and channels. Probes had of three fluidic connection prongs (from left to right: aqueous inlet, droplet outlet, and oil inlet) of 70 µm diameter with 20 µm diameter channels (B). 2 mm from the probe tip was a droplet generation tee (C) and at the tip of the probe were two inlets for "push" (left) and "pull" (right) flow. Two-channel probes were also fabricated of the same geometry but without the oil inlet or tee.

Probes were constructed with two or three fluidic channels. Two-channel probes connected one post orifice to each inlet at the probe tip for "push" and "pull" fluidic connections. Three-channel probes contained an oil inlet post. This inlet intersected with the "pull" inlet channel at 2 mm from the tip of the probe.

Fluidic Connections for Silicon Probes

Probe channels were adapted for external connections by fabrication of posts containing each channel of the probe. Posts were fabricated at the top of the probe and were 70 µm in diameter (matching the probe thickness) and 1 mm in length (Figure C.2). Channels were centered within these posts and intersected the tip of the post, providing an orifice.

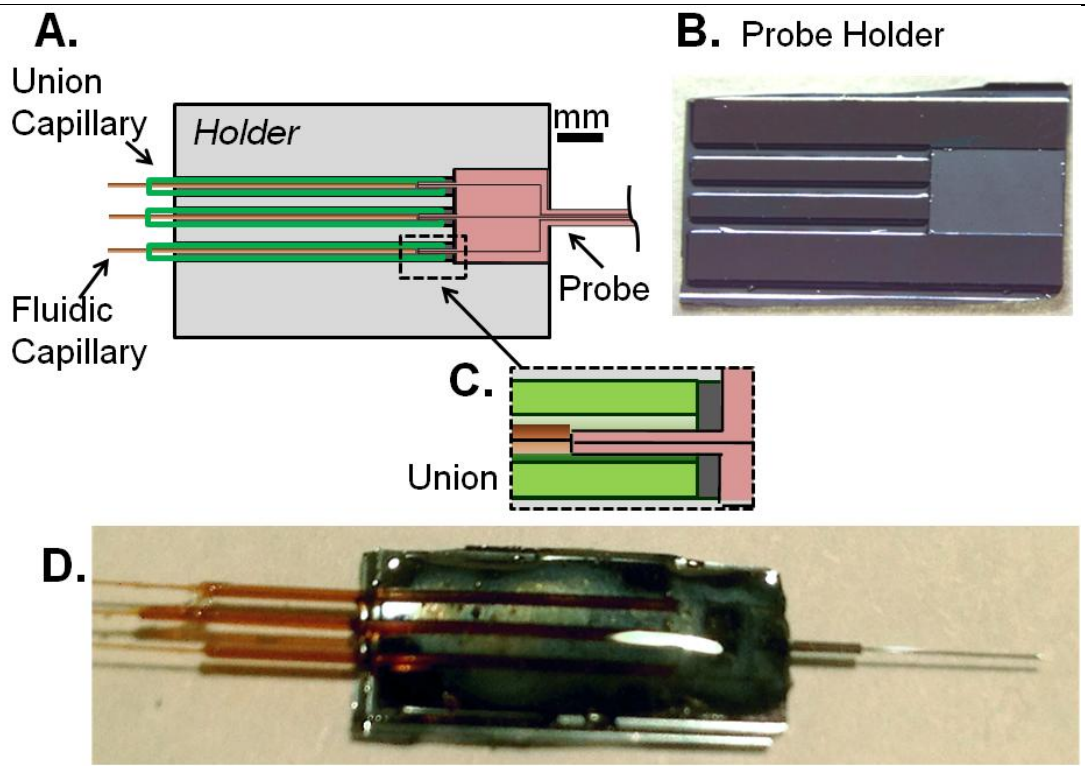

Figure C.3. Silicon probe assembly. (A) Connections from probe to capillary were made by aligning fluidic posts from the probe and fluidic capillaries (brown, 90 μm outer diameter) within a larger union capillary (green, 150 μm inner diameter). (B) Alignment was achieved by microfabricating probe holders from silicon wafers. (C) Probe posts were aligned in contact with fluidic capillaries. (D) Photograph of assembled probe, sealed by encapsulation with epoxy.

To hold probes adjacent to capillaries for unions, probe holders were fabricated from silicon wafers by DRIE. An overview of these holders is illustrated in Figure C.3. SPR 220 resist was patterned by lithography (as before) and then DRIE was utilized to etch channels of 360 μm width along the holder outline (5 mm by 10 mm rectangle) to 100 μm depth. These channels were spaced to align with silicon probe posts, and a 2 mm by 2 mm trench of 70 μm depth was etched to match the backside of the probe. As the edges of the holders were aligned with the <110> plane of the wafer, they were readily separated by cleaving.

For fluidic unions to connect to probe posts, ~10 mm lengths of 150 μm inner diameter, 360 μm outer diameter capillary were placed in the 160 μm diameter probe holder trenches (Figure C.3B). A probe was then slid into the 2 mm diameter trench so as to insert its posts into the 360 μm diameter capillary unions. The probe was fastened to the holder using epoxy. For fluidic connections, 20 μm inner diameter, 90 μm outer diameter capillaries were inserted through the opposite ends of the 360 μm outer diameter capillaries until their ends were flush against the tips of the posts. Capillaries were then sealed with additional epoxy.

Surgical Procedures

All procedures were performed according to a protocol approved by the University Committee for the Use and Care of Animals. Male Sprague-Dawley rats between 250 and 350 g were anesthetized using 65 mg/kg ketamine and 0.25 mg/kg dexmedetomidine and were placed in an ultraprecise stereotaxic frame (David Kopf, Tujunga, CA). The probe was affixed with tape to a stereotax probe holder (1770, David Kopf) in a vertical orientation. The skull was exposed and a burr hole drilled at 1 mm anterior and 2.3 mm lateral to bregma. The dura was carefully incised with a 27 gauge hypodermic needle and the surface of the cortex exposed so as to avoid damaging the probe.

During implantation, both channels of the push-pull probe were backflushed with aCSF at 200 nL/min. “Push” flow was supplied by coupling the probe inlet capillaries to a syringe pump (Fusion 400, Chemyx, Stafford, TX). The probe was lowered to a depth of 4 mm from the dura over ~2 minutes, and backflushing was immediately reduced to 50 nL/min at depth. After 8 minutes of backflushing, pull was commenced by connecting a

13 cm length of 100 μm bore capillary to the probe outlet and applying vacuum to its end (-150 mm Hg). Flow rate was monitored by measuring linear velocity of the capillary fill rate and vacuum adjusted as necessary to maintain 50 nL/min. After a capillary was filled (corresponding to 1 μL), it was transferred to an autosampler vial using gas pressure and immediately derivatized as described below. Fractions collected within the first hour were discarded. A total of three animals were measured, and between 4 and 8 fractions collected per animal (corresponding to 80 to 160 min of sampling).

Analysis of Neurotransmitters

Neurotransmitters were derivatized with benzoyl chloride and analyzed by liquid chromatography-mass spectrometry, as described in detail elsewhere[13]. To derivatize samples, reagents were added in rapid succession with intermediate vortexing immediately after collection. These reagents were 1.5 μL of 100 mM sodium tetraborate, 1.5 μL of 2% (vol.) benzoyl chloride (Sigma, St. Louis, MO) in acetonitrile, 1.5 μL of ^{13}C-labeled internal standards in dimethylsulfoxide[13] containing 1% (vol.) acetic acid, and 1 μL of 100 nM d_4-acetylcholine (CDN Isotopes, Pointe-Claire, Quebec, CA). Measured analytes included glutamate (Glu), γ-aminobutyric acid (GABA), aspartate (Asp), serine (Ser), taurine (Tau), histamine (Hist), glycine (Gly), dopamine (DA), 3,4-dihydroxyphenylacetic acid (DOPAC), 3-methoxytyramine (3-MT), homovanillic acid (HVA), norepinephrine (NE), normetanephrine (NM), serotonin (5-HT), 5-hydroxyindoleacetic acid (5-HIAA), adenosine (Ado), and acetylcholine (ACh). For calibration curves, standards were prepared which contained 0.5, 5, 10, 50 and 100 nM of ACh, 3-MT, 5-HT, DA, Hist, NE, and NM; 5, 50, 100, 500, and 1000 nM of 5-HIAA,

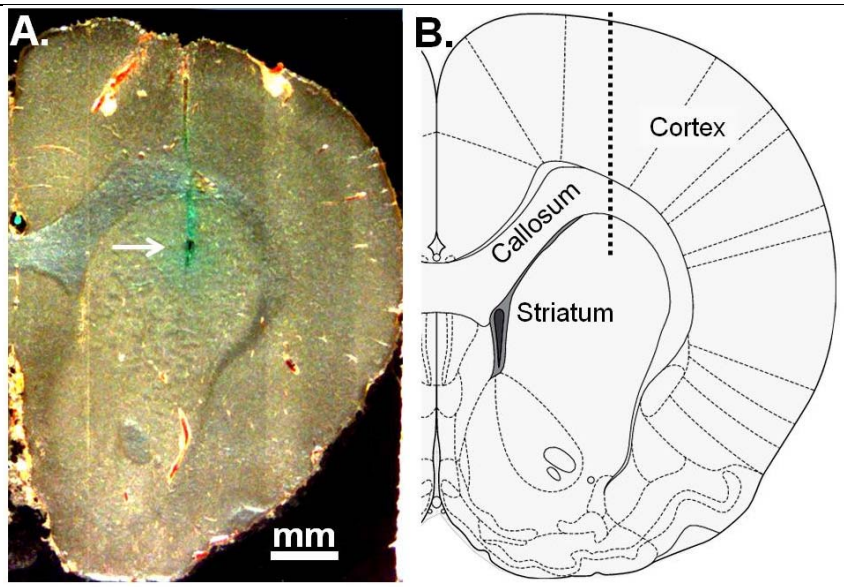

Figure C.4. Histology following sampling with a silicon probe. (A) After sampling, FastGreen FCF was infused through the probe, which labeled the sampling site (arrow) and probe track a blue-green color. (B) Sampling occurred at the tip of the probe (dashed line) within the striatum. Adapted from Paxinos and Watson[14].

Ado, Asp, DOPAC, GABA, Glu, HVA, Ser, and Tau; and 50, 500, 1000, 5000, and10000 nM of Gly, Ser and Tau respectively. Analysis was conducted using chromatographic conditions and mass spectrometer MRM parameters as described previously[13].

Histology

After sampling, 100 nL of filtered saturated FastGreen FCF was infused at 50 nL/min through the probe. Brains were placed in 10% paraformaldehyde in 100 mM phosphate buffered saline and fixed at ~4°C for at least 24 h (see Appendix B). Brains were frozen and sliced along the coronal plane using a cryostat. Slices (50 or 60 μm thick) were placed on microscope slides (SuperFrost, Fisher, Fairlawn, NJ) and imaged using an optical microscope, as shown in Figure C.4.

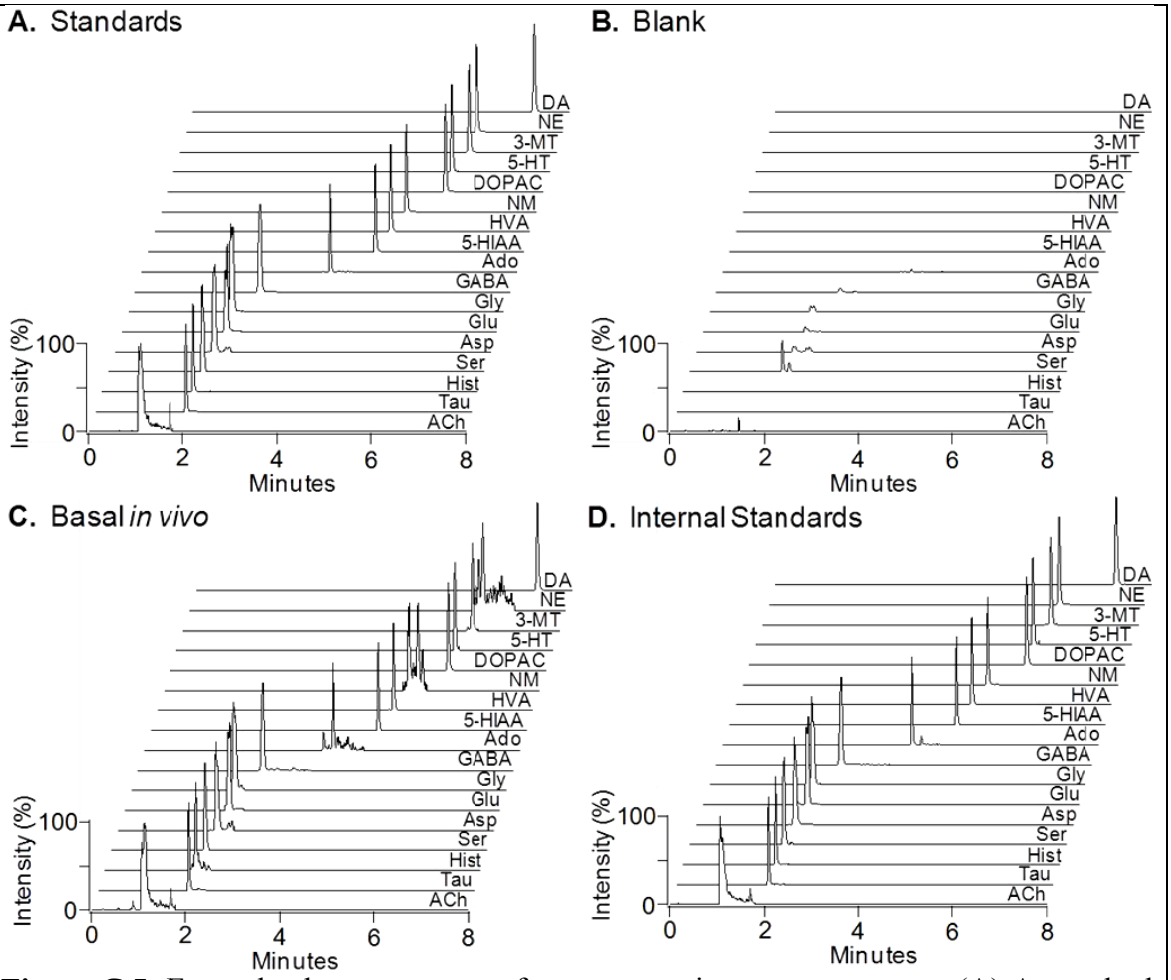

Figure C.5. Example chromatograms of neurotransmitter measurements. (A) A standard containing 50 nM of ACh, 3-MT, 5-HT, DA, Hist, NE, and NM, 500 nM of 5-HIAA, Ado, Asp, DOPAC, GABA, Glu, and HVA, and 5000 nM of Gly, Ser and Tau. (B) An aCSF blank (containing internal standard). (C) A fraction collected from the striatum, and (D) Stable isotope-labeled internal standard from the *in vivo* fraction in C.

Results and Discussion

Probe Tracking and Tissue Disruption

As shown within Figure C.4, minimal tissue disruption was observed following sampling using a microfabricated push-pull probe. As the probe diameter was only 84 μm (comparable to a human hair), less tissue is displaced during implantation than previous push-pull probe designs. Dye was necessary to locate the probe track during histology,

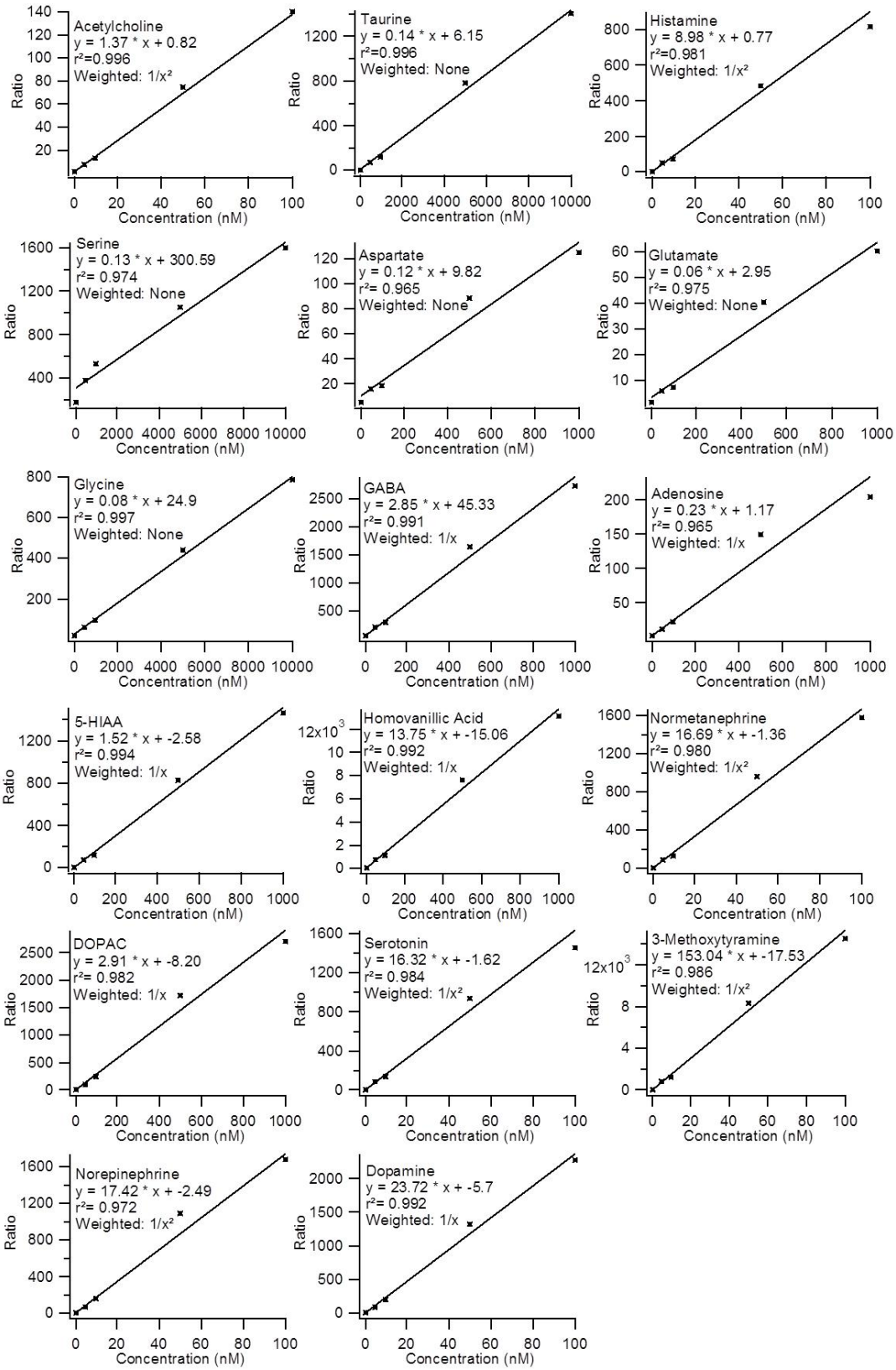

Figure C.6. Calibration curves of neurotransmitters, as ratio (analyte/internal standard peak area) vs. concentration, with weighting factors and correlation coefficients (r^2).

Neurotransmitter	Basal Concentration (nM)
ACh	26 ± 12
Tau	1500 ± 700
Hist	5.9 ± 1.5
Ser	6600 ± 1800
Asp	530 ± 110
Gly	3000 ± 600
Glu	1100 ± 500
GABA	78 ± 30
Ado	39 ± 21
5-HIAA	140 ± 80
HVA	380 ± 240
NM	0.1 ± 0.0
DOPAC	750 ± 450
5-HT	0.36 ± 0.16
3-MT	1.3 ± 0.7
NE	1.5 ± 1.3
DA	19 ± 7

Table C.1. Basal concentrations of neurotransmitters measured within the striatum of anesthetized rats (mean ± SEM, $n = 3$ animals).

given the minimal tissue disruption. No probe occlusion or bleeding was observed during these experiments.

Basal Concentrations of Neurotransmitters

As described above, each 1 μL fraction collected was labeled with benzoyl chloride, and stable isotope-labeled internal standards added. Therefore, a total of 34 ions were measured by LC-MS from each fraction, and concentrations were measured as the ratio of peak area of analyte to internal standard. Figure C.5 shows example chromatograms of a standard, a blank, an *in vivo* fraction collected from the striatum, and internal standards. No significant carry-over was observed. Calibration curves were linear, and weighting was applied to provide the best fit, as shown in Figure C.6.

Fractions collected within the first hour after probe implantation were discarded, as prior work demonstrated unstable neurotransmitter levels within the first ~30 minutes[5, 6, 11]. The average of measurements from three animals is shown in Table C.1. Basal

concentrations of dopamine and metabolites HVA and DOPAC were 11, 12 and 14-fold greater, respectively, than was observed with 220 μm diameter probes (Chapter IV), and dopamine was 3 to 10-fold greater than observed concentrations with no-net-flux microdialysis[15, 16]. A possible explanation is that this difference is attributable to the smaller probe, as electrochemical measurements have suggested that tissue in close proximity to larger probes exhibit impaired dopamine release[17]. However, the range of basal concentrations of dopamine varied 5-fold between individuals (6, 21 and 30 nM for 3 rats), which may indicate local or individual differences in dopamine within the striatum. Such differences have been observed previously with respect to dopamine activity in the ventral striatum[2].

Different neurotransmitters had differing degrees of variability within animals. To compare this variability, the relative standard deviations of neurotransmitters within each animal were calculated, and were averaged between animals. Dopamine and 3-MT were least variable, with average within-animal relative standard deviations of 12 ± 2 and 14 ± 11 percent respectively (n = 3 rats, 4 to 6 measurements each). Glycine, aspartate, serine and glutamate demonstrated the greatest variability, with within-animal standard deviations of 58 ± 22, 54 ± 30, 53 ± 23, and 42 ± 13 percent, respectively. The average within-animal variability of each neurotransmitter was 32 percent. This suggests that the amino acid neurotransmitters have a greater variability on the 20-minute timescale than the monoamine neurotransmitters.

Interestingly, taurine and GABA did not follow this trend, with 23 ± 10 and 30 ± 12 percent deviation each. A possible explanation is that this effect is due to use of ketamine anesthetic, as ketamine an n-methyl-d-aspartate (NMDA) receptor antagonist[18],

and NMDA receptor antagonists have been shown to increase excitatory amino acid concentrations.

Conclusions

Bulk micromachining of silicon wafers by reactive ion etching is a viable way to fabricate push-pull sampling probes for measuring neurotransmitters. These probes have the potential to measure many more analytes quantitatively than the 17 demonstrated in this work. These measurements also represent quantitative observations from minimally perturbed tissues which may reflect differences observed in basal levels compared with other sampling techniques. As probes are amenable to segmented flow by incorporation of a third oil channel, low-flow push-pull perfusion with silicon microprobes should provide a versatile method for high temporal resolution quantitative measurements.

References

(1) Stenken, J.; Church, M.; Gill, C.; Clough, G. *The AAPS Journal* **2010**, *12*, 73-78.
(2) Robinson, D. L.; Howard, E. C.; McConnell, S.; Gonzales, R. A.; Wightman, R. M. *Alcohol.: Clin. Exp. Res.* **2009**, *33*, 1187-1196.
(3) Wightman, R. M.; Heien, M. L. A. V.; Wassum, K. M.; Sombers, L. A.; Aragona, B. J.; Khan, A. S.; Ariansen, J. L.; Cheer, J. F.; Phillips, P. E. M.; Carelli, R. M. *Eur. J. Neurosci.* **2007**, *26*, 2046-2054.
(4) Kottegoda, S.; Shaik, I.; Shippy, S. A. *J. Neurosci. Methods* **2002**, *121*, 93-101.
(5) Slaney, T. R.; Nie, J.; Hershey, N. D.; Thwar, P. K.; Linderman, J.; Burns, M. A.; Kennedy, R. T. *Anal. Chem.* **2011**, *83*, 5207-5213.
(6) Cellar, N. A.; Kennedy, R. T. *Lab Chip* **2006**, *6*, 1205-1212.
(7) Kottegoda, S.; Pulido, J. S.; Thongkhao-on, K.; Shippy, S. A. *Molecular Vision* **2007**, *13*, 2073-2082.
(8) Johnson, M. D.; Franklin, R. K.; Gibson, M. D.; Brown, R. B.; Kipke, D. R. *J. Neurosci. Methods* **2008**, *174*, 62-70.
(9) Kipke, D. R. *Engineering in Medicine and Biology Society, 2003. Proceedings of the 25th Annual International Conference of the IEEE* **2003**, *4*, 3337-3339.
(10) Jingkuang, C.; Wise, K. D.; Hetke, J. F.; Bledsoe, S. C., Jr. *Biomedical Engineering, IEEE Transactions on* **1997**, *44*, 760-769.
(11) Cellar, N. A.; Burns, S. T.; Meiners, J. C.; Chen, H.; Kennedy, R. T. *Anal. Chem.* **2005**, *77*, 7067-7073.

(12) Kern, W.; Puotinen, D. A. *Rca Review* **1970**, *31*, 187-206.
(13) Song, P.; Mabrouk, O. S.; Hershey, N. D.; Kennedy, R. T. *Anal. Chem.* **2012**, *84*, 412-419.
(14) Paxinos, G.; Watson, C. *The Rat Brain in Stereotaxic Coordinates*; Academic Press: San Diego, CA, 2008.
(15) Sam, P. M.; Justice, J. B. *Anal. Chem.* **1996**, *68*, 724-728.
(16) Chen, N. N. H.; Lai, Y.-J.; Pan, W. H. T. *Neurosci. Lett.* **1997**, *225*, 197-200.
(17) Yang, H.; Peters, J. L.; Michael, A. C. *J. Neurochem.* **1998**, *71*, 684-692.
(18) Moghaddam, B.; Adams, B.; Verma, A.; Daly, D. *J. Neurosci.* **1997**, *17*, 2921-2927.